The Investigation of Quantum Polarisation Teleportation Protocols

Aśka Dolińska

A thesis submitted for the degree of
Bachelor of Science in Physics
The Australian National University

November, 2002

Declaration

This thesis is an account of research undertaken between February and November 2002, under the supervision of Dr Ping Koy Lam, Dr Ben Buchler and Dr Timothy Ralph. It is a partial fulfilement of the requirements for the degree of Bachelor of Science with Honours in theoretical physics at the Australian National University, Canberra, Australia.

Except where acknowledged in the customary manner, the material presented in this thesis is, to the best of my knowledge, original and has not been submitted in whole or part for a degree in any university.

Aśka Dolińska
November, 2002

StokeSpunk

Acknowledgments

My huge motivation to become a detective of the physics realm had been nurtured by the community at the Australian National University for the last 4 years. Many warm thanks goes to everyone who inspires me so much to learn more about this astounding world. The people at the Physics Department are so happy to share their insights and discoveries, that it is really thanks to them that I can build on and move forward, in this jungle of information.

Special thank you to the fellow quantum optics fans, especially my supervisors: Ping Koy Lam, Ben Buchler and Tim Ralph, for their wise advice and floods of brilliant thoughts. You make me believe that breakthroughs are not freak events but a result of hard work and dedication. Viva to perfectionism!

Thanks for all your backing Hans. (And you have no idea what a life saving raft your laptop has been during the last few weeks!)

The remaining staff at the faculty of physics deserves a big hug, like Joe, who is willing to help me with all those incomprehensible computers, John, for bringing physics to life in a very LARGE way, Thomas and Andrew for the joint time in the lab with the French music and all my previous, undergraduate lecturers. You are all such a pleasure to see everyday, listen to and talk to. I am sure to miss you!

Further, I should mention my office buddies, Prof. Nicolai and Mr Ψ-ko, for being so much fun, even when I was on the brink of madness.

To Rich for insisting I am a nerd.

To Matt B. for sharing my interests when no one else would.

And the rest of the Honours students, for surviving this year with me, and still living it up on Friday nights.

Thanks Stu for all your constructive, unbiased criticism and enthusiasm. (Now's your turn!)

Viellen Danke to Paul Cochrane for his help with atrocious Matlab code.

To dearest Kelly. You're so full of life and affection that you make me look outside my small world to enjoy your universe!

Finally, my flatmates are undoubtedly an integral part of this thesis, reminding me of the day cycles and the concept of sleep, when I was living in a time warp.

Dzięki śliczne maminku i tatinku. Jesteście wspaniałym wsparciem duchowym i moralnym!

I na koniec, całóski dla Ewci we Wrocławiu. Zawsze będziesz mi bliska, nie ważne ile słów zrozumiesz z tej księgi!

Abstract

The continuous variables regime offers much promise for quantum information and computation protocols. In particular, the continuous variable polarisation teleportation is of great interest, both theoretically and experimentally, at the moment.

In this thesis three schemes for continuous variable polarisation teleportation are analysed and their performance is rated. The double teleporter setup, the quantum nondemolition teleporter scheme and the biased entanglement teleporter setup are each discussed and evaluated. Two methods are employed for the evaluation of the teleportation success. The TV diagram which stresses the usefulness of the experimental design and the fidelity, which measures the quantum input to output state preservation. It is later shown that these two independent assessments, which consider physically different attributes, yield contradicting conclusions. Further it is shown that it is important to decide whether the objective of the polarisation teleportation is the transfer of information or the quantum state recreation before meaningful analysis using TV or fidelity can be made.

Finally, a study of a special cloning limit for a particular input state is made, related to the two of the above polarisation teleportation schemes. A new cloning fidelity limit is derived for these cases and TV cloning limits of information transfer and correlations are discussed.

Contents

List of Figures

Chapter 1

Introduction

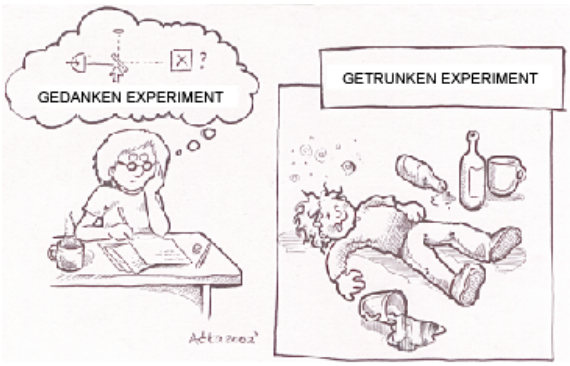

Overview

On of the aims of quantum information technology is to create communication and computing systems superior to those offered by classical physics based on the fundamental differences between the two. Quantum randomness is a tradeoff between acquiring information and creating a disturbance. It is because the outcome of a measurement has a random element that it is not possible to infer the initial state of the system from the measurement outcome. Furthermore, quantum information, as will be discussed in the later chapters, can not be copied with perfect fidelity. However, the main feature which distinguishes quantum information from its classical counterpart is the fact that it can be encoded in nonlocal correlations between different parts of a physical system, with no equivalent in classical physics, as was shown by Bell [5].

Quantum entanglement, as first discussed by Einstein, Podolsky and Rosen (EPR) [1], became an intensive field of study among those interested in the foundations of quantum theory, but more recently it came to be viewed as a potentially valuable resource. The exploitation of entangled states allows tasks that are otherwise difficult or impossible, one of which is teleportation.

The standard approach to quantum information processing has been for a long time making use of the discrete quantum entanglement, such as single photon entanglement generated by parametric down conversion, [10]. The research has raised many interesting possibilities such as quantum cryptography [7, 12, 26] and quantum teleportation [9, 11], all discussed in the references. Another protocol, quantum dense coding [20, 21], is a term given to uses of nonlocal correlations to send two pieces of information via a single quantum bit, qubit, while the classical channel at best allows only a single unit of information per bit.

Quantum computation with discrete qubits also offers exciting prospects by being able to solve a special group of problems with a completely new level of complexity not possible until now. It is also feasible to protect complicated quantum systems from the debilitating effects of decoherence, which means that quantum errors can be corrected.

We are witnessing the dawn of the age of coherent manipulation of quantum information in the laboratory, so the construction of quantum hardware is no longer a distant dream.

However, as no experimentally realised procedures exist to identify all four Bell states for any system with single photons and linear optics manipulations, (for example see paper by Zellinger *et al* [28]), the measurement central to efficiency of these discrete quantum protocols is missing. The experimental realisations have been restricted to the low efficiency inherent in photon counting experiments.

Instead of single particle entanglement, many-photon states of light can be used to convey quantum information and offer some solutions to the above problems. Their description uses continuous variables and has a distinct advantage in terms of the availability of controlled sources, efficient detectors and processing using linear elements. The use of bright beams of light allows simplification of the inverse Bell-state-like measurement, as will be shown in chapter 2. However there still exist problems with the continuous variable quantum information implementation, which must be resolved before further progress can be made.

Continuous variable systems have been shown to theoretically be equally useful in the implementation of quantum information protocols such as quantum dense coding [17, 58], quantum cryptography [41], quantum cloning [29, 30, 36] and other techniques described in papers [32, 33].

The possibility of teleportation of continuous quantum variables such as amplitude and phase quadratures of light field (section 2.2) was first suggested by the developments of L. Vaidman [52] and H. Kimble with L. Braunstein [43]. With the availability of bright squeezed states, many-photon state entanglement became relatively easy to implement [35]. The use of highly efficient homodyne detectors, (section 2.5.2) now greatly simplifies the experimental manipulation of quantum information.

A lot of investigation has been done involving quantum protocols using bright light beams, with the coding and sending of information in the fluctuations of the two orthogonal quadratures. However, the properties of the polarisation of continuous wave light are only becoming of increasing interest since they offer new opportunities for communicating quantum information. Most importantly though, they dispense with the use of costly reference or local oscillator beams.

The important advantage of these nonclassical polarisation states for quantum communication is the possibility of experimentally determining all of the relevant conjugate variables of both squeezed and entangled fields using only linear optical elements, followed by direct detection.

This thesis investigates the continuous variable regime of quantum teleportation protocols, for the polarisation states of bright beams.

It proposes several possible experimental systems designed for teleportation of all polarisation variables and evaluates their performance in the small signal limit, using two independent protocol evaluation methods. The first, fidelity, is the overlap of the input quantum state with the output, (section 2.6). The second, TV approach, deals with the amount of information transferred and the noise introduced during teleportation experiment, (section 2.7).

Thesis structure

Following this introduction chapter, in chapter 2, I will briefly outline the mathematical tools which are used in quantum optics to create models for various experimental schemes.

The standard, continuous wave teleportation scheme will then be described. It will be followed by the introduction of the two figures of merit, commonly used to evaluate a continuous variable quantum information protocol.

Chapter 3 provides extensions of the definitions in previous chapter, from quadratures to Stokes parameters used to describe polarised light. Some major difficulties with the new description are discussed. The full Stokes parameters variances are given and their meaning in the small signal limit is described.

In chapter 4 the Stokes variances are applied in an evaluation of a full polarisation teleportation system. Discussion of new behaviour and input polarisation dependence is made, in a context of imperfect setup and asymmetric squeezing.

An improved version of the polarisation state teleportation scheme is given in chapter 5, where an input of a fixed, known polarisation allows the reduction of the number of quantum resources. This scheme is called the QND-teleportation scheme. The information transfer and quantum correlation preservation is evaluated for the three Stokes parameters. A new visualisation tool, showing the dynamics of the system, is proposed.

Chapter 6 puts forward an alternative, simplified polarisation teleportation scheme, which in contrast to the previous one, optimises the teleportation fidelity. This scheme is called the BE-teleportation scheme. The transfer of information is then shown to be non optimal for such a system, and to be less than in the scheme of chapter 5. The conflicting results of fidelity and TV evaluation is then discussed.

As an interesting development motivated by chapter 6, the teleportation cloning limit of a state carrying information on a single quadrature is investigated. The fidelity cloning limits for the standard and single quadrature cases are compared and contrasted. The results of the project are summarised.

Chapter 2

Quantum optics formalism

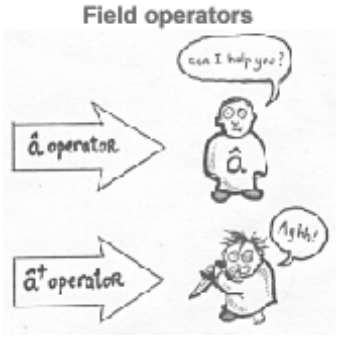

2.1 Overview of this chapter

This chapter is devoted to introducing the theoretical tools which I used in my Honours investigation of polarisation state teleportation. The first part of this chapter concentrates on the basic quantum optics concepts that will be assumed without further proof. In subsequent chapters, a list of quantum information protocols using this mathematical formalism is outlined. Finally, two important methods for evaluating the efficacy of quantum information schemes are reviewed.

2.2 The linearisation of field operators

The Heisenbergs uncertainty principle, which lies at a heart of quantum mechanics, is central to the quantum description of light, through the definition of the radiation field operator.

There are several approaches to the quantisation of the light field. However the most useful, for the following analysis, introduces the creation and annihilation field operators, $\hat{a}(t)$ and $\hat{a}^{\dagger}(t)$. These are defined as $\hat{a}(t) = \alpha_{classic} + \delta\hat{a}(t)$, and $\hat{a}^{\dagger}(t) = \alpha^{*}_{classic} + \delta\hat{a}^{\dagger}(t)$. The classical amplitude component (which is usually complex), $\alpha_{classic}$, is the expectation value, $\langle\, \hat{a}(t)\, \rangle$. The quantum operator parts $\delta\hat{a}(t)$ contain all quantum mechanical fluctuations and obey the commutation relation $[\delta\hat{a}(t), \delta\hat{a}^{\dagger}(t)] = 1$.

Hermitian and therefore observable operator combinations of these are used. The operators for amplitude and phase quadratures of light are, $\delta\hat{X}(t)^{+} = (\delta\hat{a}(t) + \delta\hat{a}^{\dagger}(t))$, and $\delta\hat{X}(t)^{-} = i\ (\delta\hat{a}(t)^{\dagger} - \delta\hat{a}(t))$. These two conjugate observables are linked by the commutation relation, $[\delta\hat{X}(t)^{+}, \delta\hat{X}(t)^{-}] = 2i$.

Most experimentally produced light states belong to a special set of Gaussian states, where the quadrature noise fluctuations obey Gaussian statistics. This means the first and second order statistical moments of a light beam, hence α and variance, are all that is necessary to describe the field fully. The variance of the quadrature operators is defined as:

$V^{\pm} = \langle(\delta\hat{X}(t)^{\pm})^2\rangle - \langle\delta\hat{X}(t)^{\pm}\rangle^2$, with $\langle\delta\hat{X}(t)\rangle$ being the expectation value of the operator $\delta\hat{X}(t)$. The linearisation principle is used, following naturally from the above definition of the creation-annihilation operators by assuming that the classical amplitude is much larger than the quantum operator. The variance in this case simplifies to $V^{\pm} = \langle(\delta\hat{X}(t)^{\pm})^2\rangle$, as the time average of fluctuations, $\langle\delta\hat{X}(t)^{\pm}\rangle$, is always zero. Often a combination of the amplitude and phase quadratures is also defined and called the quadrature amplitude $X^{\theta} = X^{+}cos\theta + X^{-}sin\theta$.

By definition, the variance of quantum vacuum fluctuations is set to unity, and any signal and modulation has $V^{\pm}$ measured relative to this noise limit. For more detail refer to texts [4, 6, 13].

For convenience the frequency spectra are given by Fourier transforming the time domain expressions above. Since there are no products, these simply change to operators describing a light field of a particular frequency. Hence the quadrature parameters $\delta X^{\pm}$ are for the remainder of this thesis assumed to be of form $\delta X^{\pm}(\omega)$.

A visualisation of the frequency description of light can be seen on figure 2.1. The modulation sideband at $\omega = \omega_{RF}$ lies on top of the vacuum noise "floor", which exists at all frequencies. The carrier α_{DC} at $\omega_{DC} = 0$ is also shown, however due to its large, relative size its uncertainty is now effectively zero.

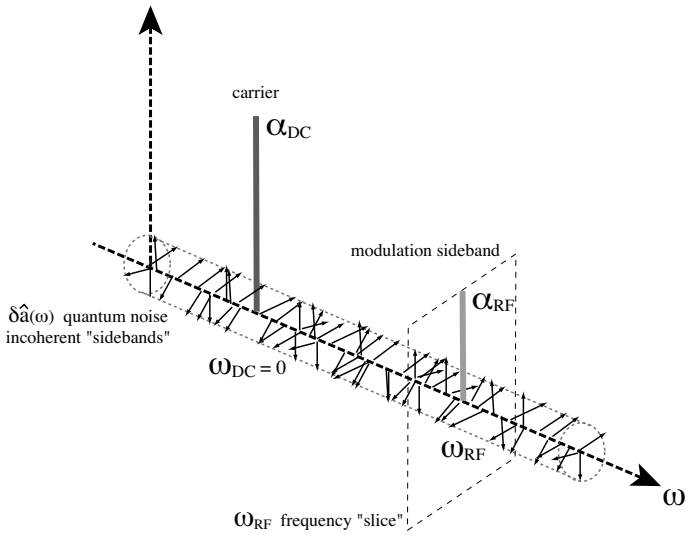

Figure 2.1: The frequency spectra of the light field in the sideband picture. α_{RF} is the modulation sideband which lies on top of the white vacuum noise, $\delta\hat{a}$. The carrier α_{DC} at $\omega_{DC} = 0$ is also shown. The ω_{RF} "slice" of this diagram inspects the properties of the light at only a single frequency.

2.3 Phase space representation

The two noncommuting and orthogonal quadratures $\hat{X}^{\pm}$ define a phase space in which a continuous variable light field can be described. To combine all the information about a light field a so called "ball-on-stick" diagram is usually constructed. This is a single frequency representation, and can be imagined as an ω_{RF} "slice" through the ω axis on figure 2.1.

Figure 2.2(a) shows the modulation signal of a carrier beam at a particular frequency for a minimum uncertainty state. The classical field amplitude α_{RF}, is the length of the "stick", while the quantum fluctuations in both the phase and the amplitude quadrature are the circular uncertainty region, or the "ball".

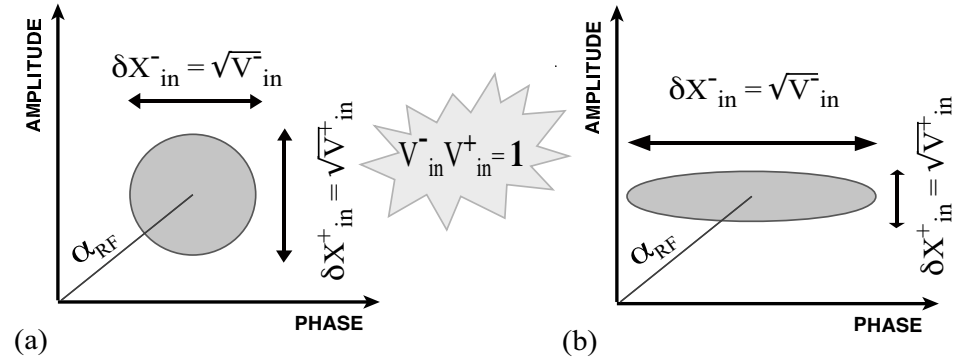

Figure 2.2: Two minimum uncertainty states: (a) coherent state, (b) amplitude squeezed state. α_{RF}: the modulation sideband amplitude, $V^{\pm}$: phase and amplitude noise variance of the light beam.

2.4 Squeezing of light

It is possible to manipulate even the quantum mechanical fluctuations of a light field. This can be done by the passage of light through a nonlinear crystal, such that correlations between the fluctuations of the two quadratures take place. In this situation the variance of the quadratures can become less than the quantum noise level, while the conjugate variance is increased to preserve the uncertainty relation, $V^+V^- \geq 1$, as shown on figure 2.2(b). [13, 23]

Light with $V < 1$ is said to be squeezed in that quadrature. In the limit of $V \to 0$ we obtain perfect squeezing however this requires infinite energy. When $V > 1$ the light is referred to as anti-squeezed or having a super-Poissonian state.

2.5 Quantum theory for experiments

Following is a summary of basic quantum optical elements, using the operator formalism introduced so far in this chapter. Quadrature variances can be detected as the fluctuations of the current and in all, experimental quantum protocols it is the transfer of these variances through the system that is analysed.

2.5.1 Beam splitters and vacuum noise

The beam splitter (BS), is an optical element central to most quantum information protocols. It introduces uncorrelated quantum noise into the system, which degrades the signal-to-noise ratio of the input and randomises the output. The figure 2.3 illustrates this. All beam splitters behave like this and are the source of the precision limit encountered by quantum optics assigned to the presence of vacuum noise.

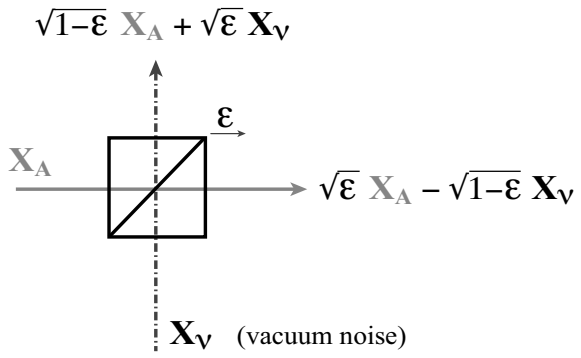

Figure 2.3: The input and output quadratures of a beamsplitter with transmittance ϵ, showing the vacuum noise fluctuations coupling to the light field, $\hat{A}$.

Many processes, like absorption, also introduce uncorrelated vacuum noise to a passing light beam. Such processes can be modelled by such a beam splitter with a transmission or efficiency of η, to keep account of the losses.

2.5.2 Standard homodyne detection

The homodyne detector is a crucial experimental tool, which facilitates the measurement of the quadrature amplitude of a light beam [6, 13, 27].

In a homodyning scheme, the signal is interfered with a bright beam of a known phase, called the local oscillator, LO. The sum and difference of the photocurrents, when LO amplitude is assumed to be much larger than the signal, are [23]

$$\begin{aligned} I_+ &\propto |\alpha_{LO}|^2 + \alpha_{LO}\ \delta X^+_{LO} \\ I_- &\propto 2\alpha_{sig}\alpha_{LO}\ \cos\theta + \alpha_{LO}(\ \delta X^-_{sig}\cos\theta\ -\ \delta X^+_{sig}\sin\theta\ ) \end{aligned}$$

This approach uses an approximation, valid if the LO is much brighter than the signal, to extract only the information about the fluctuations of the signal, which are now scaled by the bright, LO amplitude, α_{LO}. That is, the sum photocurrent I_+ is to first order approximately that of the direct detection of the LO field, δX^+_{LO}. However, depending on the relative phase of the interfering beams, any projection of the quadratures, $X^\pm_{sig}$, can be detected, and this continuous measurement of the signal quadrature amplitude is given by the difference photocurrent, I_-. The standard homodyning is hence a useful measurement in situation where the maximum squeezing quadrature is not the amplitude quadrature. The experimental setup is shown on figure 2.4.

2.5.3 Teleportation

Teleportation is a procedure by means of which two conjugate quadratures are measured, destroyed and reconstructed in an identical quantum state [43, 52]. In a classical scheme, without the use of quantum resources like entanglement, such a task is not possible, as Heisenberg's uncertainty principle prevents measuring and reconstructing both quadratures without adding external quantum noise, as the beam splitter section demonstrates.

It is the use of squeezed light and non local quantum entanglement that enables the

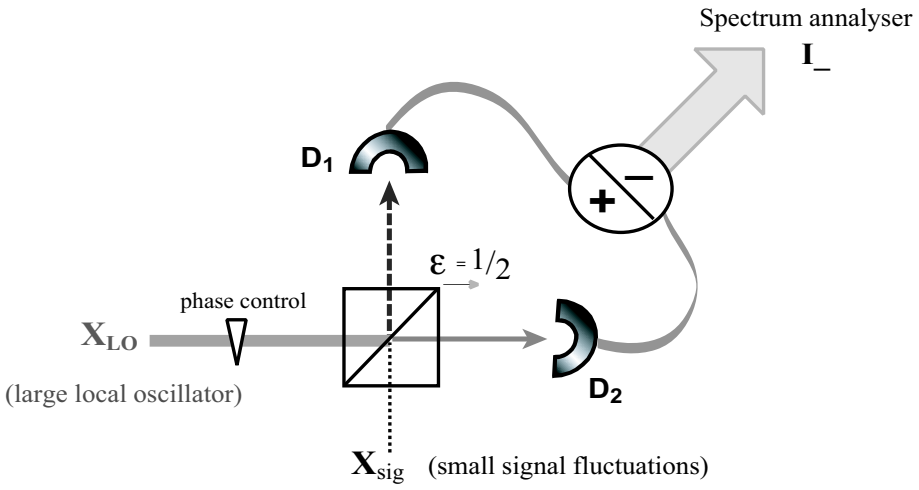

Figure 2.4: The basic principle of homodyne detection. LO amplitude is much greater than signal. The difference of the currents gives the signal fluctuations scaled by the LO, see text. D1, D2: detectors, ϵ: beam splitter transmission coefficient, +/- : electronic adder and subtracter.

teleportation scheme to surpass the classical limits, (first proposed by C. Bennett [8]). The quantum teleporter is shown in figure 2.5. The central part of the protocol is the entangled EPR pair of light beams, [1, 37]. When the EPR2 beam is injected into the BS at the sender's station, instead of introducing the usual vacuum noise, (section 2.5.1), it 'plugs' the vacuum input and correlates the noise that is mixed with the signal, so that it can be cancelled in the receiving station by EPR1 beam. If $\lambda_\pm$ are the modulator gains and the efficiency of transmission and detection is assumed ideal, the transfer of the input signal variances, ($V_{in}^{\pm}$), through the system is described by the transfer function (full expressions given in Appendix B.1) [48]

$$V_{out}^{\pm} \;=\; \frac{1}{2}|1+\lambda_\pm|^2 V_{SQ2}^{\pm} + \frac{1}{2}|1-\lambda_\pm|^2 V_{SQ1}^{\mp} + |\lambda_\pm|^2 V_{in}^{\pm} \tag{2.1}$$

If the modulator gains are adjusted to $\lambda_\pm = \pm 1$, with opposite signs, the transfer function of each quadrature reduces to

$$V_{out}^{+} = 2V_{SQ2}^{+} + V_{in}^{+} \quad \text{and} \quad V_{out}^{-} = 2V_{SQ1}^{+} + V_{in}^{-}.$$

As the amplitude squeezing of the beams increases, ($V_{SQ1,2}^{+} \to 0$), the unwanted terms above become small and the required teleportation condition of $V_{out}^{\pm} = V_{in}^{\pm}$ is obtained [47, 48].

2.5.4 Quantum nondemolition measurement

The quantum nondemolition measurement, (QND) [49, 50, 51, 53], deals with a simpler problem of reconstructing all quantum information of only one of the two conjugate observables. When for example, an experiment tries to measure position of a particle it necessarily disturbs its momentum. This momentum disturbance creates a greater uncertainty in the position reading and hence couples the noise from the unmeasured quadrature to the one being inspected. This problem is called the back action noise and QND proto-

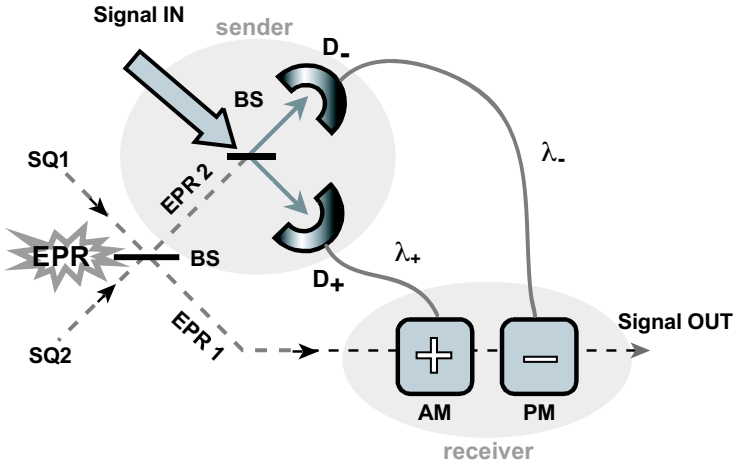

Figure 2.5: Basic experimental teleportation setup. SQ1,SQ2: two squeezed input beams; $D_{\pm}$: amplitude/ phase homodyne detectors; +/- : amplitude/ phase modulators; $\lambda_{\pm}$: amplitude/ phase modulator gains; BS: beam splitter.

cols attempt to circumvented it. The aim of QND is then to simultaneously observe and preserve the input signal [6].

A particular example of an all destructive QND circuit, used for a specific task of detecting a single light quadrature will be introduced in chapter 5. Other examples of using QND in quadrature detection can be found in references [15, 23, 39, 40].

2.6 Fidelity

Fidelity is a way to measure the success of a quantum state reconstruction of any quantum protocol. It does this by considering the overlap integral of the initial and final wave functions, $F = | < \hat{\psi}_{in} | \hat{\psi}_{out} > |^2$.

Since the statistics of a light beam are contained in the variance measurements for the special subset of states called Gaussian states, (section 2.2), simply the overlap of two Gaussian distributions in quadrature phase space can be made.

$$F = 2e^{-(k^+ + k^-)} \sqrt{\frac{V_{in}^+ V_{in}^-}{(V_{out}^+ + V_{in}^+)(V_{out}^- + V_{in}^-)}} \tag{2.2}$$

Here $k^{\pm} = \alpha_{in}^{\pm\,2}(1-|\lambda_{\pm}|)^2/(V_{out}^{\pm} + V_{in}^{\pm})$, while $\lambda_{\pm}$ is the modulation gain [54]. The square root part of the equation 2.2 deals with the overlap of the variance "balls" of input and output (see figure 2.2). The exponential part of the equation compares the amplitudes or the "stick" lengths of the two states.

Fidelity is input state dependent, as seen in the above equation, so noise inputs $V_{in}^{\pm} = 1$ are agreed upon when calculating F, for easy cross comparison of various results. At unity gain, the output is the same size as the input, and fidelity is optimum. If this is not the case the exponential term in equation 2.2 reduces fidelity considerably, even at small

deviations from unity gain condition. These assumptions, which are going to be made throughout this thesis, make the overlap equation simplify to:

$$F = \frac{2}{\sqrt{(V_{out}^{+} + 1)\ (V_{out}^{-} + 1)}} \tag{2.3}$$

This simplified version of fidelity integral is used in the remainder of my work. The coherent or Gaussian states considered in the above fidelity evaluation, are convenient due to their symmetry and experimental relevance.

The case of $F = 0$ implies the input and output are orthogonal and bare no resemblance to each other, while F =1 marks perfect reconstruction of the input. The classical limit to fidelity, without the presence of entanglement, is $0 \leq F \leq \frac{1}{2}$. This is because the output variance $V_{out}^{\pm}$, has to increase from the input unity value to at least three, as a consequence of adding two units of vacuum noise at the measuring and reconstructing stations. Only if quantum resources such as EPR are present, can these vacuum inputs be circumvented and fidelity in a quantum experiment will yield: $\frac{1}{2} < F \leq 1$.

2.7 The TV approach

Another useful way of evaluating teleportation is by considering information transfer, on a TV diagram [47]. Here two parameters are evaluated.

The first is the transfer coefficient which is simply the signal to noise ratio of the output and input beams for each quadrature :

$$T^{\pm} = \frac{SNR_{out}^{\pm}}{SNR_{in}^{\pm}} \tag{2.4}$$

This number measures the extent of signal or information transfer. Classically at unity gain, it is always below $\frac{1}{3}$ for each quadrature, (total of $T_{classical} = \frac{2}{3}$), again because of the double noise penalty which adds a unit of uncorrelated vacuum when measuring and when reconstructing the state. However for a perfect teleportation the transfer coefficient has undegraded SNR values for both quadratures, as the noise problem is circumvented, hence giving the total of T_{max} =2.

The second parameter is the conditional variance, which is a measure of the correlation between the input and the output [1] , and is defined as:

$$V_{cv}^{\pm} = V_{out}^{\pm} - \frac{< |\delta\hat{X}_{in}^{\pm}\delta\hat{X}_{out}^{\pm}|^2 >}{V_{in}^{\pm}} \tag{2.5}$$

The conditional variance is a measure of how accurately the input signal can be reproduced on the output. Classical limit at unity gain is the already discussed double vacuum noise penalty (for measurement and reconstruction), hence $V_{cv}^{classic} = 2$, while the ideal teleportation replicates the input exactly, giving $V_{cv}^{quantum} = 0$.

These two parameters can be subsequently plotted on a TV diagram as a function of the modulator gain, where $\lambda_{+} = -\lambda_{-}$ is assumed. Examples of such plots will be shown

[1] However experimentally such a correlation is impossible to measure, as the input is destroyed before the output is created, hence the two don't coexist at the same time. In order to evaluate the variance experimentally, it is possible to redefine equation 2.5 in terms of the transfer coefficient, which is an easily measurable quantity. Then: $V_{cv}^{\pm} = N_{out}^{\pm}\ (1 - T^{\pm})$. N is the output of the system with only noise input. [47].

in chapter 3. Once evaluated, both equation, 2.4, and 2.5 become independent of the input signal variances and do not critically rely on unity gain for useful results, a major advantage of the TV formulation over fidelity in an experimental situation.

2.8 Conclusion

This chapter summarises the quantum formalism necessary in understanding the later chapters of the thesis. An overview of the linearisation approach was given, followed by examples of quantum optical systems, analysed in this fashion. Finally, the fundamental ideas of protocol evaluation were given, all of which will be revisited in later chapters.

Chapter 3

Quantum Stokes operators of polarised light

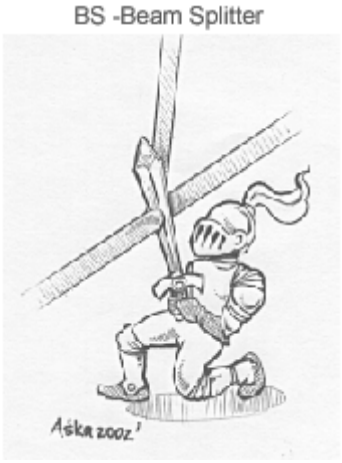

3.1 Overview of this chapter

In this chapter further definitions and discussion need to be made before a full investigation of various polarisation teleportation schemes in the later chapters.

I will outline the general transition from quadrature amplitude to polarisation teleportation and introduce some major difficulties with the latter description.

The linearised variances of the quantum Stokes parameters for polarisation modulation are then defined in the small signal limit, and two different evaluations of teleportation protocols are discussed, namely TV and fidelity.

3.2 Stokes formalism

When the light beam being teleported has an unknown polarisation state, it is no longer sufficient to describe it quantum mechanically using the two quadrature picture.

By drawing an analogy with classical Stokes parameters, [46] a new set of non commuting, Stokes polarisation operators can be defined, providing a convenient description of the polarisation properties of light. Like in the classical case, an arbitrary polarisation state is decomposed into three bases: vertical (horizontal), +(-)45 deg and LH (RH) circular, [42]. This vectorial representation can be readily visualised on a Poincaré sphere shown in figure 3.1(a). Classically, the $\hat{S}_0$ vector length equals the coherent amplitude of the light field, while its orientation describes the polarisation state. The $\hat{S}_1 - \hat{S}_2$ plane shows the ratio of horizontally to vertically polarised photons. The azimuthal deviation from this plane towards the $\hat{S}_3$ axis indicates the phase relationship between these two modes.

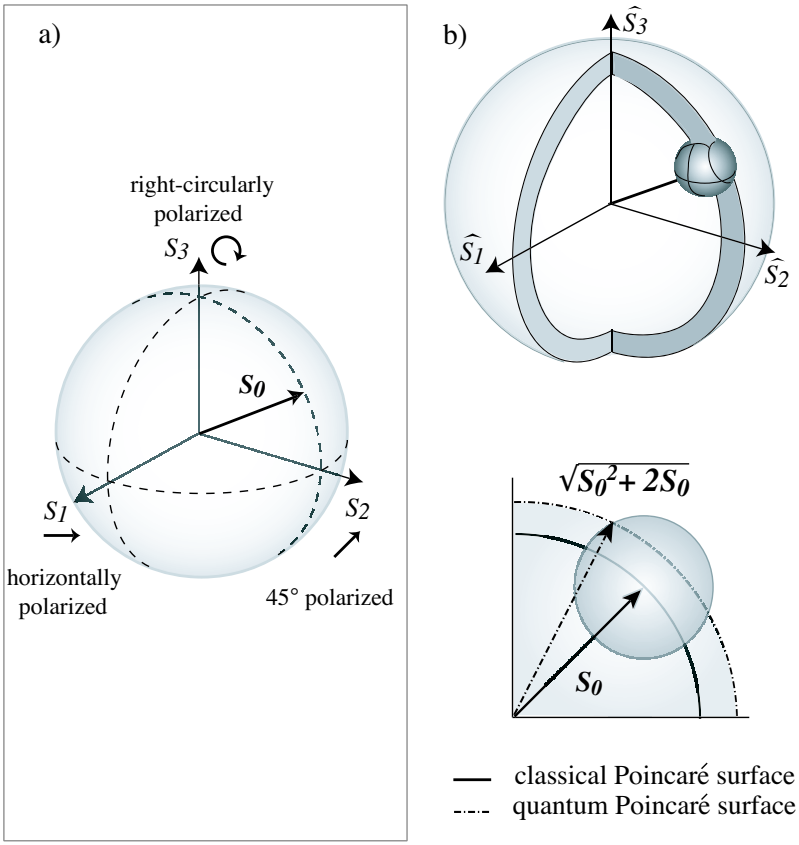

Figure 3.1: The comparison of (a) classical and (b) quantum Poincaré spheres. The explicit meaning of the "stick" is illustrated, in terms of the photon number S_0 for the classical case, and a larger value of $\sqrt{S_0^2 + 2S_0}$, due to the quantum uncertainty in the second case [34]. The presence of the uncertainty relations (eq. 3.4) noise "ball" absent in the classical picture and also indicated.

The quantum expressions for the four Stokes parameters, in terms of the field and photon number operators [19, 42], become:

$$\begin{aligned}
\hat{S}_0 &= \hat{a}_H^\dagger \hat{a}_H + \hat{a}_V^\dagger \hat{a}_V = \hat{n}_H + \hat{n}_V \\
\hat{S}_1 &= \hat{a}_H^\dagger \hat{a}_H - \hat{a}_V^\dagger \hat{a}_V = \hat{n}_H - \hat{n}_V \\
\hat{S}_2 &= \hat{a}_H^\dagger \hat{a}_V + \hat{a}_V^\dagger \hat{a}_H = \hat{n}_{+45} - \hat{n}_{-45} \\
\hat{S}_3 &= i\hat{a}_V^\dagger \hat{a}_H - i\hat{a}_H^\dagger \hat{a}_V = \hat{n}_{RC} - \hat{n}_{LC}
\end{aligned} \tag{3.1}$$

The $\hat{a}_H$ and $\hat{a}_V$ are creation (and annihilation) field operators for the horizontal and vertical polarised states, respectively.

It is experimentally convenient to rewrite the last two Stokes parameters, by explicitly including the phase angle, θ, between the two orthogonal horizontal and vertical modes. This operation is equivalent to making $\hat{a}_{H/V}$ real but keeping one mode complex through

the relative phase term.

$$\hat{S}_2 \ = \hat{a}_H^\dagger \hat{a}_V e^{i\theta} \ + \hat{a}_V^\dagger \hat{a}_H e^{-i\theta} \qquad \hat{S}_3 \ = i\hat{a}_V^\dagger \hat{a}_H e^{-i\theta} - i\hat{a}_H^\dagger \hat{a}_V e^{i\theta} \tag{3.2}$$

The equations above reduce to 3.1 if $\theta = 0$ is chosen.

In the quantum description the parameter $\hat{S}_0$ is proportional to the classical intensity of the quantum light beam, or the number of horizontal and vertical mode photons present, while the other three operators obey coupled set of commutation relations of the Pauli matrices:

$$[\hat{S}_1, \hat{S}_2] \ = 2i \ \hat{S}_3, \qquad [\hat{S}_2, \hat{S}_3] \ = 2i \ \hat{S}_1, \qquad [\hat{S}_3, \hat{S}_1] \ = 2i \ \hat{S}_2 \tag{3.3}$$

This suggests that simultaneous measurements of physical quantities described by these Stokes operators are impossible in general and their means and variances are restricted by the uncertainty relations reminiscent of those for a minimum uncertainty quadrature state.

$$V_{S2}V_{S3} \ \geq |\langle \hat{S}_1 \rangle|^2, \qquad V_{S3}V_{S1} \ \geq |\langle \hat{S}_2 \rangle|^2, \qquad V_{S1}V_{S2} \ \geq |\langle \hat{S}_3 \rangle|^2 \tag{3.4}$$

Here, $V_{Si} = \langle (S_i)^2 \rangle$ is the variance of each Stokes operator defined in the usual way.

Figure 3.1(b) shows the graphical representation of the quantum Stokes vector, and the meaning of each parameter enabling comparison to its classical counterpart. The Stokes vector length of $\sqrt{S_0^2 \ + 2S_0}$ now exceeds the classical amplitude and the Poincaré sphere has a finite thickness or "skin", due to quantum uncertainty. The coupled uncertainty relations of the Stokes variances are exhibited further in the appearance of a three dimensional noise "ball", superimposed on the Poincaré surface.

3.3 Linearisation of Stokes parameters

The linearisation of the Stokes operators is now carried out, in the fashion demonstrated in section 2.2. When the field operators $\hat{a}$, $(\hat{a}^\dagger)$ are expanded as a large classical amplitude and a quantum fluctuation, the expressions of equations 3.1-3.2 become

$$\delta\hat{S}_1 \ = \ \alpha_H \ \delta X^+{}_H \ - \ \alpha_V \delta X^+{}_V \tag{3.5}$$

$$\delta\hat{S}_2 \ = \ \alpha_H \ (\delta X^-{}_V \sin\theta + \delta X^+{}_V \ \cos\theta \ ) + \alpha_V \ (\delta X^+{}_H \ \cos\theta - \delta X^-{}_H \ \sin\theta) \tag{3.6}$$

$$\delta\hat{S}_3 \ = \ \alpha_H \ (\delta X^+{}_V \ \sin\theta - \delta X^-{}_V \ \cos\theta \ ) + \alpha_V \ (\delta X^-{}_H \ \cos\theta + \delta X^+{}_H \ \sin\theta) \tag{3.7}$$

To obtain linearisation of these equations, all terms higher than first order fluctuation are ignored.

These linearised parameters now describe the polarisation state of the "carrier", or the bright laser beam, without the presence of any modulation. The angle θ and the coherent amplitudes α_H, α_V, indicate the orientation of the light field's Stoke vector on the Poincaré sphere.

3.4 Comparison of Stokes operators with quadrature amplitudes

If the carrier light beam is phase and amplitude modulated, sidebands on either side of the input carrier frequency (ω_{DC}) appear[1]. It is the polarisation state of these that is of practical interest, since this is where the information content resides in the laser beam.

In the quadrature amplitudes picture, when the carrier is modulated, the fluctuation part of the quadrature operators, $\delta\hat{X}^{\pm}$, can be measured directly, using homodyne detection, (section 2.5.2). In phase space of $\hat{X^+}$ and $\hat{X^-}$, the phase and amplitude modulation of light at a specified frequency can be drawn as on figure 2.2. The size of the modulation sidebands, or the number of photons taking part in the modulation, is equivalent to the sum of the variances of the two axes. The photon number can be written as :

$$\delta a^{\dagger}\delta a = \tfrac{1}{4}((\delta X^+)^2 + (\delta X^-)^2 - 2)$$

Once the average is taken, the expression becomes

$$\langle\ \delta\hat{n}^X_{RF}\ \rangle = \ \tfrac{1}{4}(\ V^+ + V^- - 2)$$

This implies that it is only necessary to use homodyne detection to deduce the modulation extent on the two quadratures of a light beam, and to ignore the DC carrier amplitude. The "stick" on figure 2.2 contains $\delta\hat{n}^X_{RF}$ information only.

However the Stokes operators themselves are already photon number operators, and hence their variance $\langle(\hat{S}_i)^2\rangle$, without linearisation, will contain fourth order creation and annihilation operator terms. In this case, to quantify the polarisation modulation photon number, $\delta\hat{n}^S_{RF}$ requires the ability to perform photon counting on bright light beams. This is a task, which at the present moment is very difficult to carry out efficiently in a laboratory.

If a method similar to that of the quadrature approach is taken in analysing the polarisation of the modulation sidebands, by linearising operators and finding the variances, several problems arise.

The cyclic and dynamic commutation relations are the first major difference in the Stokes, quantum description of light from the quadrature picture, (section 2.3). There is also an increase in number of parameters. The full phase space for the Stokes operators can not consist of simply a linear combination of the quadratures, as in equations 3.5-3.7. The length of the polarisation, photon number "stick" in quadrature phase space becomes $\sqrt{2S_0 + S_0^2}$, which is more than the total photon number, S_0, due to the uncertainty "skin" of the Stokes sphere, as shown on figure 3.1(b). Both, the modulation and vacuum noise form a three dimensional ball which is superimposed on top of this uncertainty.

The problem of not being able to define a natural phase space for the Stokes operators is connected to the lack of a complete Stokes state representation. The Gaussian, coherent states can be fully defined in terms of quadratures as

$$|\alpha\ \rangle\ \equiv\ \left|\frac{1}{\sqrt{2}}\langle X^+\rangle\ + \frac{i}{\sqrt{2}}\langle X^-\rangle\right\rangle.$$

The polarisation state can be represented by a "super state", which is a product of two coherent states, each belonging to one of the horizontal or vertical modes. This can be

[1] For further discussion of the sideband picture refer to PhD thesis [6] or [23].

again expressed in terms of the quadratures of the two modes as

$$|\alpha_H\rangle|\alpha_V\rangle \equiv \left|\frac{1}{\sqrt{2}}\langle X_H^+\rangle + \frac{i}{\sqrt{2}}\langle X_H^-\rangle\right\rangle \left|\frac{1}{\sqrt{2}}\langle X_V^+\rangle + \frac{i}{\sqrt{2}}\langle X_V^-\rangle\right\rangle.$$

However, it is not possible to write the polarisation "super state" in terms of the Stokes parameters. In the quadrature example above, a product of commuting, horizontal and vertical operators exists. On the other hand, the Stokes parameter representation poses a problem, as a product of noncommuting operators is required. This suggests that values in the two kets mutually influence each other. Alternative way of explaining this limitation is that the "super state" descriptions in Stokes parameters are incomplete.

$$|\alpha_H\rangle|\alpha_V\rangle \equiv \left|\frac{1}{\sqrt{2}}\langle \hat{S}_1\rangle + \frac{i}{\sqrt{2}}\langle \hat{S}_2\rangle\right\rangle \left|\frac{1}{\sqrt{2}}\langle \hat{S}_3\rangle + \frac{i}{\sqrt{2}}\langle ??\rangle\right\rangle$$

Hence the $\hat{S}_1$, $\hat{S}_2$ and $\hat{S}_3$ are not able to fully characterise the Gaussian state without some additional measurement. The problem manifests itself further in the observation that polarisation vacuum squeezing doesn't preserve the volume of the "noise ball" [55], as in the case of the preserved area of quadrature squeezing. This also indicates that the quadratures are not a natural way to describe the polarisation operators.

The polarisation state of the RF sidebands can't be fully described in terms of the formalism introduced so far. However, despite these problems, certain special cases of polarisation modulation can be examined by looking at the Stokes parameters in quadrature space. In the next two sections I am going to use two methods to study the modulated polarised light. First I will concentrate on describing the light field by the Stokes measurements, in particular in context of teleportation. This means that only the accessible information carried by the quantum nature of the laser beam will be examined, not the complete quantum state of the modulation. However this method is still very relevant experimentally, where sending and extracting information becomes the main objective of the teleportation protocol. The evaluation of the protocol is then made using the TV method, already introduced in section 2.7. Secondly, the teleportation of the input state will be assessed, by using the full quantum mechanical description, in terms of fidelity.

3.5 TV assessment

A first step to including polarisation modulation is expanding the definition of the field operator to include classical modulation , (mod), explicitly: $\hat{a}(t) = \alpha_{DC} + \delta a(t)_{mod} + \delta\hat{a}(t)_{vac}$. Only the second fluctuation is a quantum operator, (vac), with the usual commutation relations, while the first is purely classical, hence $[\delta a(t)_{mod},\ \delta a(t)^\dagger_{mod}] = 0$. The $\delta a(t)_{mod}$ is equivalent to $\alpha(\omega)_{RF}$ because in the time domain the classical modulation is one of the time fluctuations of the carrier DC while in the frequency domain it's a sideband at ω_{RF}, as in figure 2.1. Then this $\hat{a}(t)$ expansion is substituted into Stokes equations 3.1-3.2 and the Fourier transformation of the operators is taken. The increased complexity of the quantum description of polarised light can be seen in the expanded set of Stokes operators from equations 3.5-3.7. However now, each $\delta X^\pm = \delta X^\pm_{mod} + \delta X^\pm_{vac}$, so there are two independent modes of fluctuations, the classical signal and the quantum noise. This approach is sidestepping the problem of higher order operator products discussed in the previous section by introducing a bright, DC carrier, to allow linearisation to take place. All of the small parts of the quantum system are now ignored and only the oscillations in the

direction of the bright laser beam remain. The variances, $V(\delta\hat{S}_i)$, of the Stokes operators are defined as $\langle\delta\hat{S}_i^2\rangle$, and are calculated due to linearisation in section 3.3, to take form of

$$V_{S1} = \alpha_H{}^2\,(V_H{}^+ + 1) \;+\; \alpha_V{}^2\,(V_V{}^+ + 1) \;-\; 2\alpha_H\alpha_V\,\langle\delta X^+{}_V\delta X^+{}_H\rangle \tag{3.8}$$

$$\begin{aligned} V_{S2} = {} & \alpha_H{}^2(\cos\theta)^2\,(V_V{}^+ + 1) \;+\; \alpha_V{}^2(\cos\theta)^2\,(V_H{}^+ + 1) \;+ \\ & \alpha_H{}^2\,(\sin\theta)^2\;\,(V_V{}^- + 1) \;+\; \alpha_V{}^2(\sin\theta)^2\,(V_H{}^- + 1) \;+ \\ & 2\alpha_H\alpha_V\sin\theta\;\cos\theta\,\langle\delta X^-{}_V\delta X^+{}_H\rangle \;-\; 2\alpha_H\alpha_V\sin\theta\;\cos\theta\,\langle\delta X^+{}_V\delta X^-{}_H\rangle \;+ \\ & 2\alpha_H\alpha_V\cos\theta\;\cos\theta\,\langle\delta X^+{}_V\delta X^+{}_H\rangle \;-\; 2\alpha_H\alpha_V\sin\theta\;\sin\theta\,\langle\delta X^-{}_V\delta X^-{}_H\rangle + \\ & 2\alpha_H{}^2\sin\theta\;\cos\theta\,\langle\delta X^+{}_V\delta X^-{}_V\rangle \;-\; 2\alpha_V{}^2\sin\theta\;\cos\theta\,\langle\delta X^+{}_H\delta X^-{}_H\rangle \end{aligned} \tag{3.9}$$

$$\begin{aligned} V_{S3} = {} & \alpha_H{}^2\,(\cos\theta)^2\;\,(V_V{}^- + 1) \;+\; \alpha_V{}^2(\cos\theta)^2\,(V_H{}^- + 1) \;+ \\ & \alpha_H{}^2\,(\sin\theta)^2\;\,(V_V{}^+ + 1) \;+\; \alpha_V{}^2(\sin\theta)^2\,(V_H{}^+ + 1) \;+ \\ & 2\alpha_H\alpha_V\sin\theta\cos\;\theta\,\langle\delta X^+{}_V\delta X^-{}_H\rangle \;-\; 2\alpha_H\alpha_V\sin\theta\cos\;\theta\,\langle\delta X^-{}_V\delta X^+{}_H\rangle \;- \\ & 2\alpha_H\alpha_V\cos\theta\cos\;\theta\,\langle\delta X^-{}_V\delta X^-{}_H\rangle \;+\; 2\alpha_H\alpha_V\sin\theta\sin\;\theta\,\langle\delta X^+{}_V\delta X^+{}_H\rangle \;- \\ & 2\alpha_H{}^2\sin\theta\cos\;\theta\,\langle\delta X^+{}_V\delta X^-{}_H\rangle \;+\; 2\alpha_V{}^2\sin\theta\cos\;\theta\,\langle\delta X^+{}_H\delta X^-{}_H\rangle \end{aligned} \tag{3.10}$$

The equations 3.8 to 3.10 depend on two kinds of variances, since the fluctuation operator $\delta\hat{X}^{\pm}$ was decoupled into the classical modulation (the "RF stick") and quantum operator (the "ball"). $V^{\pm}_{H/V}$ is the signal or the classical information residing in the modulation sideband, while the variance of the vacuum operator, which is assumed to be at shot noise level, is the origin of the unity term in the equations above. The classical and quantum $\delta\hat{X}^{\pm}$ parts are independent and uncorrelated, so no cross terms exist. However the classical modulation allows for correlations of various $\delta\hat{X}^{\pm}_{mod}$ quadratures with one another, and this freedom is included in the above variance expressions.

The key result of the linearisation assumption is that the Stokes variances depend on the polarisation orientation of the DC carrier beam, through scaling by the amplitude of each mode, α_H and α_V, and the phase angle between these, θ. The problem of α_{DC} scaling in quadrature modulation doesn't occur, as all terms are multiplied by a single, bright amplitude so the DC has no overall effect on the result. However in the above case, the two amplitudes will add an additional degree of freedom in redistributing the information between the quadratures, and their effect can't be simply removed by uniform re-scaling of the polarisation signal. The effects of this DC dependence will be demonstrated in the later chapters.

3.6 Fidelity assessment

With the recollection of section 2.6, fidelity measures the overlap of the two Gaussian distributions which characterise the input and (teleported) output states of the field. This actually yields a quasi-probability distribution of a Wigner function; however in the special case of Gaussian states, it can be interpreted as a real probability distribution of the two observables. Refer to figure 3.2.

Using this analogy, the fidelity of a teleported polarisation state should take form of a three dimensional overlap integral, where a Gaussian distribution, (described by the Stokes variances) is assumed for each Stokes parameter. However this is erroneous, because of the assumption that a Gaussian state can be fully described by Stokes operators, in parallel to characterisation by quadratures. This was already argued in section 3.4 to be an invalid statement.

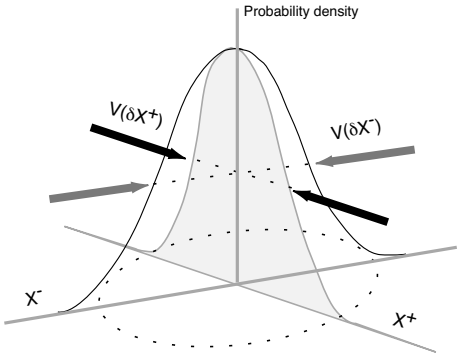

Figure 3.2: The meaning of the two dimensional Wigner function overlap integral, or fidelity, in quadrature space. Each conjugate observable is seen to be characterised by a Gaussian distribution with a given variance, and this is sufficient to describe the laser beam fully.

Hence, the open question of Stokes state description for polarised light results in inability to define fidelity in terms of Stokes variances. The three dimensional Gaussian overlap function simply doesn't exist.

$$\textit{Fidelity} \neq \int\int\int e^{\frac{x^2}{V_{S1}} + \frac{y^2}{V_{S2}} + \frac{z^2}{V_{S3}}}\, dx\, dy\, dz$$

Where $V_{Si} = V_{Si}^{mod} + V_{Si}^{vac}$, so the vacuum noise ("noise ball") and classical modulation ("stick length") are both included.

Instead, if fidelity is to be evaluated, the linearised Stokes parameter states must be expressed in full, quadrature space, including all four operators $\delta\hat{X}_H^+, \delta\hat{X}_H^-, \delta\hat{X}_V^+$ and $\delta\hat{X}_V^-$. Fidelity is then a four dimensional overlap integral, and each integration variable has its Gaussian distribution characterised by the variances $V_H^{\pm}$ and $V_V^{\pm}$.

$$\textit{Fidelity} = \int\int\int\int e^{\frac{x^2}{V_H^+} + \frac{y^2}{V_H^-} + \frac{w^2}{V_V^+} + \frac{z^2}{V_V^-}}\, dx\, dy\, dw\, dz \tag{3.11}$$

This description of the polarised quantum state is valid since the modulation is assumed to be small, and S_0 ($= \alpha_H^2 + \alpha_V^2$) is large. This makes the $\delta\hat{n}_{RF}^S$ "stick", approach the total photon number, so $S_0 \approx \sqrt{2S_0 + S_0^2}$, as $S_0 \to \infty$. The analogy with the quadrature phase space approach can be made.

Finally it is stressed, that the special nature of the input state allows this operation. I am still unable to provide a general Stokes quantum state and fidelity expressions.

3.7 Relevance

A question of relevance of the above, approach can be raised by the reader, in the light of the explanation that since there is no Stokes phase space, how is the above evaluation a correct quantum mechanical description of reality?

The answer lies in the perspective which is taken by the experiment teleporting a bright, polarised light beam. Most often the object of such a protocol is to send as much information as possible, encoded on the three degrees of freedom of a bright, polarised

carrier. The presented analysis is then perfectly valid, using linearised Stoke operators and variances, which are decomposed into quadratures and then measured. The other fluctuations that are present on the input but do not scale with the carrier are ignored, as the relative information carried by them is small hence insignificant.

This returns us to the point made in section 3.5 that, instead of scaling all terms equally as in the quadrature case, here the carrier's amplitudes in α_H and α_V modes will select special projections of signal fluctuations along the DC direction, while ignoring others. When the condition of a bright laser beam is met, this allows, through the linearisation approach, to simplify the system studied. The polarisation "super state" $|\alpha_H\rangle|\alpha_V\rangle$, has then a valid representation in the product of horizontal and vertical Gaussian-quadrature states.

3.8 Conclusion

In this chapter I have attempted to outline the procedures which will be used in the remainder of the thesis to evaluate the teleportation of the signal in polarisation modulation. The open question still remaining in connection to the full description of light in Stokes parameter phase space was discussed, and the validity of the linearised approach was justified. I then proceeded to introduce the linearised variances for the Stokes operators, which could be used in the bright carrier limit, as a useful description of information carrying polarisation. Finally the TV and fidelity methods in the context of Stokes parameters were described, to be used in later chapters.

Chapter 4

Polarisation teleportation - four squeezers

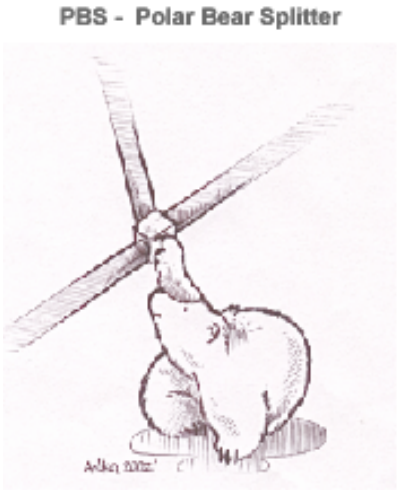

4.1 Overview of this chapter

In this chapter I will investigate the Stokes variances introduced in chapter 3, in light of information transfer, using the slightly modified TV diagrams. The most trivial, and also the most resource expensive method of implementing the polarisation teleportation protocol is then described, using two independent teleporters, hence two EPR pairs and four squeezed, bright beams.

4.2 Teleportation of the Stokes information

To experimentally teleport all the information contained in equations 3.8-3.10, the polarisation information can be broken down to the familiar quadrature amplitude information. Here a set of four bright, squeezed beams (SQ1, SQ2, SQ3, SQ4) entangled to make two sets of EPR pairs, and hence two standard, quadrature teleporters are needed. Each teleporter transfers information about one of the mutually independent modes of quantum fluctuations: horizontal and vertical. The experimental setup is shown in figure 4.1. A polarising beam splitter, PBS, first separates the signal into the horizontal and vertical components, after which each teleportation protocol is almost identical to the one discussed in section 2.5.3. The only major difference is the detection technique. Instead of using the standard homodyne detectors, each requiring a bright LO, if the EPR beam is arranged to have a carrier with equal power to that of the signal carrier, it is possible to make direct measurements which are equivalent to those that are made with vacuum EPR

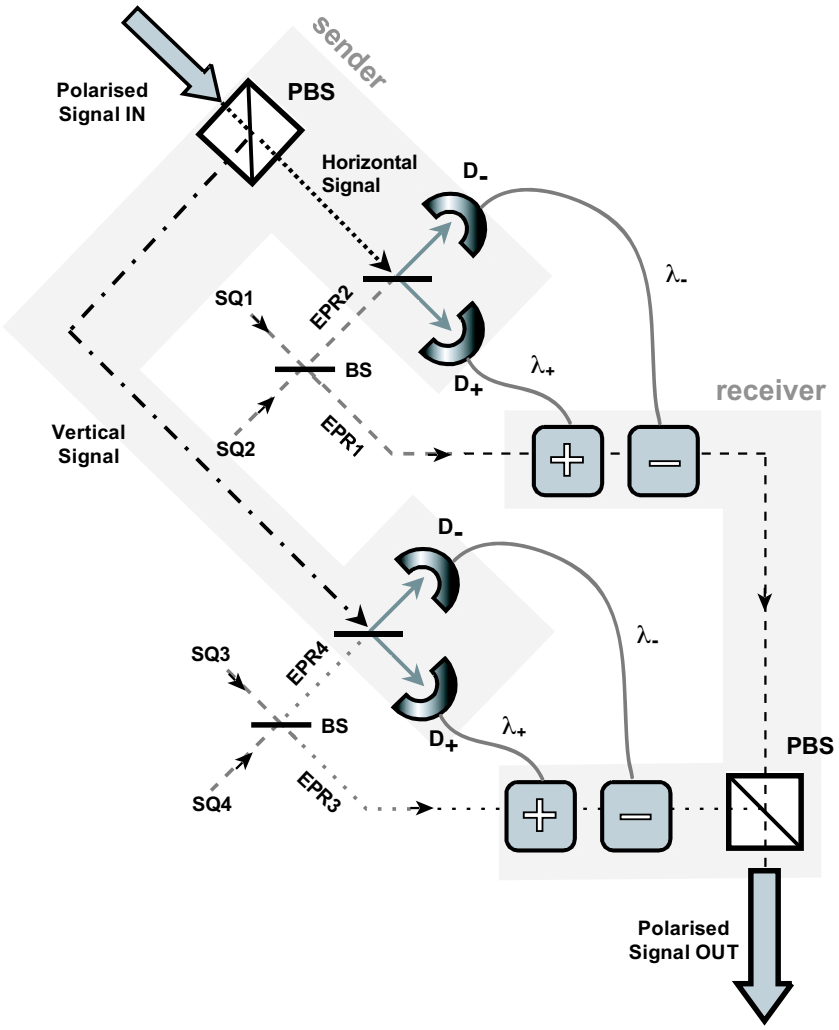

Figure 4.1: Polarisation teleportation setup which consists of a set of quadrature teleporters, with an advantage of LO free homodyne detection, (see text). SQ1-SQ4: four squeezed input beams; $D_{\pm}$: amplitude/ phase homodyne detectors; +/- : amplitude/ phase modulators; $\lambda_{\pm}$: amplitude/ phase modulator gains; PBS: polarising beam splitter.

beams and a bright LO [14]. This useful experimental modification dispenses with the use of costly LO beams in the laboratory, and offers a great advantage to the detection of polarised states. On the output, the two teleported modes of light are recombined by a second PBS into a single polarisation signal.

4.3 TV diagrams for polarisation

The TV description of teleportation introduced in section 2.7, must be now tailored to the polarisation setup described in the preceding section. A more thorough explanation of the parameters involved and examples of resulting TV diagrams will now be made.

Transfer coefficient

Transfer coefficients of the Stokes parameters, T_{S1}, T_{S2}, T_{S3}, can be evaluated by simply applying the variances of the Stokes equations 3.8-3.10 to the usual information transfer formula, (equation 2.4). The result is very complicated if all four beams have independent squeezing parameters, (shown in Appendix B.3(a)). However if the two teleporters are completely symmetric and the amplitude squeezed variance parameters $V^{+}_{SQ1,2,3,4}$ are defined as SQ1,2,3,4, the SQ1 = SQ2 = SQ3 = SQ4. In this case, the three transfer coefficients all equal to

$$T_{S\ 1,2,3} = \frac{2\lambda_+^2\ SQ}{1\ + SQ^2\ + \lambda_+^2\ (1+SQ)^2\ + 2\lambda_+\ (SQ^2-1)}, \tag{4.1}$$

where $\lambda_\pm$ is the gain from the teleportation transfer function equation 2.1, and SQ is the amplitude squeezed variance parameter of the four beams, ($V^{+}_{SQ} \leq 1$).

Conditional variance

When the correlations between the input and the output Stokes operators from equation 2.5 are found, the three conditional variances can be calculated. (Full expressions in Appendix B.3(b)). Once again, these become much simpler when the very realistic assumption of symmetric squeezing in the four beams is made[1]. All three variances then equal:

$$V_{cv}^{1,2,3}\ = \frac{1}{2\ SQ}\ - \frac{\lambda_+}{SQ}\ + \frac{\lambda_+^2}{2\ SQ}\ + \frac{SQ}{2}\ + \lambda_+\ SQ\ + \frac{\lambda_+^2\ SQ}{2} \tag{4.2}$$

The experimental assumption from section 2.7 that $V_{cv}^{1,2,3} = N_{out}^{1,2,3}\ (1 - T_{S1,2,3})$ still holds, as the variances of the quadratures in which the Stokes operators are expressed still obey Gaussian statistics.

TV diagrams

Three sets of the parameters: $V_{cv}^{1,2,3}$ and $T_{S1,2,3}$ are plotted on a TV diagram in figure 4.2. The results, (figure 4.2(a)), are identical for all Stokes parameters when symmetric squeezing is assumed on all four beams. The curves, plotted as a function of the modulator

[1] In a real experiment the mismatch of the two squeezers can be reduced down to only 0.3 dB (7 %), and over this range no significant changes to the TV description can occur.

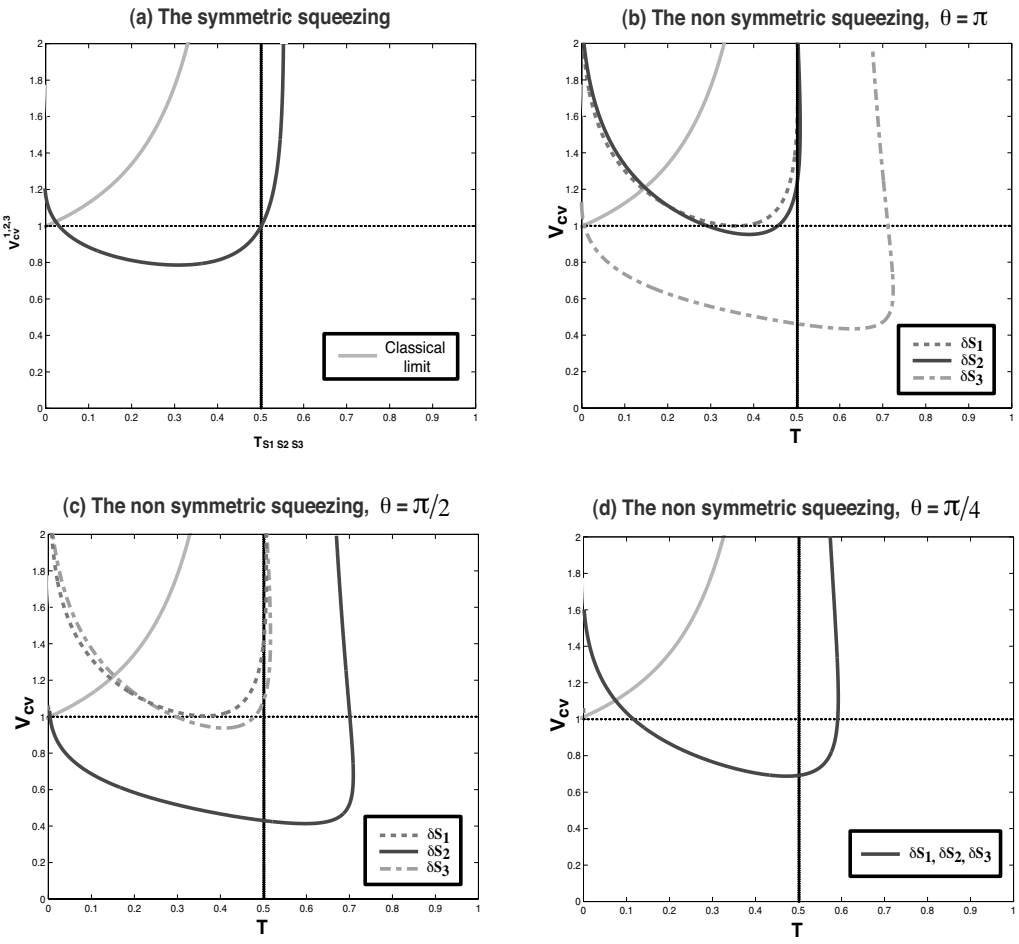

Figure 4.2: (a) The symmetric squeezing case - all three Stokes TV plots are identical and the same amount of the original polarisation information is teleported in all three Stokes parameters, hence all three polarisation components; SQ = 0.5. (b)-(d) The asymmetric squeezing case - In a non-ideal system the amount of information successfully teleported on each Stokes parameter will vary with the DC polarisation, as demonstrated for three different θ values. $\alpha_H = \frac{1}{\sqrt{7}}$, (arbitrary); SQ1 = .3, SQ2 = .6, SQ3 = .2, SQ4 =.5 The classical limit curve (pale solid line) is also indicated on all the diagrams.

gains, seem to reflect the original quadrature TV results for equal squeezing values, (SQ $\rightarrow$ $V_{SQ1,2}$).

On the other hand, when the squeezing parameters of the four entangled beams are changed independently, the teleported information becomes dependent on the polarisation of the bright carrier, carrying the input state. The main advantage of the TV formalism is that the teleportation evaluation is independent of the input signal form so any unknown state of a carrier beam gives the same result in particular experimental conditions. However this no longer holds when the squeezing is non-symmetric. In the polarisation case, the modulation can also be either represented by a "ball" of classical noise on the end of a coherent DC amplitude (time domain, figure 3.1(b)) or a RF modulation sideband (frequency domain). The DC "stick" scales these classical modulation sidebands in equations 3.8-3.10, and their relative orientation now determines the teleportation success rate.

The TV diagrams on figures 4.2(b)-(d) show the varying degrees of information and correlation preservation for each Stokes parameter, which is seen to vary as a function of the input polarisation angle θ, when the squeezing is asymmetric. The shapes of the $TV_{S1,2,3}$ curves are also determined to a small extent by the coherent DC amplitudes ratio $\alpha_V : \alpha_H$.

This dependence can be justified by imagining the polarisation modulation of a bright, DC carrier consisting of a large amplitude component along the horizontal direction $\hat{S}_1$ on the Poincaré sphere, (α_H is large). In the linearisation limit of the teleportation transfer function, only the quadrature components of $\delta\hat{S}_1$, $\delta\hat{S}_2$, $\delta\hat{S}_3$ parallel to this DC orientation are teleported, as the other quantum fluctuations are relatively small. The relevant quadrature amplitudes of the Stokes variances, (those that couple to α_H in equations 3.8-3.10), are then the only ones to be replicated. This can be also visualised as teleporting only the sideband projections onto the large DC reference (similar to the α_{proj} in figure 5.2).

The efficiency of each of the teleporters in transferring the horizontal, vertical, phase and amplitude quadratures depends on the extent of squeezing in each of the four beams. This non-symmetric teleportation efficacy means the TV evaluation results for each Stokes parameter will vary. This emphasises the dependence of TV formalism on the experimental setup.

For an arbitrary choice of input polarisation, the three $TV_{S1,2,3}$ plots will look completely different, as figures 4.2(b)-(d) demonstrate. In this example of a non-symmetric squeezing system the amount of information successfully teleported on each Stokes parameter is seen to vary with the DC polarisation. A demonstration of this for a particular squeezing combination and α_{DC} choice is shown. With $\theta = \pi$, the most successful TV evaluation occurs for the $\delta\hat{S}_3$ parameter (hence the circular polarised fluctuations component) and least impressive for $\delta\hat{S}_1$ and $\delta\hat{S}_2$. By choosing an alternate DC polarisation at $\theta = \frac{\pi}{2}$, the efficacy of the diagonal fluctuations component $\delta\hat{S}_2$ increases, but is accompanied by a significant decrease in teleportation quality of $\delta\hat{S}_3$. Alternatively to θ, the DC input polarisation could also be varied via the α_{DC} parameter, however this doesn't have a big effect on the appearance of the TV diagrams.

These results suggest that in a non-symmetric teleporter, the extent of the polarisation modulation teleported dependence on the input carrier choice could be used to the experimenter's advantage. Consequently, if the input polarisation is known, different regimes of information transfer and correlations can be reached with various squeezing parameter combinations. However the most desirable behaviour, independent of the input state when carrier polarisation is unknown, occurs only when squeezing is symmetric.

The transfer coefficients and conditional variances shown in this chapter give a good indication of how the observables of interest are reproduced on the output, and how well suited a particular experimental system is for the task (within the linearisation limit). This will be stressed in the next chapter, when an obvious contradiction between information transfer and fidelity is encountered.

4.4 Limitations of the scheme

Although the polarisation fluctuations (or classical modulation sidebands) are teleported in this scheme, the input carrier's polarisation state (or DC "stick") is not, similar to the quadrature case where the intensity of the carrier is never a parameter of interest. However in the present setup the teleportation also requires the knowledge of the relative phase angle between the two modes θ, which specifies the carrier's polarisation state. Unless this piece of information on the input is known and set to be identical at the receiving station, the protocol outlined will not work. Furthermore, there may be a possibility of reducing the number of quantum resources, which will be addressed in the next chapter.

4.5 Conclusion

In the above sections I have introduced the most trivial and resource demanding polarisation teleportation scheme, relying on the fact that the fluctuations can be decomposed into two sets of horizontal and vertical quadratures. The linearised variances for the Stokes operators, from chapter 3 were then used to evaluate the teleportation of a polarisation modulation in a Stokes TV picture. Interesting results were also discussed, revealing dependence of the signal reconstruction on DC carrier's polarisation in the linearisation limit.

Chapter 5

Polarisation teleportation and QND

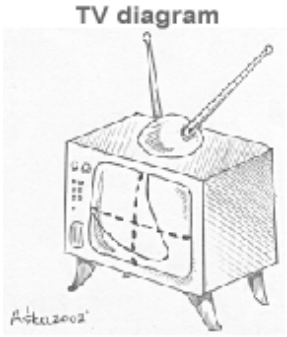

5.1 Overview of this chapter

In this chapter I will introduce a much simpler and less resource demanding experimental setup, still fully capable of teleporting polarisation encoded information. Here, I will use the fact that the average values of the Stokes parameters are classical entities which can be determined without back-action on the quantum fluctuations, to employ an all destructive QND, measurement technique.

Later I will analyse the new scheme along the same lines as chapter 4, evaluating the amount of information that can be sent in terms of the transfer coefficient and the conditional variance. Finally I will show that a modified version of the TV representation is more helpful in describing the effectiveness of the setup.

5.2 Simpler experimental scheme-teleporter and QND

It was shown previously that to experimentally reproduce all of the polarisation parameters a set of four bright, squeezed beams and two EPR pairs is needed. This implies double the complexity of the standard teleporter, and twice the entanglement resources. However when looking at the four Stokes parameters, it is clear that since $\hat{S}_0$ commutes with the rest of the Stokes parameters it can be measured classically and thus this operator, proportional to the classical intensity of the light beam, is redundant. This leaves only three parameters with quantum uncertainty relations, and indicates there could be a simpler method involved.

A closer inspection of the Stokes parameters defined in equations 3.5-3.7, reveals that once the orientation of the DC input polarisation is known, the number of quadratures involved in the description of the state can be reduced. In particular, if the polarisation of the carrier light beam is made almost vertical, (ie along the negative direction of the

$\hat{S}_1$ axis), all of the terms in equations 3.5-3.7 that scale with α_H, which is now effectively equal to zero, vanish. The expressions for the linearised Stokes operators then reduce to:

$$\delta\hat{S}_1^{QND} = -\alpha_V \delta {X^+}_V \quad (5.1)$$
$$\delta\hat{S}_2^{QND} = \alpha_V \ (\delta {X^+}_H \ \cos\theta - \delta {X^-}_H \ \sin\theta \ ) \quad (5.2)$$
$$\delta\hat{S}_3^{QND} = \alpha_V \ (\delta {X^-}_H \ \cos\theta + \delta {X^+}_H \ \sin\theta \ ) \quad (5.3)$$

The new teleportation scheme now becomes more transparent. The uncertainty relations from equation 3.4 are strongly affected by this carrier polarisation. Now both $\langle\hat{S}_2\rangle$ and $\langle\hat{S}_3\rangle$ are zero, so the only uncertainty remaining is that between $\hat{S}_2$ and $\hat{S}_3$. These two quantities must then be teleported using some quantum resource, like entanglement. The $\hat{S}_1$ parameter on the other hand can be simply detected and doesn't require a second entangled pair of bright beams for its reconstruction. In other words the equations 5.2, 5.3 are seen to completely decouple from 5.1. A standard, two quadrature teleportation is required for the horizontal teleportation of the two conjugate fluctuations in $\delta\hat{S}_2^{QND}$ and $\delta\hat{S}_3^{QND}$. However, now the vertical amplitude fluctuations of $\delta\hat{S}_1^{QND}$ can be reproduced by single quadrature measurement, which is achieved using quantum non demolition or QND, introduced in section 2.5.4. The problem of back-action noise during the QND detection is avoided as the average $\langle\hat{S}_1\rangle$ of the Stokes parameter is measured, and this quantity is classical.

The optical circuit for the simplified, QND-teleporter system is outlined on figure 5.1. The first polarising beam splitter, (PBS), extracts all of the vertical light from the signal beam, and hence reproduces the single quadrature fluctuations $\delta\hat{S}_1^{QND} \propto \delta\hat{X}_V^+$, onto the squeezed beam SQ3 . The standard teleportation protocol, using an EPR pair, transfers the information of $\delta\hat{S}_{2,3}^{QND}$ onto the output beam EPR1. Again the vertical and horizontal modes are recombined via a second PBS, and the total output signal is rotated with a variable wave plate, WP, to ensure the DC polarisation is still vertical. This last element of the new teleportation scheme must be transferred classically to allow the number of quantum resources to reduce.

The extent of squeezing on SQ3 beam enables an ideal reproduction of the single amplitude quadrature fluctuation $\delta\hat{X}_V^+$ in the QND scheme. (This is analogous to the way the squeezing of SQ1 and SQ2 beams guarantees good teleportation). The use of squeezed light in a QND scheme was first suggested by Bruckmeier *et al* [39] and implemented experimentally by Shapiro [45]. The first implementation of the all destructive QND setup considered here, was carried out by Buchler *et al* [3]. The complete polarisation teleportation system now uses only three squeezed beams and one entangled pair.

5.3 TV analysis

The linearised variances for the Stokes parameters from equations 3.8-3.10 now simplify to:

$$V_{S1}^{QND} = \alpha_V^2 \ V_V^+ \quad (5.4)$$
$$V_{S2}^{QND} = \alpha_V^2(\cos\theta)^2 \ V_H^+ + \alpha_V^2(\sin\theta)^2 \ V_H^- - 2\alpha_V^2 \sin\theta \ \cos\theta \ \langle\delta X_H^+ \delta X_H^-\rangle \quad (5.5)$$
$$V_{S3}^{QND} = \alpha_V^2(\cos\theta)^2 \ V_H^- + \alpha_V^2(\sin\theta)^2 \ V_H^+ + 2\alpha_V^2 \sin\theta\cos \ \theta \ \langle\delta X_H^+ \delta X_H^-\rangle \quad (5.6)$$

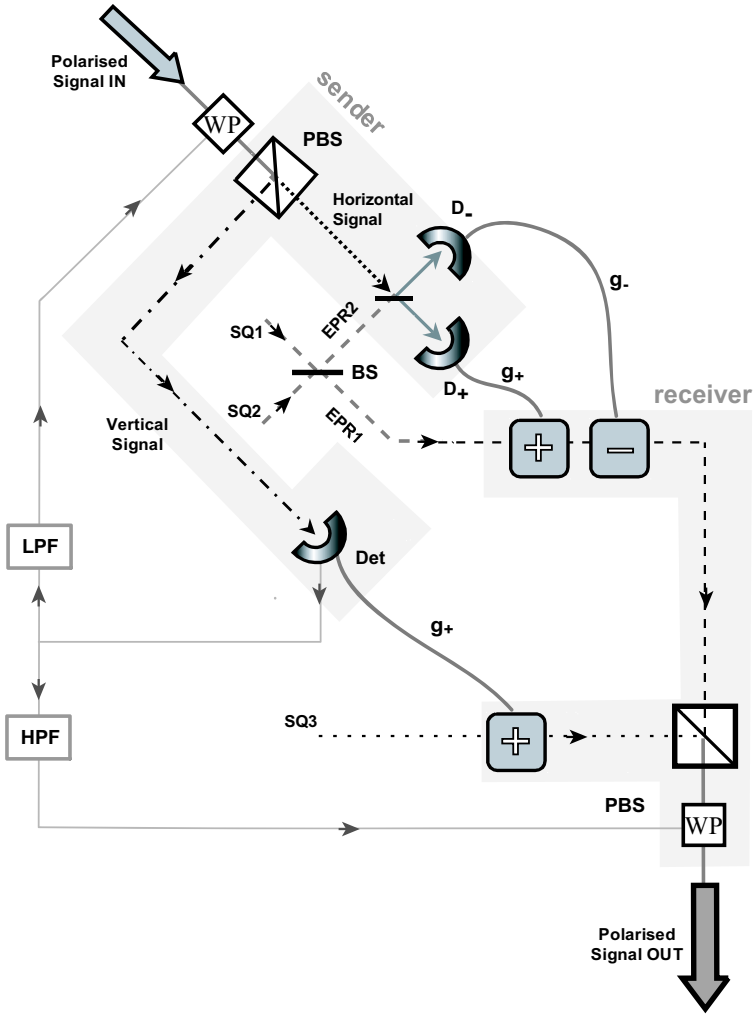

Figure 5.1: QND-teleporter experimental setup consisting of an all destructive QND and a teleportation (see fig. 4.1) circuits. $D_{\pm}$: amplitude/ phase homodyne detectors, **Det**: standard amplitude detector, **+/-** : amplitude/ phase modulators, $g_{\pm}$: amplitude/ phase modulator gains, PBS: polarising beam splitter, WP: waveplate; HPF: high pass filter in the feedforward loop; LPF: low pass filter in the feedback loop.

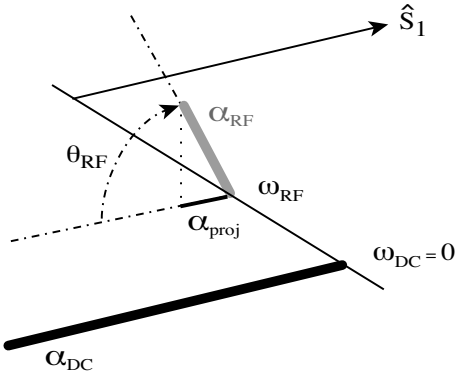

Figure 5.2: The physical meaning of the polarisation angle is shown. The choice of θ_{RF} changes the projection (α_{proj}) of the modulation sideband, measured relative to the always vertical (-$\hat{S}_1$) DC carrier.

Variances $V^{\pm}_{H/V}$ are the sum of signal and quantum fluctuation variances, $(V^{\pm}_{mod} + V^{\pm}_{vac})$. The phase angle θ gives the relative phase between the two DC modes: the very large vertical and the very small, (approximately zero) horizontal amplitude components. There is now only one type of classical input correlation $\langle \delta X^{+}_{H} \delta X^{-}_{H} \rangle$ which can be of interest.

The $\hat{S}_2$ and $\hat{S}_3$, TV evaluation

The transfer coefficient and conditional variance for $\hat{S}_2$ and $\hat{S}_3$ are now exactly equivalent to horizontal phase and amplitude fluctuation teleportation by a single teleporter, already considered in TV formalism section 2.7. The behaviour at symmetric squeezing gives two identical TV diagrams (plotting $T_{S2,S3}$ vs $V^{2,3}_{cv}$), which agree with the quadrature TV diagrams, ($T^{\pm}_{q}$ vs $V^{\pm}_{cv}$) for a given squeezing.

As with the TV analysis for the full double teleporter, a different behaviour is present for asymmetric squeezing in the QND-teleportation setup, illustrated on figures 5.3(a)-(b). The TV plots again depend on the relative phase θ of the two modes in the input polarisation state. (Full expressions for $T_{S2,S3}$ and $V^{2,3}_{cv}$ are given in Appendix B.4). In the QND-teleporter case this angle can be quite arbitrary, since there is no coherent amplitude in the horizontal direction ($\alpha_H \rightarrow 0$). The chosen, vertical polarisation of the DC carrier seems to require that $\theta = 0$ by looking at the Poincaré sphere orientation of any vertically polarised field. However once the $\alpha_H = 0$ condition is met, the absolute phase has no effect on the DC "stick" polarisation, as $\delta \hat{S}^{QND}_{1}$ (the vertical Stokes component) is now independent of θ and only proportional to α_V as seen in equation 5.1. However the relative phase does change the behaviour of the fluctuations or the sidebands, which is what the TV plots show. This allows a measurement of quadratures using the carrier as the LO, selecting the projection to be measured by manipulating the phase[1]. Subsequent changes of θ will rotate the modulation sidebands of the bright carrier in the Poincaré sphere, but wont really change their state of polarisation, as the θ parameter doesn't fully characterise the modulation polarisation as discussed in chapter 3. This can be visualised on figure 5.2.

The $T_{S2,S3}$ and $V^{2,3}_{cv}$ values are seen to always reach a maximum (or a minimum) at

[1]This is similar to the squeezed vacuum mode situation, where the statistics vary as a function of quadrature angle, although the angle itself has no absolute reference.

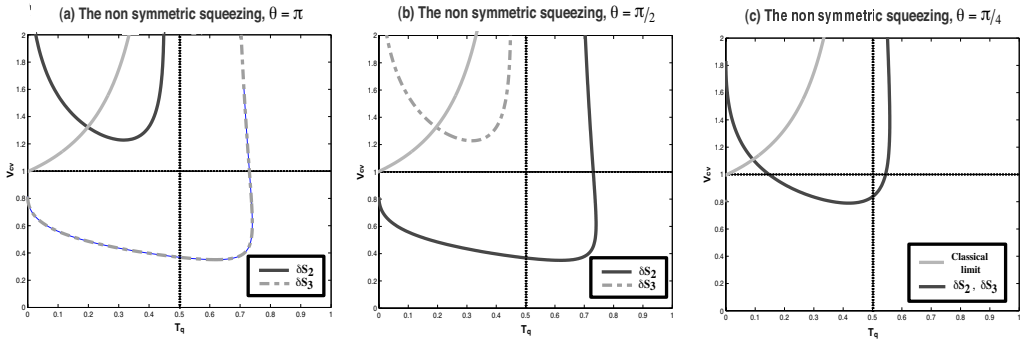

Figure 5.3: The TV_{S2} and TV_{S3} for the asymmetric squeezing case, drawn for three different θ values: (a) π; (b) $\frac{\pi}{2}$; (c) $\frac{\pi}{4}$. The classical limit (pale solid line) is again drawn as a reference. The phase delayed behaviour between the two Stokes parameters is seen (see text); SQ1 = .2, SQ2 = .7

$\theta = \pi$ (or $\frac{\pi}{2}$) for one of the two parameters, with the opposite being true for the remaining parameter. This behaviour is independent of the actual size of squeezing variances. Hence a phase delayed relationship can be observed, as the maximum curve of TV_{S3} diagram at θ_i, matches the maximum of the TV_{S2} diagram at $\theta_i + \frac{\pi}{2}$. Unlike the case of section 4.3, the two TV curves are of identical shape (at different θ values), because the $\alpha_H : \alpha_V$ ratio dependence which was the additional parameter freedom in chapter 4 is now removed.

An alternate evaluation of $\hat{S}_1$

Due to the fact that the physical system transferring the information about the $\delta\hat{X}_V^+$ quadrature is different to the teleporter, the resulting transfer function now depends on a different range of parameters than the one for $\hat{S}_2$ and $\hat{S}_3$. This means the TV analysis of this QND scheme must be kept separate to the teleportation scheme.

The conditional variance is found to be

$$V_{cv}^{S1} = \alpha_V^2 \left(1 + \eta_m \left(-1 - G^2 \left(\eta_d - 1\right)\right) + SQ3\right) \tag{5.7}$$

Here, η_m and η_d are the modulator and detector efficiencies respectively, G the modulator gain, and SQ3 the variance of the amplitude squeezed QND beam.

When the efficiencies of the system approach unity, this equation becomes gain independent and reduces to $V_{cv}^{S1} = \alpha_V^2$ SQ3. Hence the standard TV plot will fail to show any dynamics of these parameters as a function of gain, G.

The transfer coefficient is now found to be:

$$T_{S1} = \frac{G^2 \ \eta_d \ \eta_m}{1 + (G^2 - 1) \ \eta_m + SQ3} \tag{5.8}$$

which again reduces further at perfect efficiencies to $T_{S1} = \frac{G^2}{G^2+SQ3}$. Noting that both, T_{S1} and V_{cv}^{S1} depend on squeezing parameter of the QND beam, (SQ3), a new visualisation tool is proposed, which plots the two parameters as a function of G and SQ3. Figure 5.4 demonstrates the dynamics of the T_{S1} parameter as a function of both, gain and squeezing. The area above the plane shows the region of interests, where the information transfer surpasses the classical limit ($T_{S1} \geq \frac{1}{2}$).

The "equipotentials" of this surface plot are shown on figure 5.5. The SQ3 axis is

equal to the conditional variance axis, (α_V is normalised to 1), however now the transfer coefficient's "equipotential" lines are seen to asymptotically approach the G axis.

There is a physical basis behind this behaviour of the all destructive QND. It is possible to enhance the transfer of information of the system by increasing the combination of squeezing and gain, hence improving the SNR. On the other hand, the conditional variance can't be improved as there is only one beam in the setup, and all the correlations must reside in the extent of squeezing. This keeps the V_{cv}^{QND} parameter constant for a particular experimental system, and makes it impossible to characterise it on a meaningful TV diagram.

Nevertheless, an analogy with the quadrature TV in section 2.7 can be made by defining a region with $V_{cv}^{1} < 1$ and $T_{S1} > \frac{1}{2}$. This is unreachable by classical means of teleportation, and corresponds to the so called cloning limit (per quadrature) which will be discussed further in chapter 7.

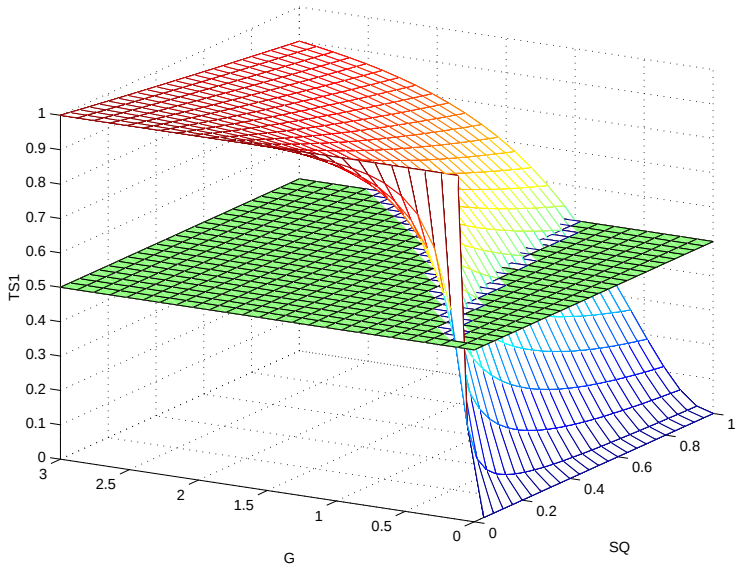

Figure 5.4: The 3-dimensional plot of T_{S1} as a function of G and SQ3. The plane shows the maximum classical value, and the surface above is the non-classical teleportation region for a single quadrature. The cross section at the plane is a parabolic.

Further discussion

The aim of teleportation is to be able to reproduce an unknown input state, regardless of its polarisation, as was already pointed out in section 4.3. From this perspective, it is desirable that TV diagrams for $\hat{S}_2$ and $\hat{S}_3$ are equal, hence symmetric squeezing is required in the teleportation setup (SQ1 = SQ2 = SQ).

Furthermore, the agreement of results for both the teleporter and the QND systems is needed. When $\lambda_{\pm} = \pm 1$, (at unity teleporter gain), $T_{S1} = T_{S2,S3}$ value occurs when the QND gain is restricted to G = $\pm\sqrt{\frac{SQ3}{SQ}}$. The second parameter equality, $V_{cv}^{1} = V_{cv}^{2,3}$, is met only when SQ3 = 2 SQ. Once this happens, G = ± 1 is needed. Hence, at unity gain for both systems and double squeezing in the EPR pair compared to that of the third QND beam, the TV points of $\hat{S}_1$, $\hat{S}_2$ and $\hat{S}_3$, overlap. There is a fundamental

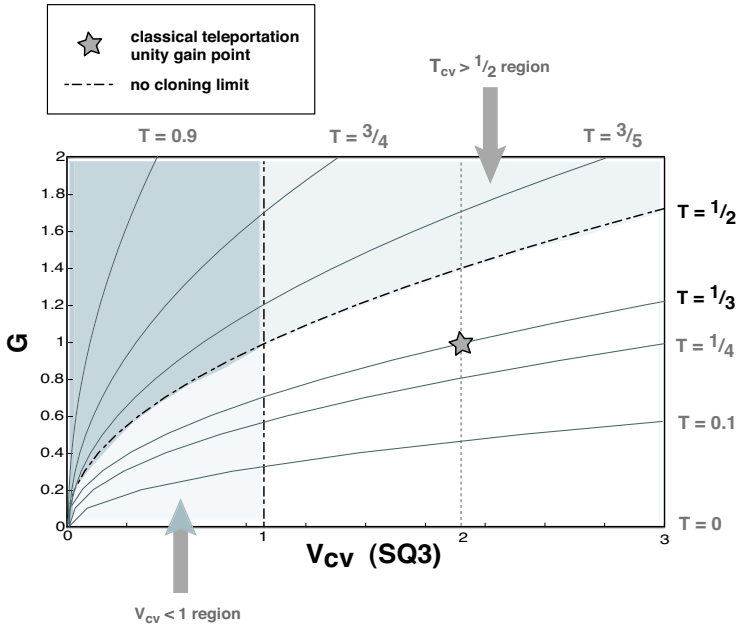

Figure 5.5: The alternative information transfer visualisation for T_{S1} in the QND case. This plot is a series of "equipotential" T_{S1} lines from the figure 5.4. The quantum teleportation regime bounded by $T_{S1} > \frac{1}{2}$ and $V_{cv}^1 < 1$ is darkened.

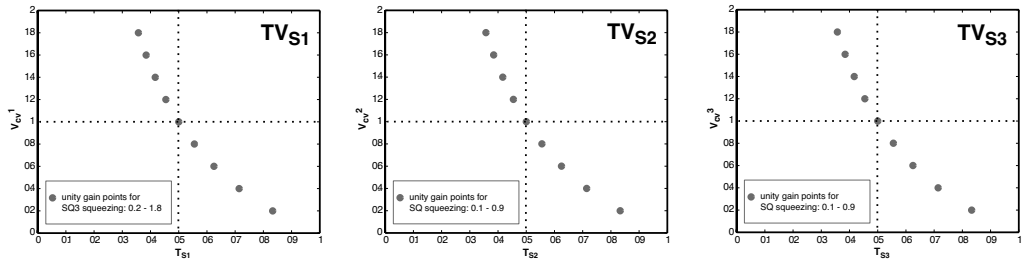

Figure 5.6: When G = 1 and SQ3 = 2 SQ the unity gain points for TV_{S1}, TV_{S2} and TV_{S3} are seen to coincide for all squeezing parameter values (in steps of 0.2 for S_1 and steps of 0.1 for $S_{2,3}$.

reason why the teleportation setup requires double the squeezing resources of the QND scheme for equal results. The teleportation protocol, as was previously discussed, admits uncorrelated noise into the system at two instances, when measuring and reconstructing the input. Hence two, so called "noise penalties" must be paid. On the other hand, in the QND measurement, only the reconstruction of the signal adds excess vacuum noise. The measurement itself avoids the back action noise by measuring the classical mean $\langle \hat{S}_1 \rangle$ of the Stokes parameter. The QND case needs to compensate for a smaller extent of incoherence introduced hence it requires less squeezing. Figure 5.6 shows how the unity gain points at various squeezing parameters for the three TV_{S1}, TV_{S2}, TV_{S3} diagrams coincide at these conditions.

5.4 Conclusion

In the above chapter an alternative way of teleporting the polarisation information was proposed. It relies on the fact that something about the input signal is known, namely the DC polarisation orientation is set to vertical, hence less parameters are required to describe the remaining information in the linearised limit. This way the resources used can be reduced to only a single teleporter and an all destructive QND scheme.

Chapter 6

Biased entanglement scheme

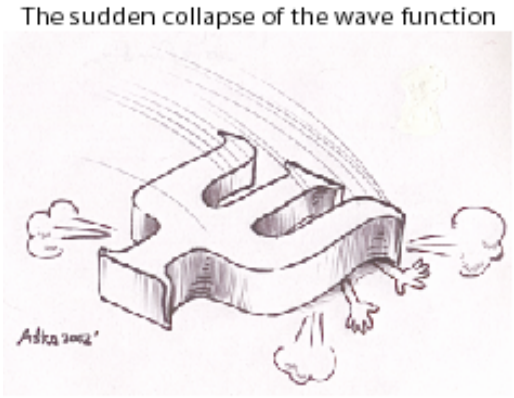

6.1 Overview of this chapter

In the following chapter I will introduce a more generalised scheme for teleportation of a single quadrature. This simplifies down to the all destructive QND measurement discussed in the previous chapter, yet allows a much better fidelity.

6.2 Motivation for improvement

It was shown that in the limit of infinite squeezing, it is possible to obtain a perfect reproduction of the signal in the QND process, hence teleport all of the polarisation quantum information possible. In the case of a signal encoded on amplitude modulation, which is the example considered previously, the output beam onto which the signal is to be imprinted needs to be amplitude squeezed, (SQ3 parameter < 1, fig 5.1), to reduce any noise in the signal quadrature. The phase quadrature, which then becomes antisqueezed and hence very noisy, ($\frac{1}{SQ3} \rightarrow$ large), is not relevant as it doesn't take part in the measurement. It carries no useful information.

This argument works well when information transfer is considered, and it is illustrated in the analysis of the previous chapter. However if the fidelity of this particular scheme is to be evaluated, it is found to be vanishingly small. This can be understood by noting that fidelity, as defined in section 2.6, measures the similarity of the complete input and output quantum states. It takes account of the quality of the reproduction of both amplitude and phase quadratures, one of which is now very noisy. Another way to express this is that when applied to single quadrature, TV evaluation preserves the classical information carried by the quantum state. However fidelity, even in this special case, still preserves the complete quantum state.

By fidelity equation 2.3, the larger the amplitude squeezing on the QND beam, the smaller the fidelity. In fact, if only measurements of $\langle \hat{S}_1 \rangle$, $\langle \hat{S}_2 \rangle$ and $\langle \hat{S}_3 \rangle$ are possible in the

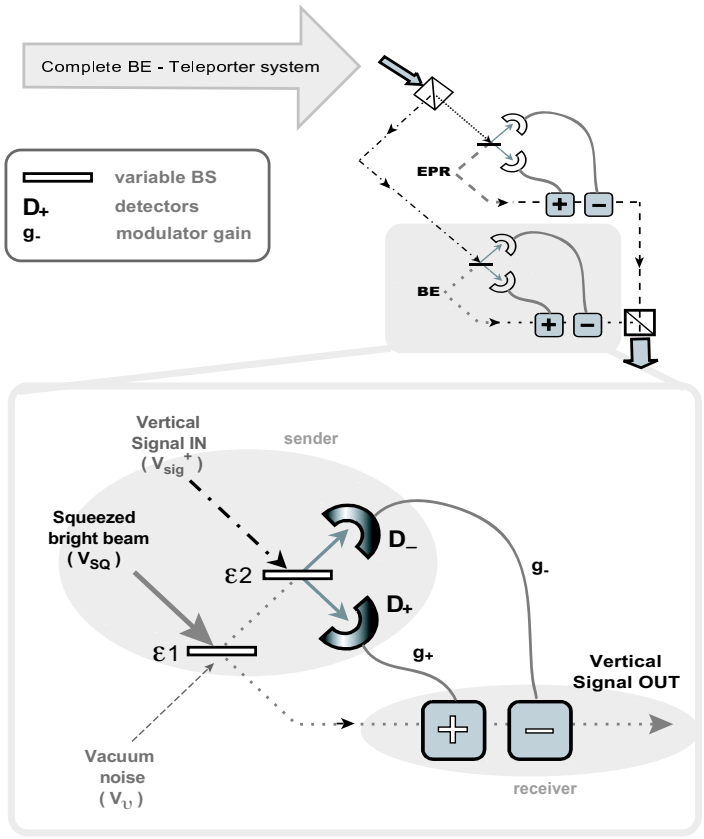

Figure 6.1: Biased entanglement and teleporter experimental setup. See text for further clarification.

teleportation scheme, then the maximum fidelity of the replicated quantum state is $F = \sqrt{\frac{2}{3}}$, attained when there is no SQ3 squeezing at all. The plot of best QND system fidelity as a function of the teleporter inputs squeezing, (SQ1 and SQ2), is shown to exceed the results of the full teleporter only below 80 % squeezing. (Figures 6.1 to 6.7, dotted line).

The aim of the following chapter is to keep to just one squeezed beam in the vertical mode, but now allow arbitrary measurements, not restricted to the Stokes parameters. The existing tradeoffs between information transfer and fidelity become apparent in this approach and the whole range of system behaviour can be examined using the scheme proposed.

6.3 Biased entanglement scheme

It is possible to design a different transfer technique, which uses non locality in the form of entanglement, to beat the above direct measurement fidelity limit. Such an experimental set up will from now on be called biased entanglement, BE and is shown on figure 6.1. It is a modification of the standard teleporter which tries to limit the resources from two bright, squeezed beams, to only one, bright, squeezed beam entangled with a vacuum port, while still achieving high fidelity. However fidelity is never expected to reach unity, as for this, entanglement of two perfectly squeezed beams is required and, as will be shown, the limiting fidelity of the BE scheme is indeed less than 1.

When the first beam splitter is set to all transmitting, $\epsilon 1 = 1$, and the second is set

to all reflective, $\epsilon 2 = 0$, the all destructive QND scheme from the previous chapter is reproduced, with no entanglement present, only a single squeezed, bright beam and direct detection of the signal (see figure 6.1). Full expressions for transfer functions of this system are given in Appendix B.5. In order to beat the $F{=}\sqrt{\frac{2}{3}}$ limit various parameters can be adjusted according to the value of squeezing injected, $V_{sq}^{\pm}$. The beam splitter transmission coefficients, $\epsilon 1$ and $\epsilon 2$, as well as the gains, are changed to optimise equation 2.3. The amplitude and phase modulators gains, g_+ and g_-, are optimised, and depend on $\epsilon 1, \epsilon 2$ and squeezing, $V_{sq}^{\pm}$ (For a more detailed analysis see Appendix B.6). Depending on the sign of g_+, there are three major cases in which the fidelity surpasses the direct detection limit. These are now discussed.

6.3.1 Case-1 : V_{sq}^{-} squeezing and g_+ positive

When the amplitude modulator gain is positive, only the squeezing of the phase quadrature along with appropriate $\epsilon 1$ and $\epsilon 2$ settings will yield $F > \sqrt{\frac{2}{3}}$. At extreme squeezing, $\epsilon 2 \rightarrow \epsilon 1 \rightarrow$ small, the output quadrature variances tend to:

$$V_{out}^{+} \rightarrow V_{sig}^{+} + 1 \qquad V_{out}^{-} \rightarrow \frac{V_{noise}^{-}}{4} + \frac{1}{4} = \frac{1}{2} \tag{6.1}$$

Here, the vertical mode is made up of the signal, (amplitude) quadrature variance, V_{sig}^{+} and the "shot noise" quadrature, V_{noise}^{-}. This limits the fidelity to:

$$F = \frac{2}{\sqrt{(1 + 0.5)(1 + 2)}} = \frac{2\sqrt{2}}{3} \tag{6.2}$$

Physically at the extremes of squeezing, almost all of the signal is directed to the amplitude detector, (D_+), while most of the phase quadrature squeezing goes directly to the output. This ensures that while the amplitude quadrature variance pays the measurement penalty by increasing the first equation of 6.1, the phase quadrature variance is lowered to half the original shot noise level.

The choice of the amplitude modulator gain sign has an effect of either correlating or anticorrelating the noise terms, which can be seen by looking at the two final terms of the V_{out}^{+} variance:

$$\begin{aligned} V_{out}^{+} \;=\; & 4\,(1-\epsilon 2)\; g_+^2\; V_{sig}^{+} \;+\; \left[V_v^{+}\; (\sqrt{(1-\epsilon 1)} \;+\; 2\; g_+\; \sqrt{\epsilon 1\; \epsilon 2}\;)^2 \right] \;+ \\ & \left\{ V_{sq}^{+}\; (2\; g_+\; \sqrt{\epsilon 2\; (1-\epsilon 1)} \;-\; \sqrt{\epsilon 1}\;)^2 \right\} \end{aligned} \tag{6.3}$$

The positive unity value of the amplitude modulator gain, g_+, implies correlations of the vacuum noise terms (square brackets) so that their addition takes place, while anticorrelating the amplitude squeezing V_{sq}^{+} contribution (curly brackets), which can be cancelled by appropriate choice of $\epsilon 1$ and $\epsilon 2$. Here V_{sig}^{+} is the signal, V_v^{+} the vacuum noise and V_{sq}^{+} the squeezed beam variance contributions. Only compensation for the vacuum noise, like squeezing, will enhance the output V_{out}^{+}, as the result is now independent of V_{sq}^{+}.

Since information is encoded only on the amplitude, the maximum transfer coefficient is the information cloning limit at unity gain, $T^{+} = \frac{1}{2}$ [54], to be discussed further in chapter 7.

The complete teleportation setup used to send polarisation encoded signals in the

vertical DC input case will also include a full teleporter for the horizontal phase and the amplitude quadrature information, hence the final fidelity of the teleported state will be the product of a standard, two quadrature teleporter result, with the optimal BE value given above. Figure 6.2, (solid line), shows the plot of maximum fidelity for such complete, polarisation teleportation system, as a function of V_{sq}^{-} squeezing. At each value of squeezing, the fidelity was numerically optimised for full the rage of parameters.

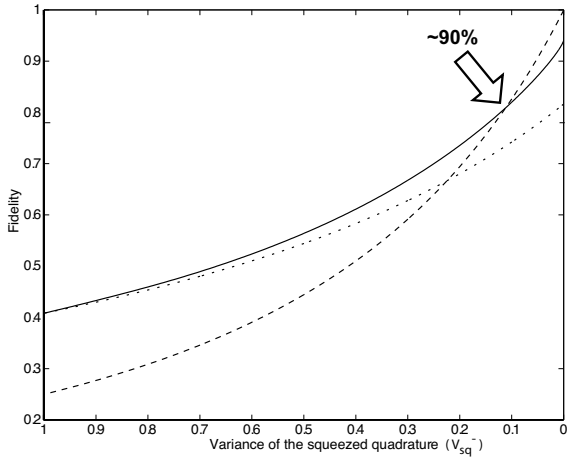

Figure 6.2: The optimal fidelity of a biased entanglement scheme, in case-1, solid line. The plot of a full QND-teleporter system fidelity is a dotted line, while the double teleporter setup is shown as a dashed line. The case-1, shows a considerable improvement to a QND system at extreme squeezing, while being more favourable than a full, double teleporter up until 90 % squeezing.

6.3.2 Case-2 : V_{sq}^{-} squeezing and g_{+} negative

With phase squeezing, ($V_{sq}^{-} < 1$) at the negative g_{+} gain, the maximum fidelity always occurs when $\epsilon 2 = 0$, and $\epsilon 1$ takes all values between 0 and 1 and is a function of V_{sq}^{-} parameter. The output quadrature variances don't approach a specific limit.

$$V_{out}^{+} = (\frac{1}{V_{sq}^{-}} - 1)\ \epsilon 1\ + 1\ + V_{sig}^{+} \qquad V_{out}^{-} = \frac{V_{sq}^{-}}{V_{sq}^{-}(1\ - \epsilon 1)\ + \epsilon 1} \tag{6.4}$$

The maximum fidelity, which can be obtained in all these variance combinations, is $F \approx 0.828$, barely beating the, QND limit of 0.816.

When V_{sq}^{-} is small, all the signal is directed to D_{+}, while the phase squeezing is delivered to D_{-}, ($\epsilon 1 \rightarrow 0$). The latter is diverted to the output beam, ($\epsilon 1 \rightarrow 1$) when V_{sq}^{-} fails to be extreme. The balancing of the transmittance of $\epsilon 1$ with the phase squeezing is crucial in keeping fidelity at this maximum.

In contrast to case-1, the negative gain, g_{+} has an effect of anti-correlating the vacuum noise and correlating the amplitude, V_{sq}^{+} contribution to:

$$V_{\nu}^{+}\ (\sqrt{1-\epsilon 1}\ -\ 2\ g_{+}\ \sqrt{\epsilon 1\ \epsilon 2})^2 \qquad and \qquad V_{sq}^{+}\ (2\ g_{+}\ \sqrt{\epsilon 2\ (1-\epsilon 1)}\ +\ \sqrt{\epsilon 1})^2 \tag{6.5}$$

Then, as $\epsilon 2 = 0$ in this case , both V_{sq}^{+} and V_{ν}^{+} limit the output to varying extent,

depending on $\epsilon 1$ value.

$$\rightarrow V_{\nu}^{+}\ (\sqrt{1-\epsilon 1})^2 \qquad and \qquad \rightarrow V_{sq}^{+}\ (\sqrt{\epsilon 1})^2 \tag{6.6}$$

The transfer coefficient for such an operation depends on the extent of phase squeezing. It can only range from $\frac{1}{2}$ at $\epsilon 1 = 0$, to 0 at $V_{sq}^{-} = 0$, a purely classical result.

Figure 6.3 shows the plot of maximum fidelity for a complete, biased entanglement, polarisation teleportation system, as a function of V_{sq}^{-} squeezing and operating in case-2.

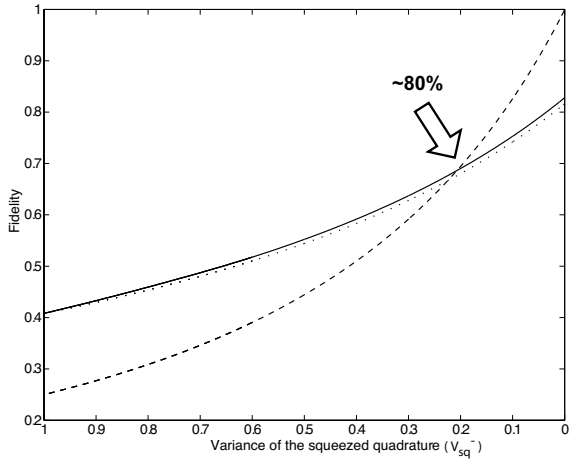

Figure 6.3: The optimal fidelity of biased entanglement scheme, in case-2, solid line. The plot of a full QND-teleporter system fidelity is dotted line, while the double teleporter setup is shown as dashed line. This case shows an almost constant and minute fidelity improvement to a QND system at all squeezing values, while, surpassing a full teleporter up until 80 % squeezing.

6.3.3 Case-3 : V_{sq}^{+} squeezing and g_{+} negative

With the amplitude modulator gain set to negative, the amplitude of the injected beam can also be squeezed. Here, as the squeezing parameter approaches zero, $\epsilon 2 \rightarrow 1$ and $\epsilon 1 \rightarrow 0$. The output variances become equal, (for unity input signal)

$$V_{out}^{+} \ \rightarrow \ V_{sig}^{+} \ + \frac{1}{4} \qquad V_{out}^{-} \ \rightarrow \ \frac{5}{4} \tag{6.7}$$

The fidelity limit grows to :

$$F \ = \frac{2}{\sqrt{(1 \ + \frac{5}{4})^2}} \ = \frac{8}{9} \tag{6.8}$$

Physically, what is occurring is that most of the signal is not detected, but is instead lost to D_{-} channel, and the little information that ends up in D_{+}, is compensated for by g_{+} gain, which is approaching infinity. So although a reasonable improvement in fidelity is observed, the infinite squeezing along with infinite gain make this a rather unphysical option.

Here, the correlation / anti-correlation of noise terms, due to the negative gain g_{+}, with the $\epsilon 1 \rightarrow 0$ and $\epsilon 2 \rightarrow 1$ has a different effect. The output variance is now limited by

a unit of vacuum noise and the extent of V_{sq}^{+} squeezing. The two terms of expression 6.5 reduce to:

$$\rightarrow V_{\nu}^{+}\ (1\ -\ 0)^2 \qquad and \qquad \rightarrow V_{sq}^{+}\ (\infty\ +\ 0)^2 \tag{6.9}$$

The information transfer coefficient for the extreme case of case-3 is a best result of $T_{out}^{+} = \frac{4}{5}$.

Figure 6.4 is again the plot of maximum fidelity for the complete BE polarisation teleportation system in case-3 as a function of V_{sq}^{+} squeezing, compared to the other two schemes discussed in previous chapters.

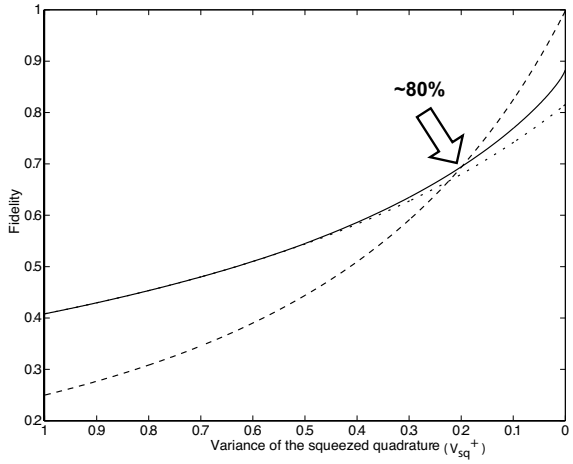

Figure 6.4: The optimal fidelity of biased entanglement scheme, in case-3, solid line. The plot of a full QND-teleporter system fidelity is a dotted line, while the double teleporter setup is shown as a dashed line. The case-3 has a modest improvement to a QND system after 50 % squeezing, while again, beating a full teleporter up until 80 % squeezing.

6.4 Further improvements with vacuum squeezing

The three cases analysed in the previous section are not the final limits on how high the fidelity of the recreated state can become. Naturally, as the asymmetric teleportation scheme, ($V_{SQ1} \neq V_{SQ2}$), approaches the full teleporter utilising two squeezed beams, the fidelity can in principle become unity. This is equivalent to optimising a full, double teleporter for the vertical DC input, to be discussed later.

The entanglement introduced in the new, BE scheme, called biased entanglement [56], differs from the maximally correlated EPR case, primarily because one of the beams, ($V_{v}^{\pm}$ vacuum), is not squeezed. Once the vacuum fluctuations variance is reduced below one, the entanglement of the two beams created after beam splitter $\epsilon 1$, (figure 6.1), enables perfect teleportation, hence a fidelity of one.

Below the three cases are analysed again, with amplitude or phase vacuum noise squeezing.

6.4.1 Case-1 with V_v^+ squeezed

Once vacuum noise squeezing variance, V_v^+ is introduced into the optimum fidelity analysis, the output variances for the two quadratures become:

$$V_{out}^+ \rightarrow V_{sig}^+ + V_v^+ \qquad V_{out}^- \rightarrow \frac{1}{1 + V_v^+} \tag{6.10}$$

This shows that, by amplitude squeezing the noise, perfect state transfer can occur. The fidelity limit is now unity as expected, $F = \frac{2}{\sqrt{(1+1)(1+1)}} = 1$. The information transfer coefficient in this case also approaches one as $T_{MAX}^+ = \frac{1}{1+V_v^+}$. In the limit considered, this system reduces to a symmetric teleporter. (See "Complete cross comparison" section).

6.4.2 Case-2 with no vacuum squeezing

Fidelity is not improved in this case by any further vacuum squeezing, being optimum at $V_v^\pm = 1$. This makes sense, as most of the squeezing compensation for the noise comes from the balance of V_{sq}^- and $\epsilon 1$ parameters.

The information transfer coefficient can again take a range of values, but this time the upper limit is determined by vacuum squeezing, $T_{MAX}^+ = \frac{1}{1+V_v^+}$. To keep fidelity optimum, the squeezing must remain one, but if $V_v^+ \rightarrow 0$, the information transfer can grow, at a cost to fidelity.

6.4.3 Case-3 with V_v^- squeezed

Finally, the variances of the outputs in this case are now:

$$V_{out}^+ \rightarrow V_{sig}^+ + \frac{V_v^+}{4} \qquad V_{out}^- \rightarrow \frac{1}{V_v^+} + \frac{1}{4} \tag{6.11}$$

Again, a compromise must be made, while squeezing one vacuum quadrature, not to increase the other in the process, because of the V_v^+ dependence. The optimum fidelity is found when the noise phase quadrature, V_v^- is squeezed to ≈ 0.395.

The value of the maximum fidelity is then not unity, but $F = \frac{4}{9}(\sqrt{10}-1) \approx 0.961$, which, as I will show later, is an equivalent of a cloning limit for single quadrature detection. The transfer coefficient for this system is $T_{out}^+ = \frac{1}{1+\frac{1}{4V_v^-}}$ It is a monotonically decreasing function, which has its maximum value, $T_{out}^+ = 1$, where F=0, at perfect vacuum amplitude squeezing. It decreases to $T_{out}^+ \approx 0.6126$, at the optimum fidelity. Information transfer can once again be seen to improve only at a cost to the fidelity.

Complete cross comparison

It should be pointed out that the curve of fidelity as a function of squeezing for a full, four squeezer teleporter in the figures 6.2-6.4, (dashed line), could also be optimised for the amplitude coded signal. This can be achieved in the similar manner as was done in this chapter for BE teleportation scheme, and is in fact equivalent to the results of section 6.4.

This optimisation involves similar equations to the ones already introduced, only this time both inputs are squeezed. A more in depth analysis is presented in Appendix B.7. If the squeezing of the two beams is assumed symmetric and the beamsplitter transmissions

adjusted at each squeezing parameter, then a much better fidelity curve is obtained. Two cases can also be seen to emerge, limits of which are analysed in sections 6.4.1-6.4.3. However only the biggest improvement fidelity curve is considered here. This, along with the non optimised four squeezer case and the BE teleporter curve, is shown on figure 6.5. The BE and optimised full teleporter schemes are seen to be equivalent up to 0.5, (3

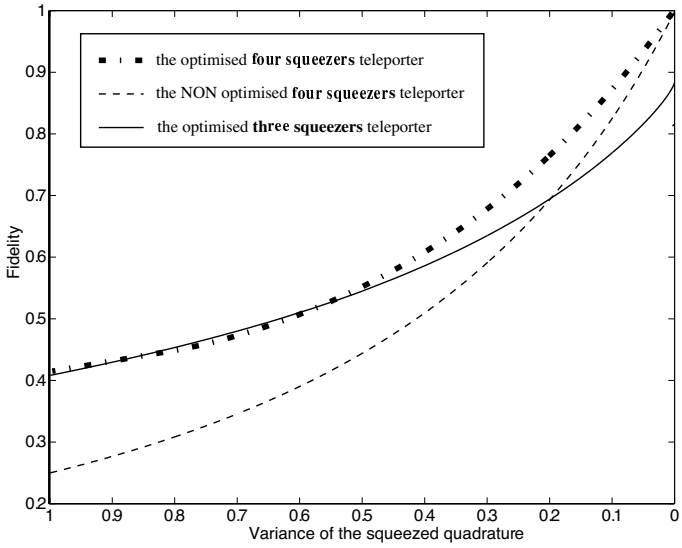

Figure 6.5: The optimised four squeezer teleporter (thick, dotted-dashed line), compared with the optimised three squeezer case, the BE-teleporter scheme (solid line). The non optimised fidelity curve for the full teleporter is also shown (thin, dashed line). The two optimised systems show comparable results at lower squeezing parameters, even though the full teleporter is more demanding in resources.

dB) squeezing, after which the latter increased, as expected, up to ideal fidelity at perfect squeezing.

The advantage of using the BE-teleporter setup is seen, as the scheme yields comparable results, while using less resources than the four squeezed beams teleporter, while acquiring lower squeezing parameters, within experimental reach.

6.5 Conclusion

In this chapter I have shown that if the preservation of the total quantum state, and hence a good fidelity, is the objective of the polarisation teleportation, then an alternative experimental design is required to the one proposed in chapter 5.

This new setup uses non local operations, namely entanglement, to surpass the otherwise present $F_{QND}= \sqrt{\frac{2}{3}}$ limit. The design uses less resources than a full teleporter, containing only one squeezed, bright beam. It surpasses it in fidelity until V_{sq}^{-} reduces to ≈ 0.1 (≈ 10 dB), a squeezing value which to date has not been achieved experimentally.

Additionally, by introducing vacuum fluctuations squeezing, the fidelity limit can be increased further in special circumstances, as the regime of full teleporter, with two entangled, bright beams is entered.

It is clear from the above analysis that success of information transfer is not necessarily linked to an improvement in fidelity, as poor signal, input-output overlap is compensated for by a better phase noise overlap. A clear decision on what is most important to a particular quantum protocol needs to be made before deciding which tools are to be used when evaluating it. In fact for perfect information transfer the scheme of chapter 5, with no second entanglement resource, is a sufficient solution and the BE teleporter setup introduced above becomes an overkill.

Chapter 7

The alternative cloning limit

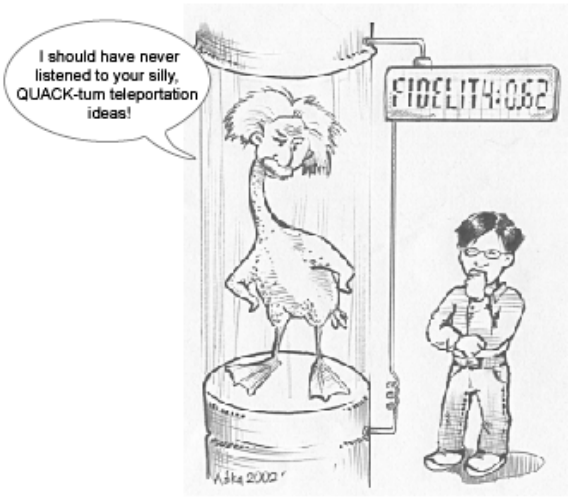

7.1 Overview of this chapter

In this chapter I will introduce an idea analogous to that of the quantum cloning of quadrature amplitudes.

First, the cloning analysis for the well known quadrature cloner will be outlined, where two quadratures of a state are copied and measured. This includes a discussion of information cloning limit. Following is the introduction of a special case of cloning, where information resides on a single conjugate variable hence only one quadrature of the output is measured.

An interesting fidelity limit, of $F=\frac{4}{9}(\sqrt{10}-1)$, will be seen to reappear, from investigation in chapter 6.

7.2 The standard cloning limit

7.2.1 The fidelity cloning limit

In contrast to its counterpart in the single particle regime [16, 57], cloning of continuous variables [29] has only been investigated over the last few years. The linearity of quantum mechanics demands that copies of conjugate observables of a state can't be ideal, as minimum noise has to be introduced in the cloning process, hence giving rise to an absolute bound on the fidelity.

The Gaussian cloning machines are of greatest interest as they apply to the amplitude and phase quadrature description, and experimentally realisable coherent states. They are so called as they yield copies that are Gaussian distributions centred on the original value.

The question of optimal quantum cloning addresses a problem of to what extent can the copies resemble the original, or what is the optimum tradeoff between the two variable errors brought about when cloning. It was shown by Rottenberg *et al* [30] that the clones obey Heisenberg like uncertainty relation, where the product of the first copy's amplitude variance with second copy's phase variance remains bounded by $(\frac{\hbar}{2})^2$.

The simplest demonstration of such a Gaussian cloner was proposed by Iblisdir *et al* [44] and is now discussed.

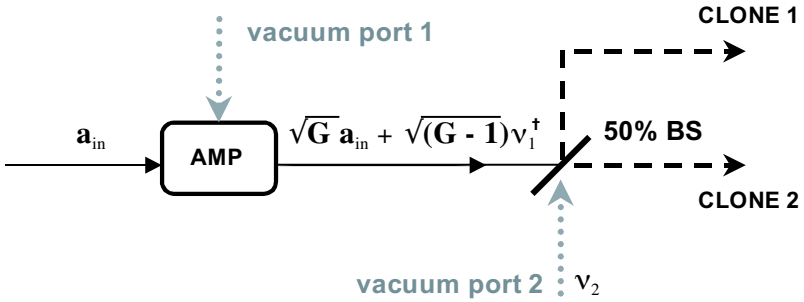

Figure 7.1: The optimum quantum Gaussian cloning machine, for complete two quadrature copies.

Figure 7.1 shows a simple system, containing a phase insensitive amplifier, AMP, followed by a classical beam splitter, BS. The input, field, $\hat{a}_{in}$, is analysed by considering the amplifier's transfer function, as was done for other protocols in section 2.5. An operator $\hat{a}_{in}$, is mixed with the quantum noise field, $\hat{\nu}_1^{\dagger}$, via the gain coefficient, G, as shown. The beam splitter then divides the amplified beam into two outputs, chosen to be equal by setting $\epsilon = 0.5$, and adds further uncorrelated noise, $\hat{\nu}_2$. To determine what is the best possible fidelity of each copy, the output quadrature variances

$$V^{\pm}_{CLONE1} \;=\; V^{\pm}_{CLONE2} \;=\; V^{\pm}_{a}\,\frac{G}{2} \;+\; V^{\pm}_{\nu 1}\,\frac{(G-1)}{2} \;+\; \frac{V^{\pm}_{\nu 2}}{2} \tag{7.1}$$

are substituted into fidelity equation 2.3. To set the maximum possible fidelity in such a process, (hence overall unity gain), a value of G = 2 is required, which gives $F = \frac{2}{3}$.

This consequence of the "no cloning theorem", ensures that the two separate measurements of the clones will not yield better knowledge about the input than direct measurement of the state itself. $F = \frac{2}{3}$ can be thought of, as on average, the number of times one gets the correct "answer" about the original state, when taking a measurement of a clone.

The proof that this cloning limit is the upper bound[1] and further discussion of the limit's importance are given in references [36, 44].

The signal to noise ratios of each clone can also be calculated.

$$SNR^{+}_{out} \;=\; \frac{2\;SNR^{+}_{in}}{(2\;+V^{+}_{\nu 2}\;+V^{+}_{\nu 1})} \qquad\qquad SNR^{-}_{out} \;=\; \frac{2\;SNR^{-}_{in}}{(2\;+\frac{1}{V^{-}_{\nu 2}}\;+\frac{1}{V^{-}_{\nu 1}})} \tag{7.2}$$

These, at the agreed, shot noise level of vacuum inputs, $(V_\nu = 1)$, are equal and given by $SNR^{\pm}_{out} = \frac{1}{2}SNR^{\pm}_{in}$. Hence the best clone will have its SNR halved in the process, so the

[1] for a coherent state $|\alpha\rangle$

standard, Gaussian cloning system is limited to a purely classical result.

7.2.2 The information and correlation cloning limits

An equivalent argument exists in the TV formalism, described by the transfer coefficient and conditional variance in sections 2.7, 5.3 and 6.3. The idea is illustrated in figure 7.2. In a protocol such as teleportation it is also possible to clone the signal but at a price

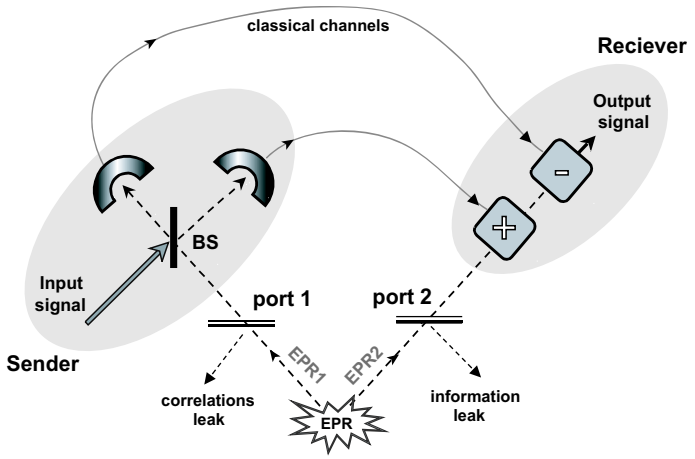

Figure 7.2: The teleportation setup with two taps at ports 1 and 2. Quantum correlation loss occurs at port 1, and information loss at port 2. The cloning limits for the two TV parameters are $T_{LIM} \leq \frac{1}{2}$ and $V_{cv}^{LIM} \geq 1$, per quadrature.

of the information transfer or conditional variance. In an ideal teleportation protocol, the input signal is mixed with EPR1 beam, and all information is masked completely by the large noise statistics of the entangled beam. There is no detectable information in the classical channel, and with ideal squeezing the conditional variance reduces to zero while the information transfer can reach unity for each quadrature. This marks an ideal teleportation as the second, EPR2 beam cancels all of the noise at the receiving station.

If some of the EPR1 beam is tapped-off at port 1, partial quantum correlations can be used at the classical channel (somewhere other than the receiving station), to extract partial information about the input. Therefore cloning of the signal takes place. However the noise statistics of EPR1 are subsequently interfered with and reduced. When the signal is mixed with this modified EPR1 beam at BS, it is no longer completely masked by the EPR noise, and the correlations between EPR1 and EPR2 are degraded. Some variation of the input signal can now be detected in the classical channel due to the loss of some entanglement at port 1, so it is necessary that the noise penalty increases. There is now a lower bound to the uncertainty of input reproduction and the value of *the correlation cloning limit* is $V_{cv}^{LIM} = 1$ (per single quadrature). Since the two TV parameters are not independent of one another, the total transfer coefficient is also restricted to the well known (unity gain) cloning limit of $T \leq \frac{2}{3}$.

Alternatively, some of the EPR2 beam can also be tapped-off at port 2 and subsequently used in order to deduce some of the signal in the classical channel. This is once again equivalent to cloning, however because the EPR2 beam has now been partially detected, the complete cancellation of the EPR noise at the receiving station can't take

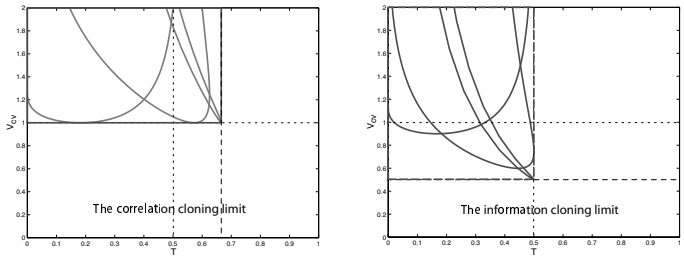

Figure 7.3: The two cloning regimes of the TV diagram, depending on the tap-off port. The correlation cloning regime (dashed box), $T \leq \frac{2}{3}$ and $V_{cv} \geq 1$. The information cloning regime (solid box), $T \leq \frac{1}{2}$ and $V_{cv} \geq \frac{1}{2}$, per quadrature. Examples of TV curves are given at three squeezing values: $V_{SQ} = 0.5, 0.1, 0.001$.

place, so the information transfer is reduced. *The information transfer cloning limit* is $T_{LIM} = \frac{1}{2}$ (per single quadrature). The conditional variance in this case is also restricted and increases from its ideal, zero value to $V_{cv} \geq \frac{1}{2}$. Both of these TV cloning regimes are shown on figure 7.3.

7.3 The single quadrature cloning limit

Optimum cloning is thought of as a restriction placed by the Heisenberg's uncertainty principle between two conjugate parameters being copied [30]. For a case of information on a single quadrature, where only one of the conjugate observables is being measured and copied it could be easy to make a misleading conclusion that there will not be such a cloning limit. However the quantum mechanics still places a restriction on the fidelity of such clones. This makes it impossible for a set of clone-measurements to determine the original, input distribution with greater precision, (ie. smaller variance).

In the process of investigating the biased entanglement scheme in chapter 6, it became apparent that for the special case of teleportation, of an input state carrying information on one quadrature only, a different cloning process would be required. As a result of only one quadrature being measured, all efforts of error suppression are biasing one variable only. Therefore a new cloning limit, with a much higher, harder to beat fidelity emerges in such a scenario and is now discussed.

The analog of a simple, single quadrature Gaussian "cloner" is shown on figure 7.4. It

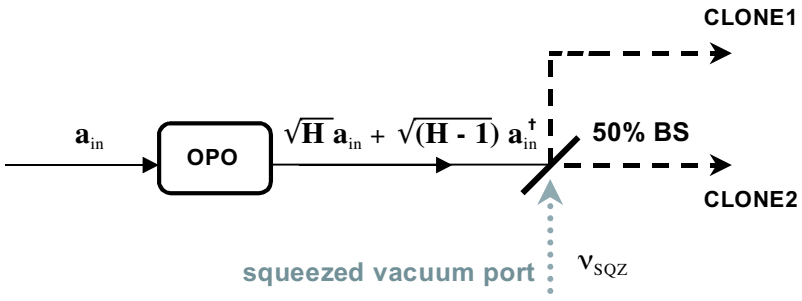

Figure 7.4: The single quadrature quantum cloner. H is the OPO gain.

consists of a phase sensitive amplifier, or a nonlinear device called an optical parametric oscillator, (OPO), [6, 13, 23, 24, 25]. It is followed by a phase sensitive beam splitter, BS, with squeezed vacuum noise, injected in the dark port, $\hat{\nu}_{SQZ}$. The transfer function of an OPO shows that on output, the input field, $\hat{a}_{in}$, is correlated with its conjugate, $\hat{a}^{\dagger}_{in}$, via the OPO gain constant, H, as shown.

Again, to ensure two equal copies, $\epsilon = 0.5$. After passing through the beam splitter, the variances of the output quadratures are:

$$V^{\pm}_{CLONE1} \;=\; V^{\pm}_{CLONE2} \;=\; \frac{V^{\pm}_{a}}{2}\,(\sqrt{H-1} \;\pm \sqrt{H})^2 \;+\; \frac{V^{\pm}_{\nu}}{2} \tag{7.3}$$

Setting the gain to H = $\frac{9}{8}$ is needed for maximum fidelity, (overall unity gain). The minimum uncertainty state of input noise, where $V^{+}_{\nu} \;= \frac{1}{V^{-}_{\nu}}$, is also assumed. This gives a limiting fidelity of:

$$F \rightarrow \frac{2}{\sqrt{(\frac{5}{4} + \frac{1}{2V^{+}_{\nu}})(2 \;+ \frac{V^{+}_{\nu}}{2})}} \tag{7.4}$$

The function 7.4 reaches a maximum when vacuum phase quadrature squeezing becomes $V^{-}_{\nu} = \sqrt{\frac{5}{8}}$, (so $V^{+}_{\nu} = \sqrt{\frac{8}{5}}$). Maximum fidelity of such a "clone" is then $\frac{4}{9}(\sqrt{10}-1)$. This is precisely the maximum fidelity value which could be obtained with vacuum squeezing in the BE-teleporter scheme, when g_{+} was negative and V^{+}_{sq} was perfectly squeezed. It suggests that the regime 3 of sections 6.3.3 and 6.4.3, reduces to a cloner in this limit of parameter values, and points to the reason why, unlike a teleporter, it is never able to achieve a perfect reproduction of the input. More discussion of the cloning limits is given in section 7.5.

An equivalent operation of to injecting squeezed vacuum into the unused port is to instead insert two independent OPO's in each output arm of the cloner. This is shown on figure 7.5.

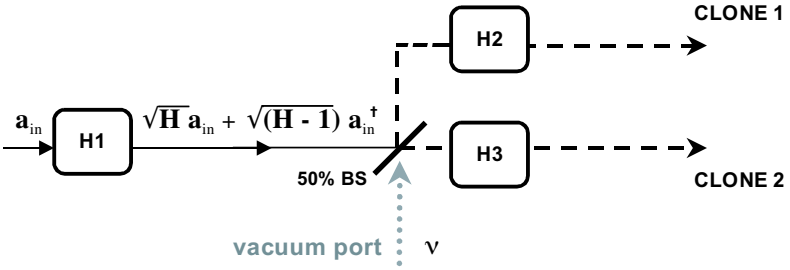

Figure 7.5: Equivalent single quadrature quantum cloner design. H1, H2 and H3 are the gains of the three OPOs.

The first OPO gain, H1, is then unrestricted, as the later, H2, (H3) gain in each arm will be chosen in compensation, to give the best fidelity possible. Squeezing the vacuum port $\hat{\nu}$, doesn't improve the result, which still remains at the previous limit of $F = \frac{4}{9}(\sqrt{10}-1)$.

The SNR^{+} of the individual amplitude quadrature clones is found to be:

$$SNR^{+}_{out} \;= \frac{2\;SNR^{+}_{in}}{(2 \;+ V^{+}_{\nu})} \tag{7.5}$$

With optimised fidelity at $V_\nu^+ = \sqrt{\frac{5}{8}}$, the above expression reduces to $SNR_{out}^+ = \frac{5\ SNR_{in}^+}{5+\sqrt{10}} \approx 0.6125\ SNR_{in}^+$. This is a greater value than the single quadrature average SNR in the previous case, so it lies outside the classical regime.

The SNR of the summed quadrature of two cloned amplitude quadratures, $X_{SUM}^+ = X_{CLONE1}^+ + X_{CLONE2}^+$, is always independent of the vacuum squeezing parameter and gives $SNR_{out}^+ = 1$. The noise outputs of the phase and amplitude quadratures are very close to the minimum uncertainty product. (The perfect fulfilment of the $V^+V^- = 1$ condition requires unity fidelity which is forbidden by the no cloning theorem.) The implications of these results are discussed in the next section.

7.4 Is this the optimum "cloner"?

In the standard cloning limit, the value of $F{=}\frac{2}{3}$ was shown to be the best clone fidelity possible using the fundamental commutation relations of the conjugate observables [44]. In the single quadrature case, no such analogy can be made, and hence the question of whether the above scheme is an optimum one remains open. However there are arguments suggesting this indeed is the case.

Firstly, the new approach is analogous to the standard "cloner" set-up, and it is hard to imagine how the phase sensitive amplification and phase sensitive beam splitter combination could be improved upon.

Secondly, the sum of signal to noise ratios, SNR_{out}^+, of the two clones gives unity, and the output noise is almost a minimum uncertainty state, indicating that the system as a whole doesn't introduce any external noise, which could somehow be cancelled.

However, although these are promising arguments, they don't constitute a proof as various fidelities, (and hence various combinations of $V_{out}^\pm$ values), can yield the same SNR^+. This can be illustrated by noticing that the signal resides on amplitude quadrature only, hence SNR^+ is fixed by the size of the cloner's input V_a^+. However fidelity also depends on the extent of the noise variance on the V_a^- quadrature, and if this value happens to be different to the assumed shot noise level of unity, fidelity will change, while the SNR^+ remains the same.

7.5 Equivalent information and correlation cloning limits ?

The cloning limit fidelity of $F{=}\frac{4}{9}(\sqrt{10}-1)$ can not be obtained in any of the three regimes of squeezing, discussed in section 6.3, unless the entanglement is made less asymmetric by introducing vacuum noise squeezing, (section 6.4).

In the case of ideal V_{sq}^+ squeezing and negative gain, the single quadrature cloning limit is only just reached when the vacuum port becomes phase squeezed at $V_{optimum}^- \approx 0.395$, as mentioned in section 6.4.3. At these parameter values, yielding optimum cloning fidelity, the transfer coefficient and conditional variance are found numerically to be: $T_{lim}^+ \approx 0.6126$ and $V_{cv_{lim}}^+ \approx 0.6325$.

The other case of ideal V_{sq}^- squeezing and positive gain, section 6.4.1, can reach a fidelity of $\frac{4}{9}(\sqrt{10}-1)$ with a minimum threshold amplitude vacuum squeezing of $V_{threshold}^+ \approx 0.7644$. The resulting transfer coefficient and conditional variance information limits are $T_{lim}^+ \approx 0.5668$ and $V_{cv_{lim}}^+ \approx 0.7644$.

The limits of these two cases are not equal as the systems considered, case-1 and case-3 are physically different, the first reducing to a full teleporter while the latter to a cloner.

	Teleporter	2 teleporters	QND-teleporter	BE-teleporter	
Fidelity	$\frac{1}{2} \rightarrow$	$\frac{1}{4}$ (classical)	-	$\frac{4}{9}(\sqrt{10}-1)$	(single quadrature cloning)
limits	$\frac{2}{3} \rightarrow$	$\frac{4}{9}$ (cloning)	-	$\frac{2\sqrt{2}}{3}$	(ideal, no V_ν squeezing)
	$1 \rightarrow$	1 (ideal)	$\sqrt{\frac{2}{3}}$ (ideal)	1	(ideal, with V_ν squeezing)
				Regime 1	Regime 3
$T_q^{cloning}$	$T_q^+ =$	$\frac{1}{2}$	$T_V^+ = \frac{1}{2}$	T_V^+=0.567	T_V^+=0.613
(per quadrature)	$T_q^- =$	$\frac{1}{2}$	$T_H^\pm = \frac{1}{2}$	$T_H^\pm = \frac{1}{2}$	$T_H^\pm = \frac{1}{2}$
$V_{cv}^{cloning}$	$V_{cv}^+ =$	1	V_{Vcv}^+ =1	V_{Vcv}^+ =0.764	V_{Vcv}^+ =0.633
(per quadrature)	$V_{Hcv}^\pm =$	1	$V_{Hcv}^\pm$ =1	$V_{Hcv}^\pm$ =1	$V_{Hcv}^\pm$ =1

Table 7.1: This is a table summarising results for the three, polarisation teleportation schemes in the text. Where cloning fidelity limits exist, T_q^+ and V_{cv}^+ are calculated for the set of relevant parameters.

Both of these are first optimised to the best possible fidelity, which doesn't regard the T_{lim}^+ and $V_{cv}{}_{lim}^+$ from the two systems on equal footing. The results in both cases are more stringent than the requirements of the no cloning theorem for both quadratures, as discussed in section 7.2.2.

By comparing the schemes discussed in previous chapters, the results of the cloning limits are summarised in table 7.1. These are the two-quadrature teleporter, (section 2.5.3), the double polarisation teleporter, (section 4.3), the QND-teleporter, (section 5.3), and the BE-teleporter setup, (sections 6.3 and 6.4). The table lists various fidelity limits and the T_{lim}^+ and $V_{cv}{}_{lim}^+$ for the appropriate parameters at the no cloning limit boundaries.

7.6 Conclusion

I have demonstrated the existence of another cloning limit and the found, corresponding information and correlation cloning limits, for the special case of single quadrature input.

I also argued that although the fidelity limit, $F=\frac{4}{9}(\sqrt{10}-1)$, is not necessarily the highest possible, there is a good indication that it is indeed, the absolute upper bound for cloning a single quadrature measured state.

Future prospects

Back in 5 min...

The field of experimental quantum optics in the continuous-variable regime has made many significant advances in recent years. The development of its technology, readily allowing production of optical entanglement from a multitude of different optical systems, has resulted in the demonstration of many quantum communication protocols, including the discussed quantum teleportation as well as quantum cryptography, entanglement swapping and quantum secret sharing.

The quantum Stokes parameters offer a useful tool for the description of the polarisation of a light beam. The novel approach to quantum information processing that exploits quantum continuous variables has stimulated interest in these non classical polarisation states.

The formalism of quantum Stokes operators was recently used to describe the mapping of the polarisation state of a light beam on to the spin variables of atoms in excited states, [2, 22]. The correspondence between the algebras of the Stokes operators and the spin operators enables an efficient transfer of quantum information from a freely propagating optical carrier to a matter system. These developments show promise in designing a quantum teleportation scheme of atomic states, a first step in the much anticipated matter teleportation.

A successful generation of a light-atom interspecies entanglement would allow a development of technology to transfer, store, exchange, and read-out quantum information between photons and atoms. While photonic systems are ideal for information transmission, atomic systems are ideal as a storage medium. The ability to map the quantum state of atoms using light and vice versa is hence an important step towards the realisation of a quantum communication network.

There have so far been several proposals on interspecies entanglement. Examples of these include: atomic entanglement via cavity QED, ions or atoms in traps and lattices and the continuous variable light and atomic spin ensemble entanglement. In atomic ensemble experiments, the quantum information is stored in the form of spin-states that can be

interrogated at specific Larmor frequencies in a magnetic field. In the near future such experiments will investigate the possibility of generating a novel macroscopic quantum state, such as the Schrödinger cat state and macroscopical entanglement.

The shared EPR entanglement between the sender and the receiver allows some further interesting applications to emerge.

In a non polarised beam, if the sender and receiver randomly decide to make a set of measurements of either phase or amplitude, each time they simultaneously choose the same quadrature their measurement results will agree, as their beams are entangled. This string of results can be subsequently used as a key to encrypt information and any message sent between the two parties can be made absolutely unbreakable as there is no way for an external agent to deduce the quantum key. The message is encoded in the correlation between the transmitted string and the key. The sring of qubits itself, carries no information where the key is unknown to the eavesdropper. This protocol is called quantum cryptography [41].

The proposal to apply the bright polarisation-entangled beams to a continuous-variable quantum cryptography protocol, [31, 41], will avoid using the experimentally costly local oscillator techniques. The advantages of using continuous-variable polarisation, such as the intense sources of EPR entanglement and efficient direct detection, will open way to a secure quantum communication with bright light.

A possibility of creating a quantum channel able to convey information to several receivers is also an attractive prospect. A multiuser quantum channel would allow simultaneous distribution of "cloned", (and hence only partial) pieces of information to several remote receivers, and is termed telecloning [38].

To teleport a quantum state precisely from one sender to many receivers one at the time was first proposed by using multiparticle entanglement state, [37]. Another method involves building a quantum device using continuous variable switch teleportation, first suggested by [18]. Such scheme relies on an EPR entanglement produced by mixing a pair of two-mode (or polarisation) squeezed beams, shared by the sender and receivers. By changing the squeezed component of one of the two polarised beams between amplitude and phase, or by adjusting the relative phase angle θ between the horizontal and vertical modes, the original input can be conditionally teleported to either of the two output stations, alternatively, [59].

Overall, the field of quantum information is just emerging, with experimental solutions to the proposed protocols being developed at a rapid speed all around the world. At the frontier of the field is the continuous wave quantum optics regime, and especially the study of non classical polarisation states of light. The promising results outlined above, so far predict a bright future for quantum computing, quantum teleportation, quantum cryptography and many other non classical schemes which are more practical and easier to manipulate when applied to many particle systems.

This thesis is one of the first steps taken towards characterisation and analysis of the experimental aspects of this area and in particular in the context of the teleportation protocols which lie at the heart of quantum information processing.

I am personally looking forward with anticipation towards the accumulation of knowledge and rapid progress in the not so distant future of this field. It is my true belief that a completely new level of logic and problem solving is on the verge of appearing in our lives, along side the quantum information revolution.

Matlab Programs

Below are the two Matlab programs which were used to generate the Stokes TV diagrams, for double teleporter and QND-teleporter setups.

A.1 The double teleporter

```
% Plot of 4 squeezer teleportation as function of gains
% However here the Stoke parameters are characterised, not
quadratures!
clear;

VHpin=5; 'Signal + Noise quadrature inputs';
VHmin=5;
VVpin=5;
VVmin=5;
NHpin=1; 'this is the vacuum noise on the SIGNAL, not the squeezed
beam!';
NHmin=1;
NVpin=1;
NVmin=1;

'**************   VERTICAL DC carrier polarisation info !
****************';
Ah=1/sqrt(3);       % DC coherent amplitudes, normalized to one
Av=sqrt(1-Ah^2);
TH=pi/4;            % THETA, the phase angle between the two!

SQ1=.3;             % Squeezing variances for the four beams
SQ2=.6;
SQ3=.2;
SQ4=.5;

V1m=1/SQ1;          % These are the Vertical teleporter squeezed
beams,
V1p=SQ1;            %  minimum uncertainty states
V2m=1/SQ2;
V2p=SQ2;

V3m=1/SQ3;          % These are the Horizontal teleporter squeezed
beams,
V3p=SQ3;            %  minimum uncertainty states
V4m=1/SQ4;
V4p=SQ4;
```

```
% These are all the possible correlations due to the modulation
BEFORE, between 1 or -1
X1vCX1hIN=0;
X2vCX2hIN=0;
X1vCX2hIN=0;
X2vCX1hIN=0;
X1vCX2vIN=0;
X1hCX2hIN=0;

%%%%%%%%%%%%%%%%%%%%%%%%%%%%%%%%%%%%%%%%%%%%%%%%%%%%%%%%%%%%%%%%%%%%%%%%%%%%

'((((((((((((((((TELEPORT as funct of gain h))))))))))))))))';

Nc=1;'transmission efficiencies, assumed ideal';
Nd=1;
Ne=1;'detection efficiency';

hm = -1*linspace(0,2,600);'gain arrays, always opposite sign';
hp = 1*linspace(0,2,600);
Shm = hm.*hm;             'this is gain squared array, to make
calculations easier';
Shp = hp.*hp;

'below is calculated from Vout with Vin = Nin, ie the noise only';
NHmout=0.5*(sqrt(Nd)+hm*sqrt(Ne*Nc)).*(sqrt(Nd)+hm*sqrt(Ne*Nc))*V4m +
...
0.5*(sqrt(Nd)-hm*sqrt(Ne*Nc)).*(sqrt(Nd)-hm*sqrt(Ne*Nc))*V3p +
Shm*Ne*NHmin+...
(1-Nd)+Shm*(1-Nc*Ne);

NHpout=0.5*(sqrt(Nd)+hp*sqrt(Ne*Nc)).*(sqrt(Nd)+hp*sqrt(Ne*Nc))*V4p +
...
0.5*(sqrt(Nd)-hp*sqrt(Ne*Nc)).*(sqrt(Nd)-hp*sqrt(Ne*Nc))*V3m +
Shp*Ne*NHpin+...
(1-Nd)+Shp*(1-Nc*Ne);

NVmout=0.5*(sqrt(Nd)+hm*sqrt(Ne*Nc)).*(sqrt(Nd)+hm*sqrt(Ne*Nc))*V2m +
...
0.5*(sqrt(Nd)-hm*sqrt(Ne*Nc)).*(sqrt(Nd)-hm*sqrt(Ne*Nc))*V1p +
Shm*Ne*NVmin+...
(1-Nd)+Shm*(1-Nc*Ne);

NVpout=0.5*(sqrt(Nd)+hp*sqrt(Ne*Nc)).*(sqrt(Nd)+hp*sqrt(Ne*Nc))*V2p +
...
0.5*(sqrt(Nd)-hp*sqrt(Ne*Nc)).*(sqrt(Nd)-hp*sqrt(Ne*Nc))*V1m +
Shp*Ne*NVpin+...
(1-Nd)+Shp*(1-Nc*Ne);
```

```
'the TRANSFER function for the quadratures in the two teleporters';
'the atteniuations, etc are assumed to have equall values...';
VHmout=0.5*(sqrt(Nd)+hm*sqrt(Ne*Nc)).*(sqrt(Nd)+hm*sqrt(Ne*Nc))*V4m +
0.5*(sqrt(Nd)...
-hm*sqrt(Ne*Nc)).*(sqrt(Nd)-hm*sqrt(Ne*Nc))*V3p +
Shm*Ne*VHmin+(1-Nd)+Shm*(1-Nc*Ne);

VHpout=0.5*(sqrt(Nd)+hp*sqrt(Ne*Nc)).*(sqrt(Nd)+hp*sqrt(Ne*Nc))*V4p +
0.5*(sqrt(Nd)...
-hp*sqrt(Ne*Nc)).*(sqrt(Nd)-hp*sqrt(Ne*Nc))*V3m +
Shp*Ne*VHpin+(1-Nd)+Shp*(1-Nc*Ne);

VVmout=0.5*(sqrt(Nd)+hm*sqrt(Ne*Nc)).*(sqrt(Nd)+hm*sqrt(Ne*Nc))*V2m +
0.5*(sqrt(Nd)...
-hm*sqrt(Ne*Nc)).*(sqrt(Nd)-hm*sqrt(Ne*Nc))*V1p +
Shm*Ne*VVmin+(1-Nd)+Shm*(1-Nc*Ne);

VVpout=0.5*(sqrt(Nd)+hp*sqrt(Ne*Nc)).*(sqrt(Nd)+hp*sqrt(Ne*Nc))*V2p +
0.5*(sqrt(Nd)...
-hp*sqrt(Ne*Nc)).*(sqrt(Nd)-hp*sqrt(Ne*Nc))*V1m +
Shp*Ne*VVpin+(1-Nd)+Shp*(1-Nc*Ne);

%%%%%%%%%%%%%%%%%%%%%%%%%%%%%%%%%%%%%%%%%%%%%%%%%%%%%%%%%%%%%%%%%%%%%%%%%%%

'Defining the INPUT Stoke variances';
VS1in = Ah^2*VHpin + Av^2*VVpin - 2*Ah*Av*(X1vCX1hIN); 'These include
correlations';

VS2in = Ah^2*(cos(TH))^2*VVpin+Av^2*(cos(TH))^2*VHpin+Ah^2*(sin(TH))^2*...
        VVmin+Av^2*(sin(TH))^2*VHmin+2*Ah*Av*sin(TH)*cos(TH)*(X2vCX1hIN)-...
2*Ah*Av*sin(TH)*cos(TH)*(X1vCX2hIN)+2*Ah*Av*cos(TH)*cos(TH)*...
(X1vCX1hIN)-2*Ah*Av*sin(TH)*sin(TH)*(X2vCX2hIN)+2*Ah^2*sin(TH)*...
cos(TH)*(X1vCX2vIN)-2*Av^2*sin(TH)*cos(TH)*(X1hCX2hIN);


VS3in = Ah^2*(cos(TH))^2*VVmin+Av^2*(cos(TH))^2*VHmin+Ah^2*(sin(TH))^2*...
        VVpin+Av^2*(sin(TH))^2*VHpin+2*Ah*Av*sin(TH)*cos(TH)*(X1vCX2hIN)-...
2*Ah*Av*sin(TH)*cos(TH)*(X2vCX1hIN)-2*Ah*Av*cos(TH)*cos(TH)*...
(X2vCX2hIN)+2*Ah*Av*sin(TH)*sin(TH)*(X1vCX1hIN)+2*Av^2*sin(TH)*...
cos(TH)*(X1hCX2hIN)-2*Ah^2*sin(TH)*cos(TH)*(X1vCX2vIN);

%INPUT Stokes parameters Noise
NS1in = Ah^2*NHpin + Av^2*NVpin;          'no correlations for
noise!';

NS2in =
Ah^2*(cos(TH))^2*NVpin+Av^2*(cos(TH))^2*NHpin+Ah^2*(sin(TH))^2*NVmin+...
```

```
Av^2*(sin(TH))^2*NHmin;

NS3in =
Ah^2*(cos(TH))^2*NVmin+Av^2*(cos(TH))^2*NHmin+Ah^2*(sin(TH))^2*NVpin+...

Av^2*(sin(TH))^2*NHpin;


X1vCX1hOUT = X1vCX1hIN* hp.*hp *Ne;      % output correlations, if any
X2vCX2hOUT = X2vCX2hIN* hm.*hm *Ne;
X1vCX2hOUT = X1vCX2hIN* abs(hp.*hm) *Ne;
X2vCX1hOUT = X2vCX1hIN* abs(hp.*hm) *Ne;
X1vCX2vOUT = X1vCX2vIN* abs(hp.*hm) *Ne;
X1hCX2hOUT = X1hCX2hIN* abs(hp.*hm) *Ne;


'these are the Stoke OUTPUTS after the TELEPORTERS, ie 4 squeezers!';
VS1out = Ah^2*VHpout + Av^2*VVpout - 2*Ah*Av*(X1vCX1hOUT);

VS2out = Ah^2*(cos(TH))^2*VVpout+Av^2*(cos(TH))^2*VHpout+Ah^2*(sin(TH))^2*...
         VVmout+Av^2*(sin(TH))^2*VHmout+2*Ah*Av*sin(TH)*cos(TH)*...
 (X2vCX1hOUT)-2*Ah*Av*sin(TH)*cos(TH)*(X1vCX2hOUT)+2*Ah*Av*...
 cos(TH)*cos(TH)*(X1vCX1hOUT)-2*Ah*Av*sin(TH)*sin(TH)*(X2vCX2hOUT)...
 +2*Ah^2*sin(TH)*cos(TH)*(X1vCX2vOUT)-2*Av^2*sin(TH)*cos(TH)*...
 (X1hCX2hOUT);


VS3out = Ah^2*(cos(TH))^2*VVmout+Av^2*(cos(TH))^2*VHmout+Ah^2*(sin(TH))^2*...
         VVpout+Av^2*(sin(TH))^2*VHpout+2*Ah*Av*sin(TH)*cos(TH)*...
 (X1vCX2hOUT)-2*Ah*Av*sin(TH)*cos(TH)*(X2vCX1hOUT)-2*Ah*Av*...
 cos(TH)*cos(TH)*(X2vCX2hOUT)+2*Ah*Av*sin(TH)*sin(TH)*(X1vCX1hOUT)...
         +2*Av^2*sin(TH)*cos(TH)*(X1hCX2hOUT)-2*Ah^2*sin(TH)*cos(TH)*...
 (X1vCX2vOUT);


%%%%%%%%%%%%%%%%%%%%%%%%%%%%%%%%%%%%%%%%%%%%%%%%%%%% Stokes Noise on OUTPUT
NS1out = Ah^2*NHpout + Av^2*NVpout;

NS2out = Ah^2*(cos(TH))^2*NVpout+Av^2*(cos(TH))^2*NHpout+Ah^2*(sin(TH))^2...
         *NVmout+Av^2*(sin(TH))^2*NHmout;

NS3out = Ah^2*(cos(TH))^2*NVmout+Av^2*(cos(TH))^2*NHmout+Ah^2*(sin(TH))^2...
         *NVpout+Av^2*(sin(TH))^2*NHpout;

'Now find three transfer coefficients';

TS1=(VS1out./NS1out-1)./(VS1in/NS1in-1);
```

```
TS2=(VS2out./NS2out-1)./(VS2in/NS2in-1);
TS3=(VS3out./NS3out-1)./(VS3in/NS3in-1);

% below are the correlations of the input-output Stokes calculated in
Mathematica
% These are used to fing conditional variance of each parameter
CORsqr1 = hp.^2*Ne*(Ah^2*VHpin + Av^2*VVpin - 2*Ah*Av* X1vCX1hIN )^2;

CORsqr2 = (1/4)*Ne*(-Av^2*hm*VHmin + Av^2*hp*VHpin - Ah^2*hm*VVmin +...
          Ah^2*hp*VVpin + 2*Ah*Av*hp* X1vCX1hIN + 2*Ah*Av*hm* X2vCX2hIN +...
          (Av^2*(hm*VHmin+hp*VHpin) + Ah^2*(hm*VVmin+hp*VVpin) +...
          2*Ah*Av*(hp*X1vCX1hIN - hm*X2vCX2hIN))*cos(2*TH) + (hm -...
          hp)*(Av^2*X1hCX2hIN + Ah*Av*(X1vCX2hIN - X2vCX1hIN) - Ah^2 *...
          X1vCX2vIN)*sin(2*TH)).^2;

CORsqr3 = (1/4)*Ne*(Av^2*hm*VHmin - Av^2*hp*VHpin + Ah^2*hm*VVmin -...
          Ah^2*hp*VVpin - 2*Ah*Av*hp* X1vCX1hIN - 2*Ah*Av*hm* X2vCX2hIN +...
          (Av^2*(hm*VHmin+hp*VHpin) + Ah^2*(hm*VVmin+hp*VVpin) +...
          2*Ah*Av*(hp*X1vCX1hIN - hm*X2vCX2hIN))*cos(2*TH) + (hm -...
          hp)*(Av^2*X1hCX2hIN + Ah*Av*(X1vCX2hIN - X2vCX1hIN) - Ah^2 *...
          X1vCX2vIN)*sin(2*TH)).^2;

% conditional variances
B1=CORsqr1./VS1in;
B2=CORsqr2./VS2in;
B3=CORsqr3./VS3in;

CV1 = (VS1out-B1);
CV2 = (VS2out-B2);
CV3 = (VS3out-B3);

% This is the alternative method of finding conditional variance.
% It is a function of the above transfer coefficients and both
evatuations
% prove to be equal
C1=(1-TS1).*NS1out; 'This is still true for most symmetric cases,
correlations or none!';
C2=(1-TS2).*NS2out;
C3=(1-TS3).*NS3out;

%%%%%%%%%%%%%%%%%%%%%%%%%%%%%%%%%%%%%%%%%%%%%%%%%%%%%%%%%%%%%%%%%%%%%%%%%%%

'((((((((((((((((((((((((((( PLOT))))))))))))))))))))))))))';
m1 = 1+0*linspace(0,3,300);
n1 = linspace(0,3,300);
plot(n1,m1,'k.');          % here the horizontal axis is plotted
m2 = linspace(0,10,500);
n2 = .5+0*linspace(0,3,500);
```

```
hold on;
plot(n2,m2,'k.');          % here the vertical axis is plotted

AXIS([0 1 0 2])

plot(TS3, CV3, 'r-');     % here a chosen pair of parameters T and CV
for either
YLABEL('CV');             % of the 3 Stokes is plotted.
XLABEL('T');
zoom on;
```

A.2 The QND-teleporter program

```
% Plot of teleportation and QND schemes as function of gains
% Stoke parameters are characterised, (not quadratures!)
clear;

VHpin=10; 'Signal + Noise quadrature inputs';
VHmin=10;
VVpin=10;
NHpin=1; 'this is the vacuum noise on the SIGNAL, not the squeezed
beam!';
NHmin=1;
NVpin=1;

'**************     VERTICAL DC carrier polarisation info !    ';

Av=1;      % amplitude normalised to one
TH= pi/1;  % THETA, the phase angle between the two!

SQ2=.4;    % Squeezing variances for the three beams
SQ3=.2;
SQ4=.7;

V2p=SQ2;   % This is SQ3, QND beam in the text

V3p=SQ3;   % These are the teleporter squeezed beams,
V3m=1/SQ3; %  minimum uncertainty states
V4p=SQ4;
V4m=1/SQ4;

'These are the correlations due to the modulation, either 1 or -1 !!';
X1hCX2hIN=0;

%%%%%%%%%%%%%%%%%%%%%%%%%%%%%%%%%%%%%%%%%%%%%%%%%%%%%%%%%%%%%%%%%%%%%%%%%%%

'((((((((((((((((TELEPORT as funct of gain h))))))))))))))))';

Nc=1;'transmission efficiencies, assumed ideal';
Nd=Nc;
Ne=Nc;'detection efficiency';

hm = -1*linspace(0,2.2,300);'gain arrays, always opposite sign';
hp = linspace(0,2.2,300);''

'below is calculated from Vout with Vin = Nin, ie the noise only';
NHmout=0.5*(sqrt(Nd)+hm*sqrt(Ne*Nc)).*(sqrt(Nd)+hm*sqrt(Ne*Nc))*V4m +...
       0.5*(sqrt(Nd)-hm*sqrt(Ne*Nc)).*(sqrt(Nd)-hm*sqrt(Ne*Nc))*V3p + ...
       Ne*NHmin+(1-Nd)+(1-Nc*Ne);
```

```
NHpout=0.5*(sqrt(Nd)+hp*sqrt(Ne*Nc)).*(sqrt(Nd)+hp*sqrt(Ne*Nc))*V4p +...
       0.5*(sqrt(Nd)-hp*sqrt(Ne*Nc)).*(sqrt(Nd)-hp*sqrt(Ne*Nc))*V3m + ...
       Ne*NHpin+(1-Nd)+(1-Nc*Ne);

'the TRANSFER function for the quadratures in the two teleporters';
'the attenuations, etc are assumed to have equal values';
VHmout=0.5*(sqrt(Nd)+hm*sqrt(Ne*Nc)).*(sqrt(Nd)+hm*sqrt(Ne*Nc))*V4m +...
       0.5*(sqrt(Nd)-hm*sqrt(Ne*Nc)).*(sqrt(Nd)-hm*sqrt(Ne*Nc))*V3p + ...
       Ne*VHmin+(1-Nd)+(1-Nc*Ne);

VHpout=0.5*(sqrt(Nd)+hp*sqrt(Ne*Nc)).*(sqrt(Nd)+hp*sqrt(Ne*Nc))*V4p +...
       0.5*(sqrt(Nd)-hp*sqrt(Ne*Nc)).*(sqrt(Nd)-hp*sqrt(Ne*Nc))*V3m + ...
       Ne*VHpin+(1-Nd)+(1-Nc*Ne);

%%%%%%%%%%%%%%%%%%%%%%%%%%%%%%%%%%%%%%%%%%%%%%%%%%%%%%%%%%%%%%%%%%%%%%%%%%%%
'((((((((((((((((QND as funct of gain h))))))))))))))))';

Vdet=1;   'detection loss noise';
Vmodm=1;  'modulator noise';
nm=Nc;    'electronic transfer efficiency';
nd=Nc;    'signal detection efficiency';

G=linspace(0,2.5, 600);'the in loop gain of QND';

'transfer of the signal';
VVpout = nm*((nd*(VVpin) + (1-nd)*Vdet)*G.^2) + V2p + (1-nm)*Vmodm;

NVpout = nm*((nd*(NVpin) + (1-nd)*Vdet)*G.^2) + V2p + (1-nm)*Vmodm;

'Conditional variance';
Vqq = VVpout - nm*nd*G.^2*(VVpin);

'Transfer coefficient for signal';
Tss=nd*nm*G.^2*NVpin./(nm*((1-nd)*G.^2*Vdet + V2p + nd*G.^2*NVpin) +
(1-nm)*Vmodm);
%%%%%%%%%%%%%%%%%%%%%%%%%%%%%%%%%%%%%%%%%%%%%%%%%%%%%%%%%%%%%%%%%%%%%%%%%%%%


X1hCX2hOUT = X1hCX2hIN* abs(hm.*hp) *Ne; % output correlations, if any

%%%%%%%%%%%%%%%%%%%%%%%%%%%%%%%%%%%%%%%%%%%%%%%%%%%%%%%%%%%%%%%%%%%%%%%%%%%%

'((((((((((((((Defining the Stoke variances))))))))))))))';

'these are the Stoke INPUTS before the TELEPORTER';
VS1in = Av^2*VVpin; 'These include correlations';
```

```
VS2in = Av^2*(cos(TH))^2*VHpin+Av^2*(sin(TH))^2*VHmin-
2*Av^2*sin(TH)*cos(TH)*...
(X1hCX2hIN);

VS3in = Av^2*(cos(TH))^2*VHmin+Av^2*(sin(TH))^2*VHpin+
2*Av^2*sin(TH)*cos(TH)*...
(X1hCX2hIN);

NS1in = Av^2*NVpin; 'no correlations for noise!';
NS2in = Av^2*(cos(TH))^2*NHpin + Av^2*(sin(TH))^2*NHmin;
NS3in = Av^2*(cos(TH))^2*NHmin + Av^2*(sin(TH))^2*NHpin;

'these are the Stoke OUTPUTS after the TELEPORTER, ie 3 squeezers!';
VS1out = Av^2*VVpout;

VS2out = Av^2*(cos(TH))^2*VHpout + Av^2*(sin(TH))^2*VHmout -
2*Av^2*sin(TH)...
*cos(TH)*(X1hCX2hOUT);

VS3out = Av^2*(cos(TH))^2*VHmout + Av^2*(sin(TH))^2*VHpout +
2*Av^2*sin(TH)...
*cos(TH)*(X1hCX2hOUT);

%%%%%%%%%%%%%%%%%%%%%%%%%%%%%%%%%%%%%%%%%%%%%%%%%%%%%%%%%%%% Stokes
Noise on OUTPUT
NS1out = Av^2*NVpout;
NS2out = Av^2*(cos(TH))^2*NHpout+Av^2*(sin(TH))^2*NHmout;
NS3out = Av^2*(cos(TH))^2*NHmout+Av^2*(sin(TH))^2*NHpout;

'Now find three Stokes transfer coefficients';

TS1=(VS1out./NS1out-1)./(VS1in/NS1in-1);
TS2=(VS2out./NS2out-1)./(VS2in/NS2in-1);
TS3=(VS3out./NS3out-1)./(VS3in/NS3in-1);
% below are the correlations of the input-output Stokes calculated in
Mathematica
% These are used to fing conditional variance of each parameter
CORv1 = nm*nd*(G.^2)*VVpin^2;

CORv2 = (Ne/4)*(-(Av^2)*hm*VHmin + (Av^2)*hp*VHpin + (Av^2)*(hm*VHmin...
       + hp*VHpin)*cos(2*TH) + (Av^2)*(hm - hp)* X1hCX2hIN *sin(2*TH)).^2;

CORv3 = (Ne/4)*((Av^2)*hm*VHmin - (Av^2)*hp*VHpin + (Av^2)*(hm*VHmin...
       + hp*VHpin)*cos(2*TH) + (Av^2)*(hm - hp)* X1hCX2hIN *sin(2*TH)).^2;

% conditional variances
CV1 = (VS1out-CORv1./VS1in);
CV2 = (VS2out-CORv2./VS2in);
```

```
CV3 = (VS3out-CORv3./VS3in);

% This is the alternative method of finding conditional variance.
% It is a function of the above transfer coefficients and both
evatuations
% prove to be equal
C1 = (1-TS1).*NS1out;
C2 = (1-TS2).*NS2out;
C3 = (1-TS3).*NS3out;

%%%%%%%%%%%%%%%%%%%%%%%%%%%%%%%%%%%%%%%%%%%%%%%%%%%%%%%%%%%%%%%%%%%%%%%%%%%%

'((((((((((((((((((((((((( PLOT))))))))))))))))))))))))))';

m1 = 1+0*linspace(0,3,300);
n1 = linspace(0,3,300);
plot(n1,m1,'k.');          % here the horizontal axis is plotted
m2 = linspace(0,10,500);
n2 = .5+0*linspace(0,3,500);
hold on;
plot(n2,m2,'k.');          % here the vertical axis is plotted

AXIS([0 1 0 2])

plot(TS3, CV3, 'r-');     % here a chosen pair of parameters T and CV
for either
YLABEL('CV');             % of the 3 Stokes is plotted.
XLABEL('T');
zoom on;

% NOTE: The T1 and CV1 are better visualised on the scheme
% outlined in Chapter 5.
%%%%%%%%%%%%%%%%%%%%%%%%%%%%%%%%%%%%%%%%%%%%%%%%%%%%%%%%%%%%%%%%%%%%%%%%%%%%
```

A.3 Fidelity optimisation code

Below is the code for generating maximum fidelity values by optimising the parameters in the biased entanglement scheme. It demonstrates the approach for a given range of regime 1, which was repeated for the entire parameter spectrum. It is followed by the retieving and plotting code.

```
%%%%%%%%%%%%%%%%%%%%%%%%%%%%%%%%%%%%%%%%%%%%%%%%%%%%%%%%%%%%%%%%%%%%%%%%%%%%%%%
% Program for finding the optimum fidelity for a given squeezing parameter
% Positive g+ case
% Phase squeezing  (regime 1)

clear

VamVec = 0.1:.006:.3;    % Range of squeezing
V3 = VamVec;             % vector to be saved to file

% Due to the limited computational time and memory I had to conduct the
% calculation in various ranges of parameters. The optimum fidelity regions
% for each squeezing parameter were first estimated using contour plots in
% Mathematica.

N = 0.2:.0025:.45;       % BS1 - epsilon1 chosen optimum range
E = 0.11:.0009:.2;       % BS2 - epsilon2 chosen optimum range

% Looping over all the V squeezing, E and N values

for i = 1:length(VamVec)

  Vap = 1/VamVec(i);

  for j = 1:length(E)
      e = E(j);

  for k = 1:length(N)
          n = N(k);
          FidelityPosGain1(j,k) = (2*((-1+e).*(-1+(-1+Vap)*e.*(n-1)...
  +n-Vap*n)).^(1/2))./((((-2 + 2*(Vap-1)*e.*(n-1) + n - ...
  Vap*n).*(-3 + n - Vap*n - 2*(1-Vap)*((e-1).*(n-1).*e.*n).^(1/2)...
          + (3-2*n+Vap*(2*n-1)).*e))).^(1/2));
      end
  end

  FNMaxR(i) = max(max(FidelityPosGain1));
  % here maximum fidelity value is found in the matrix

  [x,y]=find(FNMaxR(i)==FidelityPosGain1);
  % the corresponding BS transmittivities are found and put into a matrix
```

```
  eANDn(i,1) = E(x(1));      % first column = E values
  eANDn(i,2) = N(y(1));      % second column = N values

end

FNMaxR3 = FNMaxR;
eANDn3 = eANDn;
save Data3 FNMaxR3 V3 eANDn3 % the results of optimisation are saved

%%%%%%%%%%%%%%%%%%%%%%%%%%%%%%%%%%%%%%%%%%%%%%%%%%%%%%%%%%%%%%%%%%%%%%%%%%%%








%%%%%%%%%%%%%%%%%%%%%%%%%%%%%%%%%%%%%%%%%%%%%%%%%%%%%%%%%%%%%%%%%%%%%%%%%%%%
% The program for retrieving and plotting the optimal fidelity data
clear;

load Data3 V3 FNMaxRneg3;     % retrieve data from the files
FNM = FNMaxRneg6;             % the optimal fidelity values
Vsq = V6;                     % the corresponding variances of the squeezed beam

SQv=1;                        % vacuum squeezing parameter

'((((((((((((((((TELEPORT as funct of gain h))))))))))))))))';

SQa=Vsq;                         'the squeezing parameter, smaller, the better!';
SQb=SQa;

Vam=SQa;
Vap=1./SQa;
Vbm=SQb;
Vbp=1./SQb;

Vinm=1;
Vinp=1;                          'noise + signal';

Vvm=SQv;                         'quantum noise, can be squeezed!!';
Vvp=1/SQv;

N=0.5;                           'beam splitter ratio';
Nc=1;                            'transmission efficiencies';
Nd=1;
```

```
Ne=1;                              'detection efficiency';

hm = 1;                            % fixed unity gains;
hp = -1;

%the TRANSFER function of the Biased Entanglement teleporter

Voutm=0.5*(sqrt(Nd)+hm*sqrt(Ne*Nc))*(sqrt(Nd)+hm*sqrt(Ne*Nc))*Vam + ...
      0.5*(sqrt(Nd) - hm*sqrt(Ne*Nc))*(sqrt(Nd)-hm*sqrt(Ne*Nc))*Vbp + Ne*Vinm...
  + (1-Nd) + (1-Nc*Ne);

Voutp=0.5*(sqrt(Nd)+hp*sqrt(Ne*Nc))*(sqrt(Nd)+hp*sqrt(Ne*Nc))*Vap + ...
      0.5*(sqrt(Nd) - hp*sqrt(Ne*Nc))*(sqrt(Nd)-hp*sqrt(Ne*Nc))*Vbm + Ne*Vinp
  + (1-Nd) + (1-Nc*Ne);

%%%%%%%%%%%%%%%%%%%%%%%%%%%%%%%%%%%%%%%%%%%%%%%%%%%%%%%%%%%%%%%%%%%%%%%%%%%%

'((((((((((((((((((((((((( FIDELITY))))))))))))))))))))))))';
FID = (2./((Voutm + 1).*(1 + Voutp)).^(1/2));
% single teleporter fidelity for the Horizontal fluctuations.

TotFID = FID.* FNM;
% 3-sqz OPTIMISED system, the above fidelity times the optimal Vertical value
'((((((((((((((((((((((((( PLOT))))))))))))))))))))))))';

plot(Vsq, TotFID, 'r-');          % optimised system - 3sqz
hold on;
plot(Vsq, FID*sqrt(2/3), 'b-');   % system with perfect QND, 2sqz
plot(Vsq, FID.^2, 'g-');          % 4sqz, NON optimal system
zoom on;
axis([0,1,0.2,1])

YLABEL('Fidelity');
XLABEL('Variance of the squeezed quadrature');

%%%%%%%%%%%%%%%%%%%%%%%%%%%%%%%%%%%%%%%%%%%%%%%%%%%%%%%%%%%%%%%%%%%%%%%%%%%%
% This procedure was repeated for the entire Vsqueezed range,
% and the three regimes
```

The supplement of full mathematical expressions

In this appendix, full mathematical expressions derived on Mathematica, which did not fit in the thesis text, will be listed.

B.1 (a) **

These are the standard teleporter output quadrature expressions

$$X_{out}^{+} = \frac{X^{+}_{sQ2}\ \sqrt{n_d}}{\sqrt{2}} + \frac{X^{-}_{sQ1}\ \sqrt{n_d}}{\sqrt{2}} + \sqrt{1-n_d}\ X^{+}_{v4} - \frac{\lambda_{+}\sqrt{n_c}\ \sqrt{n_e}\ X^{-}_{sQ1}}{\sqrt{2}} + \frac{\lambda_{+}\sqrt{n_c}\ \sqrt{n_e}\ X^{+}_{sQ2}}{\sqrt{2}} + \lambda_{+}\sqrt{n_e}\ X^{+}_{sig} + \lambda_{+}\sqrt{1-n_c}\ \sqrt{n_e}\ X^{+}_{v1} + \lambda_{+}\sqrt{1-n_e}\ X^{+}_{v2}$$

$$X_{out}^{-} = \frac{X^{-}_{sQ2}\ \sqrt{n_d}}{\sqrt{2}} - \frac{X^{+}_{sQ1}\ \sqrt{n_d}}{\sqrt{2}} + \sqrt{1-n_d}\ X^{-}_{v4} + \frac{\lambda_{-}\sqrt{n_c}\ \sqrt{n_e}\ X^{-}_{sQ2}}{\sqrt{2}} - \lambda_m\sqrt{n_e}\ X^{-}_{sig} + \lambda_{-}\sqrt{1-n_c}\ \sqrt{n_e}\ X^{-}_{v1} + \frac{\lambda_{-}\sqrt{n_c}\ \sqrt{n_e}\ X^{+}_{sQ1}}{\sqrt{2}} + \lambda_{-}\sqrt{1-n_e}\ X^{-}_{v3}$$

B.1 (b) Reference to section 2.5.3 ** ** ** ** ** ** ** ** ** ** ** ** **

These are the standard teleporter output variances, the full expressions (eq 2.1) Full expressions contain the transmission (η_c, η_d) and detection (η_e) efficiency terms. The vacuum inputs are already assumed to be $V_v^{\pm} = 1$.

$$V_{out}^{-} = \frac{1}{2}\left(\sqrt{\eta_d} + \lambda_{-}\sqrt{\eta_c\,\eta_e}\right)^2 V_{SQ2}^{-} + \frac{1}{2}\left(\sqrt{\eta_d} - \lambda_{-}\sqrt{\eta_c\,\eta_e}\right)^2 V_{SQ1}^{+} + \lambda_{-}^{2}\,\eta_e\,V_{in}^{-} + 1 - \eta_d + \lambda_{-}^{2}\,(1-\eta_c\,\eta_e)$$

$$V_{out}^{+} = \frac{1}{2}\left(\sqrt{\eta_d} + \lambda_{+}\sqrt{\eta_c\,\eta_e}\right)^2 V_{SQ2}^{+} + \frac{1}{2}\left(\sqrt{\eta_d} - \lambda_{+}\sqrt{\eta_c\,\eta_e}\right)^2 V_{SQ1}^{-} + \lambda_{+}^{2}\,\eta_e\,V_{in}^{+} + 1 - \eta_d + \lambda_{+}^{2}\,(1-\eta_c\,\eta_e)$$

B.2 Reference to section 4.3 ** ** ** ** ** ** ** ** ** ** ** ** ** **

These are the Stokes cross-correlation expressions: $|\langle \delta S_{in}\ \delta S_{out}\rangle|^2$

used for conditional variance calculation: $V^{Si}_{cv} = V^{Si}_{out} - \frac{|\langle \delta S_{in}\ \delta S_{out}\rangle|^2}{V^{Si}_{in}}$

the input variances notation VHpin $= V^{+}_{H}$

and input quadratures notation XHpin $= X^{+}_{H}$

Ne = all detection and transmission efficiencies, assumed symmetric for both teleporters

The cross correlated classical terms notation: XHpinXVpin $= \langle X^{+}_{H}\ X^{+}_{V}\rangle$

$$|\langle \delta S1_{in}\,\delta S1_{out}\rangle|^2 = \lambda_+^{2}\,\mathrm{Ne}\left(\alpha_H^2\,\mathrm{VHpin} + \alpha_V^2\,\mathrm{VVpin} - 2\,\alpha_H\,\alpha_V\,\mathrm{XHpinXVpin}\right)^2$$

$$\begin{aligned}|\langle \delta S2_{in}\,\delta S2_{out}\rangle|^2 = \frac{1}{4}\,\mathrm{Ne}\Big(&-\alpha_V^2\,\lambda_-\,\mathrm{VHmin} + \alpha_V^2\,\lambda_+\,\mathrm{VHpin} - \alpha_H^2\,\lambda_-\,\mathrm{VVmin} + \alpha_H^2\,\lambda_+\,\mathrm{VVpin} +\\ &2\,\alpha_H\,\alpha_V\,\lambda_-\,\mathrm{XHminXVmin} + 2\,\alpha_H\,\alpha_V\,\lambda_+\,\mathrm{XHpinXVpin} +\\ &\big(\alpha_V^2\,(\lambda_-\,\mathrm{VHmin} + \lambda_+\,\mathrm{VHpin}) + \alpha_H^2\,(\lambda_-\,\mathrm{VVmin} + \lambda_+\,\mathrm{VVpin}) +\\ &\alpha_H\,\alpha_V\,(-2\,\lambda_-\,\mathrm{XHminXVmin} + 2\,\lambda_+\,\mathrm{XHpinXVpin})\big)\,\mathrm{Cos}[2\,\theta] +\\ (\lambda_- - \lambda_+)&\left(\alpha_V^2\,\mathrm{XHminXHpin} + \alpha_H\,\alpha_V\,(\mathrm{XHminXVpin} - \mathrm{XHpinXVmin}) - \alpha_H^2\,\mathrm{XVminXVpin}\right)\mathrm{Sin}[2\,\theta]\Big)^2\end{aligned}$$

$$\begin{aligned}|\langle \delta S3_{in}\,\delta S3_{out}\rangle|^2 = \frac{1}{4}\,\mathrm{Ne}\Big(&\alpha_V^2\,\lambda_-\,\mathrm{VHmin} - \alpha_V^2\,\lambda_+\,\mathrm{VHpin} + \alpha_H^2\,\lambda_-\,\mathrm{VVmin} - \alpha_H^2\,\lambda_+\,\mathrm{VVpin} -\\ &2\,\alpha_H\,\alpha_V\,\lambda_-\,\mathrm{XHminXVmin} - 2\,\alpha_H\,\alpha_V\,\lambda_+\,\mathrm{XHpinXVpin} +\\ &\big(\alpha_V^2\,(\lambda_-\,\mathrm{VHmin} + \lambda_+\,\mathrm{VHpin}) + \alpha_H^2\,(\lambda_-\,\mathrm{VVmin} + \lambda_+\,\mathrm{VVpin}) +\\ &\alpha_H\,\alpha_V\,(-2\,\lambda_-\,\mathrm{XHminXVmin} + 2\,\lambda_+\,\mathrm{XHpinXVpin})\big)\,\mathrm{Cos}[2\,\theta] +\\ (\lambda_- - \lambda_+)&\left(\alpha_V^2\,\mathrm{XHminXHpin} + \alpha_H\,\alpha_V\,(\mathrm{XHminXVpin} - \mathrm{XHpinXVmin}) - \alpha_H^2\,\mathrm{XVminXVpin}\right)\mathrm{Sin}[2\,\theta]\Big)^2\end{aligned}$$

B.3 (a) Reference to section 4.3 ** ** ** ** ** ** ** ** ** ** ** ** ** **

These are the Stokes TRANSFER COEFFICIENTS for the double teleporter scheme when the four squeezing parameters and non symmetric.

All efficiencies are assumed ideal for both teleporters

Unity gain is assumed for compact, analytical solution

$$T_{S1} = \frac{1}{1 - 2\left(-1 + \alpha_H^2\right)\mathrm{SQ2} + 2\,\alpha_H^2\,\mathrm{SQ4}}$$

$$T_{S2} = \frac{1}{\left(1 + 2\,\alpha_H^2\,(\mathrm{SQ2} - \mathrm{SQ4}) + 2\,\mathrm{SQ4}\right)\mathrm{Cos}[\theta]^2 + \left(1 + 2\,\alpha_H^2\,(\mathrm{SQ1} - \mathrm{SQ3}) + 2\,\mathrm{SQ3}\right)\mathrm{Sin}[\theta]^2}$$

$$T_{S3} = \frac{1}{\left(1 + 2\,\alpha_H^2\,(\mathrm{SQ1} - \mathrm{SQ3}) + 2\,\mathrm{SQ3}\right)\mathrm{Cos}[\theta]^2 + \left(1 + 2\,\alpha_H^2\,(\mathrm{SQ2} - \mathrm{SQ4}) + 2\,\mathrm{SQ4}\right)\mathrm{Sin}[\theta]^2}$$

B.3 (b) **

These are the Stokes CONDITIONAL VARIANCES for the double teleporter scheme when the four squeezing parameters and non symmetric.

$$\begin{aligned}V_{CV}^{S1} = \frac{1}{2\,\mathrm{SQ1}\,\mathrm{SQ3}}\Big(&(2 + 2\,\mathrm{SQ1}\,\mathrm{SQ2} + 2\,(-1 + \mathrm{SQ1}\,\mathrm{SQ2}))\,\mathrm{SQ3} +\\ &\alpha_H^2\,\mathrm{SQ1}\,(2 - 2\,\mathrm{SQ2}\,\mathrm{SQ3} + 2\,\mathrm{SQ3}\,\mathrm{SQ4} - 2\,(1 + \mathrm{SQ2}\,\mathrm{SQ3} - \mathrm{SQ3}\,\mathrm{SQ4})\end{aligned}$$

$$\begin{aligned}V_{CV}^{S2} = \mathrm{SQ3} + \alpha_H^2\,(\mathrm{SQ1} + \mathrm{SQ2} - \mathrm{SQ3} - \mathrm{SQ4}) +&\\ \mathrm{SQ4} + \left(-\mathrm{SQ3} + \mathrm{SQ4} + \alpha_H^2\,(-\mathrm{SQ1} + \mathrm{SQ2} + \mathrm{SQ3} - \mathrm{SQ4})\right)&\mathrm{Cos}[2\,\theta]\end{aligned}$$

$$\begin{aligned}V_{CV}^{S3} = \mathrm{SQ3} + \alpha_H^2\,(\mathrm{SQ1} + \mathrm{SQ2} - \mathrm{SQ3} - \mathrm{SQ4}) +&\\ \mathrm{SQ4} + \left(\mathrm{SQ3} - \mathrm{SQ4} + \alpha_H^2\,(\mathrm{SQ1} - \mathrm{SQ2} - \mathrm{SQ3} + \mathrm{SQ4})\right)&\mathrm{Cos}[2\,\theta]\end{aligned}$$

B.4 (a) Reference to section 5.3 ** ** ** ** ** ** ** ** ** ** ** ** ** **

These are the Stokes TRANSFER COEFFICIENTS and CONDITIONAL VARIANCES for S_1 and S_3, in the QND-teleporter scheme.

All efficiencies are assumed ideal.

$$V_{cv}^{S2} = -\frac{1}{4\,SQ3\,SQ4}$$
$$((1 + SQ3\,SQ4 + 2\,\lambda_+\,(-1 + SQ3\,SQ4) + \lambda_+^2\,(1 + SQ3\,SQ4))\,(-SQ3 - SQ4 + (SQ3 - SQ4)\,\mathrm{Cos}[2\theta]))$$

$$T_{S2} = (2\,\lambda_+^2\,SQ3\,SQ4) /$$
$$(SQ4\,(1 + SQ3\,SQ4 + 2\,\lambda_+\,(-1 + SQ3\,SQ4) + \lambda_+^2\,(1 + SQ3\,(2 + SQ4)))\,\mathrm{Cos}[\theta]^2 +$$
$$SQ3\,(1 + SQ3\,SQ4 + 2\,\lambda_+\,(-1 + SQ3\,SQ4) + \lambda_+^2\,(1 + (2 + SQ3)\,SQ4))\,\mathrm{Sin}[\theta]^2)$$

B.4 (b) **

$$V_{cv}^{S3} = \frac{1}{4\,SQ3\,SQ4}$$
$$((1 + SQ3\,SQ4 + 2\,\lambda_+\,(-1 + SQ3\,SQ4) + \lambda_+^2\,(1 + SQ3\,SQ4))\,(SQ3 + SQ4 + (SQ3 - SQ4)\,\mathrm{Cos}[2\theta]))$$

$$T_{S3} = (2\,\lambda_+^2\,SQ3\,SQ4) /$$
$$(SQ3\,(1 + SQ3\,SQ4 + 2\,\lambda_+\,(-1 + SQ3\,SQ4) + \lambda_+^2\,(1 + (2 + SQ3)\,SQ4))\,\mathrm{Cos}[\theta]^2 +$$
$$SQ4\,(1 + SQ3\,SQ4 + 2\,\lambda_+\,(-1 + SQ3\,SQ4) + \lambda_+^2\,(1 + SQ3\,(2 + SQ4)))\,\mathrm{Sin}[\theta]^2)$$

The T_{S2} and T_{S3} as well as V_{cv}^{S2} and V_{cv}^{S3} are seen to depend on polarisation angle θ with a π rad difference which makes their behaviour "out of phase". This can be seen in section 5.3

B.5 Reference to section 6.3 ** ** ** ** ** ** ** ** ** ** ** ** ** **

These are the output quadrature and variance expressions for the BE-teleporter scheme.

$$X_{out}^{+} = 2\,\sqrt{1-\epsilon 2}\;g_+\;X_{sig}^{+} +$$
$$X_v^{+}\;\left(\sqrt{1-\epsilon 1} + 2\,\sqrt{\epsilon 2}\;g_+\;\sqrt{\epsilon 1}\right) + X_{sq}^{+}\;\left(2\,\sqrt{\epsilon 2}\;g_+\;\sqrt{1-\epsilon 1} - \sqrt{\epsilon 1}\right)$$

$$X_{out}^{-} =$$
$$-2\,\sqrt{\epsilon 2}\;g_-\;X_{noise}^{-} + X_v^{-}\;\left(\sqrt{1-\epsilon 1} + 2\,\sqrt{1-\epsilon 2}\;g_-\;\sqrt{\epsilon 1}\right) + X_{sq}^{-}\;\left(2\,\sqrt{1-\epsilon 2}\;g_-\;\sqrt{1-\epsilon 1} - \sqrt{\epsilon 1}\right)$$

$$V_{out}^{+} =$$
$$4\,(1-\epsilon 2)\,g_+^2\,V_{sig}^{+} + V_v^{+}\;\left(\sqrt{1-\epsilon 1} + 2\,\sqrt{\epsilon 2}\;g_+\;\sqrt{\epsilon 1}\right)^2 + V_{sq}^{+}\;\left(2\,\sqrt{\epsilon 2}\;g_+\;\sqrt{1-\epsilon 1} - \sqrt{\epsilon 1}\right)^2$$

$$V_{out}^{-} =$$
$$4\,\epsilon 2\,g_-^2\,V_{noise}^{-} + V_v^{-}\;\left(\sqrt{1-\epsilon 1} + 2\,\sqrt{1-\epsilon 2}\;g_-\;\sqrt{\epsilon 1}\right)^2 + V_{sq}^{-}\;\left(2\,\sqrt{1-\epsilon 2}\;g_-\;\sqrt{1-\epsilon 1} - \sqrt{\epsilon 1}\right)^2$$

B.6 Reference to section 6.3 ** ** ** ** ** ** ** ** ** ** ** ** ** **

The fidelity expressions which were optimised in chapter 6.

The noise terms are all assumed to be minimum uncertainty states (shot noise)

Firstly:

the amplitude modulator gain was fixed to the UNITY gain condition for optimum fidelity,

$$g_+ = \frac{1}{2\sqrt{1-\epsilon 2}}$$

The fidelity then becomes:

$$\text{FIDELITY} = \left(4\sqrt{(-1+\epsilon 2)\,V_{sq}^{+}}\right) \Big/ \left(\sqrt{\left(\left(-5+4\epsilon 2-2\sqrt{-(-1+\epsilon 2)\,\epsilon 2}+\left(-1+2\sqrt{-(-1+\epsilon 2)\,\epsilon 2}\right)V_{sq}^{+}\right)\left(1+4\sqrt{1-\epsilon 2}\,g_-\left(-1+V_{sq}^{+}\right)+3V_{sq}^{+}+4g_-^{2}\left(1+\epsilon 2\left(-1+V_{sq}^{+}\right)+V_{sq}^{+}\right)\right)\right)}\right)$$

(4 variables = $\epsilon 1$, $\epsilon 2$, V_{sq}^{+}, g_-)

Secondly:

the phase modulator gain was fixed to the value optimising fidelity,

$$g_- = \frac{-\sqrt{1-\epsilon 2}\;V_{sq}^{+}\;\sqrt{1-\epsilon 1}\;\sqrt{\epsilon 1}\;+\;\sqrt{1-\epsilon 2}\;V_{v}^{+}\;\sqrt{1-\epsilon 1}\;\sqrt{\epsilon 1}}{2\;\epsilon 2\;V_{sq}^{+}\;V_{v}^{+}\;+\;2\;(1-\epsilon 2)\;V_{v}^{+}\;(1-\epsilon 1)\;+\;2\;(1-\epsilon 2)\;V_{sq}^{+}\;\epsilon 1}$$

The fidelity then becomes:

$$\text{FIDELITY} = 2 \Big/ \left(\sqrt{\left(-\left(\left(1+V_{v}^{+}+V_{sq}^{+}\;\epsilon 1-V_{v}^{+}\;\epsilon 1+\epsilon 2\left(-1-V_{v}^{+}+V_{sq}^{+}\left(1+V_{v}^{+}-2\epsilon 1\right)+2V_{v}^{+}\;\epsilon 1\right)\right)\right.\right.$$
$$\left(2\epsilon 2^{3/2}\left(V_{sq}^{+}-V_{v}^{+}\right)\sqrt{-(-1+\epsilon 1)\,\epsilon 1}+2\sqrt{\epsilon 2}\left(-V_{sq}^{+}+V_{v}^{+}\right)\sqrt{-(-1+\epsilon 1)\,\epsilon 1}+\right.$$
$$\sqrt{1-\epsilon 2}\left(2+V_{v}^{+}+V_{sq}^{+}\;\epsilon 1-V_{v}^{+}\;\epsilon 1\right)+$$
$$\left.\left.\sqrt{1-\epsilon 2}\;\epsilon 2\left(-2+V_{sq}^{+}-2V_{sq}^{+}\;\epsilon 1+V_{v}^{+}\;(-1+2\epsilon 1)\right)\right)\right) \Big/$$
$$\left.\left.\left((1-\epsilon 2)^{3/2}\left((-1+\epsilon 2)\,V_{sq}^{+}\;\epsilon 1+V_{v}^{+}\;\left(-1+\epsilon 1-\epsilon 2\left(-1+V_{sq}^{+}+\epsilon 1\right)\right)\right)\right)\right)\right)$$

(3 variables = $\epsilon 1$, $\epsilon 2$, V_{sq}^{+})

For BE scheme, 3 squeezed beams fidelity optimisation vacuum V_v^+ was assumed to be 1

For the double teleporter, 4 squeezed beams fidelity optimisation the V_v^+ term was squeezed/ antisqueezed.

B.7 Reference to section 6.4 ** ** ** ** ** ** ** ** ** ** ** ** **

this is the optimisation of the **full teleporter** for the amplitude coded signal
1,2 = SQUEEZED BEAM FIELDs, η = BS1, e = BS2
b = SIGNAL field, but we know it is only REAL

everything up to this point is the same as in BE-teleporter optimisation

$$xoutp = 2\sqrt{1-e}\, g_+ Xbp + Xvp\left(\sqrt{1-\eta} + 2\sqrt{e}\, g_+ \sqrt{\eta}\right) + Xap\left(2\sqrt{e}\, g_+ \sqrt{1-\eta} - \sqrt{\eta}\right);$$

$$xoutm = -2\sqrt{e}\, g_- Xbm + Xvm\left(\sqrt{1-\eta} + 2\sqrt{1-e}\, g_- \sqrt{\eta}\right) + Xam\left(2\sqrt{1-e}\, g_- \sqrt{1-\eta} - \sqrt{\eta}\right);$$

now Xvp/ Xvm become the other squeezed BRIGHT beam

$$Xoutp = 2\sqrt{1-e}\, gp\, Xbp + X1p\left(\sqrt{1-\eta} + 2\sqrt{e}\, gp \sqrt{\eta}\right) + X2p\left(2\sqrt{e}\, gp \sqrt{1-\eta} - \sqrt{\eta}\right);$$

$$Xoutm = -2\sqrt{e}\, gm\, Xbm + X1m\left(\sqrt{1-\eta} + 2\sqrt{1-e}\, gm \sqrt{\eta}\right) + X2m\left(2\sqrt{1-e}\, gm \sqrt{1-\eta} - \sqrt{\eta}\right);$$

$$Voutp = 4(1-e)\, g_+^2\, Vbp + V1p\left(\sqrt{1-\eta} + 2\sqrt{e}\, g_+ \sqrt{\eta}\right)^2 + V2p\left(2\sqrt{e}\, g_+ \sqrt{1-\eta} - \sqrt{\eta}\right)^2;$$

$$Voutm = 4e\, g_-^2\, Vbm + V1m\left(\sqrt{1-\eta} + 2\sqrt{1-e}\, g_- \sqrt{\eta}\right)^2 + V2m\left(2\sqrt{1-e}\, g_- \sqrt{1-\eta} - \sqrt{\eta}\right)^2;$$

^^

Vinp = Vbp;
Vinm = 1; shot noise only in this quadrature

V1m = 1 / V1p; minimum uncertainty states
V2m = 1 / V2p;

$$g_+ = \frac{1}{2\sqrt{1-e}};$$ Gain for positive quadrature

$$\left\{\left\{g_- \to \frac{\sqrt{1-e}\, V1p \sqrt{1-\eta}\sqrt{\eta} - \sqrt{1-e}\, V2p \sqrt{1-\eta}\sqrt{\eta}}{2e\, V1p\, V2p\, Vbm + 2(1-e)\, V1p(1-\eta) + 2(1-e)\, V2p\, \eta}\right\}\right\}$$ optimum gain

$$FIDELITY = \frac{2}{\sqrt{(Vinp + Voutp) * (Vinm + Voutm)}}$$

assuming shot noise in both input quadratures Vbm/p = 1

Assume a symetric teleporter but two beams are antisqueezed! V1p = 1/V2p

FIDELITY =

$$2\Big/\left(\sqrt{\left(-\left((1+V1p)\,(V1p+\eta-V1p\,\eta+e\,(-1+V1p)\,(-1+2\eta))\left(2\,V1p+\eta-2\sqrt{-(-1+e)\,e}\sqrt{-(-1+\eta)\,\eta} + V1p^2\left(1-\eta+2\sqrt{-(-1+e)\,e}\sqrt{-(-1+\eta)\,\eta}\right)+e\,(1-2\,V1p-2\eta+V1p^2\,(-1+2\eta))\right)\right)\Big/\left((-1+e)\,V1p\,(-V1p^2\,(-1+\eta)+\eta+e\,(-1+V1p)\,(V1p\,(-1+\eta)+\eta))\right)\right)}\right);$$

e = n is the BEST combination

$$FIDELITY = \frac{2}{\sqrt{\dfrac{(-2+2e-V1p)\,(1+V1p)\,(-2e\,(-1+V1p)+2e^2\,(-1+V1p)+V1p)}{(-1+e)\,(V1p^2+e\,(1+V1p-2\,V1p^2)+e^2\,(-1+V1p^2))}}}$$

This function was optimised for e BS1, BS2 choices...

Bibliography

[1] N Rosen A Einstein, B Podolsky. Can quantum-mechanical description of physical reality be considered complete? *Phys. Rev*, 47:777, 1935.

[2] E S Polzik A Kuzmich. Atomic quantum state teleportation and swapping. *Phys. Rev. Lett*, 85:5639, 2000.

[3] T C Ralph B C Buchler, P K Lam. Enhancement of quantum nondemolition measurements with an electro-optic feedforward amplifier. *Phys. Rev. A*, 60:4943, 1999.

[4] H A Bachor. *A guide to experiments in quantum optics.* VCH Publishers, New York, 1 edition, 1998.

[5] J S Bell. *Physics*, 1:195, 1964.

[6] B C Buchler. *Electro optic control of Quantum measurement.* PhD thesis, 2001.

[7] G Brassard C H Bennett. *SIGACT News*, 20:78, 1989.

[8] G Brassard C H Bennett. Experimental realization of teleporting an unknown pure quantum state via dual classical and einstein-podolsky-rosen channels. *Phys. Rev. Lett.*, 70:1895, 1993.

[9] F De Martini L Hardy S Popescu D Boschi, S Branca. Experimental realization of teleporting an unknown pure quantum state via dual classical and einstein-podolsky-rosen channels. *Phys. Rev. Lett*, 80:1121, 1998.

[10] A Zelinger D Bouwmeester, A Ekert. *The Physics of Quntum Information.* Springer, Berlin, Heidelberg, 2000.

[11] K Mattle M Eibl H Weinfurter A Zelinger D Bouwmeester, J W Pan. Experimental quantum teleportation. *Nature*, 390:575, 1997.

[12] A K Ekert. Quantum cryptography based on bell's theorem. *Phys. Rev. Lett*, 67:661, 1991.

[13] D F Walls G J Milburn. *Quantum Optics.* Springer-Verlag, New York, 1994.

[14] C Silberhorn N Korolkova G Leuchs, T C Ralph. *J. Mod. Opt*, 46:1471, 1999.

[15] Ph. Grangier, J. F. Roch, and G. Roger. Observation of backaction-evading measurement of an optical intensity in a three-level atomic nonlinear system. *Phys. Rev. Lett.*, 66:1418, 1991.

[16] C A Fuchs R Jozsa B Schumacher H Barnum, C M Caves. Noncommuting mixed states cannot be broadcast. *Phys. Rev. Lett.*, 76:2818, 1996.

[17] K C Peng J Zhang. Quantum teleportation and dense coding by means of bright amplitude-squeezed light and direct measurement of a bell state. *Phys. Rev A*, 62:064302, 2000.

[18] K C Peng J Zhang, C D Xie. *J Opt. B*, 3:293, 2001.

[19] J M Jauch and F Rochrlich. *The Theory of Photons and Electrons.* Springer, Berlin, 2 edition, 1976.

[20] P Kwiat A Zellinger K Mattle, H Weinfurter. Dense coding in experimental quantum communication. *Phys. Rev. Lett.*, 76:4656, 1996.

[21] T Mukai K Shimizu, N Imoto. Dense coding in photonic quantum communication with enhanced information capacity. *Phys. Rev. A*, 59:1092, 1999.

[22] P Zoller E S Polzik L M Duan, J I Cirac. Quantum communication between atomic ensembles using coherent light. *Phys. Rev. Lett*, 85:5643, 2000.

[23] P K Lam. *Applications of Quantum Electro-Optic Control and Squeezed Light.* PhD thesis, 1998.

[24] P. K. Lam, T. C. Ralph, E. H. Huntington, and H.-A. Bachor. Noiseless signal amplification using positive electro-optic feed-forward. *Phys. Rev. Lett.*, 79:1471, 1997.

[25] P.K. Lam, Ralph T.C., Buchler B.C., McClelland D.E., Bachor H.-A., and Gao J. Optimization and transfer of vacuum squeezing from an optical parametric oscillator. *J. Opt. B*, 1:469, 1999.

[26] N Lutkenhaus. Estimates for practical quantum cryptography. *Phys. Rev. A*, 59:3301, 1999.

[27] C W Gardiner M J Collett, R Loudon. *J. Mod. Opt*, 34:881, 1987.

[28] H Weinfurter A Zellinger M Michler, K Mattle. Interferometric bell-state analysis. *Phys. Rev A*, 53:1209, 1996.

[29] S Iblisdir N J Cerf. Optimal n-to-m cloning of conjugate quantum variables. *Phys. Rev. A*, 62:040301, 2000.

[30] X Rottenberg N J Cerf, A Ipe. Cloning od continuous quantum variables. *Phys. Rev. Lett.*, 85:1754, 2000.

[31] G Leuchs N Korolkova, C Silberhorn. Iqec 2000 nice,. *Conference Digest QMB6*, page p. 8.

[32] G Leuchs N Korolkova, C Silberhorn. Quantum key distribution with bright entangled beams. *Phys, Rev Lett*, 88:167902, 2002.

[33] O Glockl S Lorenz C Marquardt G Leuchs N Korolkova, C Silberhorn. *Eur. Phys J D*, 18:229, 2001.

[34] R Loudon T C Ralph C Silberhorn N Korolkova, G Leuchs. Polarisation squeezing and continuous-variable polarisation entanglement. *Phys. Rev. A*, 65:052306, 2002.

[35] H Weinfurter A Zellinger P G Kwiat, K Mattle. New high intensity source of polarisation-entangled photon pairs. *Phys. Rev. Lett*, 75:4337, 1995.

[36] F Grosshans P. Grangier. Quantum cloning and teleportation criteria for continuous quantum variables. *Phys. Rev. A*, 64:010301, 2001.

[37] S L Braunstein P Loock. Multipartite entanglement for continuous variables: A quantum teleportation network. *Phys. Rev Lett*, 84:3482, 2000.

[38] S L Braunstein P Loock. Telecloning of continuous quantum variables. *Phys. Rev Lett*, 87:247109, 2001.

[39] S Schiller J Mlynek R Bruckmeier, H Hansen. Realization of a paradigm for quantum measurements: The squeezed light beam splitter. *Phys. Rev. Lett.*, 79:43, 1997.

[40] S. Schiller J. Mlynek R. Bruckmeier, K. Schneider. Quantum nondemolition measurements improved by a squeezed meter input. *Phys. Rev. Lett.*, 78:1243, 1997.

[41] T C Ralph. Continuous variable quantum cryptography. *Phys. Rev. A*, 61:010303, 2000.

[42] B A Robson. *The Theory of Polarisation Phenomena*. Clarendon, Oxford,, 1947.

[43] H. J. Kimble S. L. Braunstein. Teleportation of continuous quantum variables. *Phys. Rev. Lett.*, 80:869, 1998.

[44] S Iblisdir P Loock S Massar S L Braunstein, N J Cerf. Optimal cloning of coherent states with linear amplifier and beam splitters. *Phys. Rev. Lett*, 86:4938, 2001.

[45] J.H. Shapiro. Optical waveguide tap with infinitesimal insertion loss. *Opt. Lett.*, 5:351, 1980.

[46] G G Stokes. *Trans. Camb. Phil. Soc*, 9:399, 1852.

[47] P K Lam T C Ralph. Teleportation with bright squeezed light. *Phys. Rev. Lett.*, 81:5668, 1998.

[48] R E S Polkinghorne T C Ralph, P K Lam. Characterising teleportation in optics. *J. Opt. B , Opt 1,*, page 483, 1999.

[49] K. S. Thorne, R. W. P. Drever, C. M. Caves, M. Zimmermann, and V. D. Sandberg. Quantum nondemolition measurements of harmonic oscillators. *Phys. Rev. Lett.*, 40:667, 1978.

[50] F Ya Khalili V B Braginsky, Yu I Vorontsov. *Sov. Phys. JETP*, 46:705, 1977.

[51] K S Thorne V B Braginsky, Yu I Vorontsov. Quantum nondemolition measurements. *Science*, 209:547, 1980.

[52] L Vaidman. Teleportation of quantum states. *Phys. Rev A*, 49:1473, 1994.

[53] Yu. I Voronsov V.B. Braginsky. Quantum-mechanical limitations on macroscopic experiments and modern experimetnal techniques. *Sov. Phys. Usp.*, 17:644, 1975.

[54] B C Buchler R Schnabel T C Ralph H Bachor T Symul P K Lam W Bowen, N Trepps. Experimental investigation of continuous variable quantum teleportation. *pre-print archive : quant-ph/0209001.*

[55] R Schnabel H Bachor W Bowen, P K Lam. Polarization squeezing of continuous variable stokes parameters. *Phys. Rev. Lett*, 88:093601, 2002.

[56] T C Ralph W Bowen, P K Lam. Biased epr entanglement and its application to teleportation. *accepted by J. Mod. Opt.*

[57] W H Zurek W K Wootters. *Nature*, 299:802, 1982.

[58] J Jing J Zhang C D Xie K C Peng X Y Li, Q Pan. Quantum dense coding exploiting a bright einstein-podolsky-rosen beam. *Phys. Rev Lett*, 88:047904, 2002.

[59] M Watanabe Y Zhang, K Kasai. Continuous variables quantum switch teleportation using two-mode squeezed light. *accepted by Eur. Phys J D.*